Characterization of the Mitochondrial Phenotype Associated with Primary Biliary Cholangitis

By

Filip Wysokinski

A thesis submitted in partial fulfillment of the requirement for the degree of

Master of Science

Department of Medicine

University of Alberta

Abstract

Primary Biliary Cholangitis (PBC) is a chronic liver disease characterized by the immune-mediated destruction of intra-hepatic bile ducts. The autoimmune nature of PBC involves humoral and cell-mediated responses that target endogenous mitochondrial proteins. It is thought that the breakdown of immune tolerance relates to the aberrant localization of mitochondrial proteins to the cell surface of PBC patient bile ducts. Mitochondrial dysfunction, altered expression of metabolic regulators, and modified redox homeostasis have also been implicated in disease pathogenesis; however, exactly how these processes relate to the pathogenesis of PBC remains unclear. Here we have characterized metabolic and mitochondrial function in PBC patients' cultured biliary epithelial cells (BEC) relative to liver disease controls. Shotgun-proteomics of cultured BEC illustrated elevated expression of enzymes related to aerobic glycolysis, fatty acid degradation, the mitochondrial compartment and redox homeostasis. Subsequent, functional assays revealed that both aerobic glycolysis and mitochondrial respiration are elevated in PBC BEC *in vitro.* Elevated levels of mtDNA copy number are also observed in PBC BEC. These studies support that PBC BEC show a novel phenotype with metabolic and mitochondrial changes, which may be related to disease pathogenesis. Given that mitochondrial function plays critical roles in both cellular viability and immunity, further work dissecting this phenotype in PBC may provide novel insight into disease pathogenesis and illustrate future targets for therapeutic intervention.

Preface

This thesis is an original work by Filip Wysokinski. No part of this thesis has been previously published.

Several individuals have contributed to the work discussed herein. Ishwar Hosamani helped with sample extractions, cell culture, experimental design, and optimization of the extraction protocol. Chelsea McDougal also aided in the culture and collection of samples, as well as the optimization of the extraction protocol. Dr. L. Xu, Dr. I. Wong and Dr. S. Wasilenko completed the microarray studies. Dr. I. Wong performed the lactate secretion, oxygen biosensor, and Akt qPCR experiments. Jasper Bitner in collaboration with Dr. C. Zwingmann (U Montreal) performed the ^{1}H-NMR glucose tracing experiment. Dr. B. Meng, Dr. W. Wang, and Dr. R. Fahlman's proteomic core (U Alberta) completed the sample extractions, LC-MS/MS and primary analysis. I completed the final pathway analysis for the proteomic studies.

Tracy Jordan performed DNA extractions for the mitochondrial DNA quantitative PCR. I designed and performed the quantitative PCR experiment with the advice of Dr. Michelakis' group. For the Seahorse experiments I performed cell culture, ran the Seahorse assay and performed analysis with the aid of the Michelakis group. I also performed the biliary epithelial cell extraction protocol and general cell culture for several samples included in this thesis. I also performed the statistical analysis on the oxygen biosensor experiment and aesthetically modified all graphs included.

This study was approved by the University of Alberta, Research Ethics Committee. (Pro00005105)

Acknowledgement

I am deeply indebted to all of the individuals who have supported me throughout my Master's degree. Committee members, lab mates, friends and family have all helped me through this experience.

To begin, I would like to express sincere gratitude to my supervisor, Dr. Andrew Mason for his patience, encouragement, and understanding. With his mentorship I have gained invaluable knowledge and skills that I can carry with me for the rest of my life. I also extend many thanks to my committee members Dr. David Marchant and Dr. Evangelos Michelakis. Their input and guidance has benefited me greatly in my training as a master's student. It was a pleasure working with such esteemed researchers.

I would also like to thank the Canadian Institute of Health Research for their funding in support of my work and the Mason group.

I am thankful for having the opportunity to work with current and former members of the Mason and Wong labs including Dr. Steven Willows, Chelsea McDougall, Tracy Jordan, Sandra O'Keefe, Dr. Guangzhi Zhang, Dr. Weiwei Wang, Dr. Kerolous Messeha, Dr. Hiatem Abofayed, Yitian Guo and Dr. Mohammed Sarhan. I would like to extend extra thanks to Mandana Rahabari for the patience, conversation and company during many late nights at the beginning of my degree. I would like to extend thanks to Dr. Ellina Lytvyak for her advice on statistical analysis and general support. I would also like to extend great thanks to our lab manager, Ishwar Hosamani, for his persistent motivation, the countless hours he has spent helping me with my experiments, and the delightful conversations we've had both about science and life. He was there on the hardest of days and I would not have made it this far without his support. I must also extend endless thanks to Dr. David Sharon, one of the most patient, kind, and selfless individuals I have ever had the pleasure of knowing.

I would also like to thank the members of the Michelakis lab for welcoming me into their lab space and their help with experiments. I must extend extra thanks to Dr. Sotirios Zervopoulos and Dr. Aristeidis Boukouris who were kind enough to help me with experimental design and sacrificed a great deal of their time teaching me techniques. I'd like to thank David Kramer from Dr. Fahlman's group, for his help with data collection and teaching me the basics of proteomic analysis. I'd like to thank Dr. Misagh Alipour and Michael Bording-Jorgensen for help with immunocytochemistry and general help not included in this thesis. Furthermore, I'd like to thank Karen Seeberger for her help with immunohistochemistry studies not included in this thesis.

I would like to thank my parents, Lucyna and Jarek Wysokinski for their tireless support and care. I would also like to thank my sister, Agata Wysokinski, whose creativity, courage and resolve are an inspiration to say the least. Finally, I would like to thank my girlfriend, Paige Durling, for her boundless compassion, courage and optimism.

Table of Contents

List of Tables

List of Figures

List of Abbreviations

Abbreviation	Meaning
2-OADC	2-oxoacid dehydrogenase complexes
2-OA	2-octynoic acid
6-BH	6-Bromohexoanate
A1AT	Alpha-1 Antitrypsin deficiency
ADI	Alberta Diabetes Institute
ADP	Adenosine diphosphate
AIH	Autoimmune hepatitis
Akt	V-Akt Murine Thymoma Viral Oncogene Homolog
AldoA	Aldolase, Fructose-Bisphosphate A
ALF	Acute liver failure
AMA	Anti-mitochondrial antibody
ATP	Adenosine triphosphate
B2M	Beta-2-microglobulin
BCA	Bicinchoninic acid assay

BEC	Biliary epithelial cells
BGM	Biliary epithelial cell growth media
BSA	Bovine serum albumin
C_t	Cycle threshold
CRYPTO	Cryptogenic Cirrhosis
DAVID	Database for Annotation, Visualization, and Integrated Discovery
DMEM	Dulbecco modified eagle medium
DTT	Dithiothreitol
ECAR	Extracellular acidification rate
EDTA	Ethylenediaminetetraacetic acid
ENO1	Enolase 1 (Alpha)
ENO2	Enolase 2 (Gamma, Neuronal)
EM	Electron microscopy
ERR	Estrogen-related receptor
ETC	Electron Transport Chain
ETOH	Alcoholic liver disease
F12	Nutrient mixture F12
FAO	Fatty acid oxidation
FFPE	Formalin fixed paraffin embedded
GSD	Glycogen storage disease
GSH	Reduced glutathione
GWAS	Genome wide association studies
HBRV	Human betaretrovirus
HCC	Hepatocellular carcinoma
HBV	Hepatitis B Virus
HCV	Hepatitis-C virus
HEMA	Hemachromatosis
HGF	Hepatocyte growth factor
HI-FBS	Heat inactivated fetal bovine serum
HIF1α	Hypoxia-inducible factor 1 alpha
HKII	Hexokinase II

HLA	Human leukocyte antigen
HSP60	Heat shock protein 60
IBD	Inflammatory bowel disease
IHC	Immunohistochemistry
IL	Interleukin
IQR	Inter-quartile range
JAK	Janus kinase
KEGG	Kyoto Encyclopedia of Genes and Genomes
LDHA	Lactate dehydrogenase
LN	Lymph node homogenate
LC-MS/MS	Liquid chromatography tandem mass spectrometry
MDV	Mitochondrial derived vesicle
MMTV	Mouse mammary tumour virus
mTOR	Mammalian Target of Rapamycin
mtDNA	Mitochondrial DNA
NOD	Non-obese diabetic
OCR	Oxygen consumption rate
OXPHOS	Oxidative phosphorylation
PAGE	Poly-acrylamide gel electrophoresis
PBC	Primary biliary cholangitis
PBS	Phosphate buffered saline
PBST	Phosphate buffer saline supplemented with tween 20
PCR	Polymerase chain reaction
PDC	Pyruvate dehydrogenase complex
PDC-E1α	E1α subunit of the pyruvate dehydrogenase complex
PDC-E2	E2 subunit of the pyruvate dehydrogenase complex
PDC-E3BP	E3 binding protein, a subunit of the pyruvate dehydrogenase complex
PDK4	Pyruvate Dehydrogenase complex 4
PI3K	Phosphatidylinositol-4,5-bisphosphate 3-kinase
PMSF	Phenylmethylsulfonyl fluoride
PGC-1α	Peroxisome proliferator-activated receptor gamma coactivator 1-alpha

PSC	Primary sclerosing cholangitis
QC	Quality control
qPCR	Quantitative PCR
R^2	Pearson correlation coefficient
RIPA	Radioimmunoprecipitation assay buffer
RPM	Rotations per minute
ROS	Reactive oxygen species
SDS	Sodium dodecyl sulfate
SE	Standard error of the mean
STAT	Signal transducer and activator of transcription
STRING	Search Tool for the Retrieval of Interacting Genes/Proteins
TCA	Tricaboxylic Acid Cycle
TNF	Tumour necrosis factor
UDCA	Ursodeoxycholic acid
UK	United Kingdom
US	United States of America
VDAC	Voltage-dependent anion channel

Chapter 1: Introduction

1.1 Introduction

Primary Biliary Cholangitis (PBC) is a chronic autoimmune liver disease characterized by the immune-mediated destruction of the biliary epithelial cells (BEC) lining the intra-hepatic bile ducts. The autoimmune nature of the disease is characterized by humoral and cell-mediated reactivity to endogenous mitochondrial proteins. It is suspected that the breakdown of immune tolerance is related to the aberrant cell-surface localization and increased expression of mitochondrial enzymes in BEC, referred to as the "mitochondrial-phenotype". To date the mechanism behind the mitochondrial phenotype and its relationship to mitochondrial function in BEC have not been well characterized. Herein, we aim to further assess whether PBC BEC show modifications in mitochondrial function and cellular metabolism.

1.2 Primary Biliary Cholangitis

PBC is a chronic liver disease characterized by destruction of the small intra-hepatic bile ducts leading to cholestasis, fibrosis and an eventual progression to liver cirrhosis. Late-stage patients may advance to the point of liver failure where liver transplant becomes necessary to prolong life[1]. PBC accounts for 5% to 10% of liver transplants in North America and Europe, imposing a significant societal and economic burden[2]. PBC is ten times more prevalent in women than men and usually presents during

mid life (fifth or sixth decade)[1]. Disease prevalence also shows geographic disparity, ranging from 1.91 to 40.20 per 100 000 people[3]. Currently there is only one licensed therapy, the naturally occurring bile-acid ursodeoxycholic acid (UDCA), which has been shown to be effective in delaying histological progression, improving hepatic biochemistries and prolonging transplant-free survival. Furthermore, patients that develop a biochemical response to UDCA have an overall survival similar to that of the general population; however, UDCA is not a curative treatment and approximately 40% of PBC patients develop progressive disease, leaving a substantial need for the development of alternate therapies[1].

PBC is considered a model autoimmune disease with both auto-reactive humoral and cell-mediated immune responses to self-proteins. The main diagnostic criterion of PBC is the presence of anti-mitochondrial antibodies (AMA), present in 95% of patient sera[4]. AMA targets subunits of the 2-oxacid dehydrogenase complexes (2-OADC), a group of related mitochondrial complexes that play a variety of roles in cellular metabolism (Table 1.1). AMA specifically recognizes a conserved lipoic acid domain present in all of the 2-OADC complexes. The immunodominant antigen of AMA is the E2 subunit of the pyruvate dehydrogenase complex (PDC-E2), a complex that connects glycolysis to the citric acid cycle by converting pyruvate to acetyl-CoA[5]. Both CD4+ and CD8+ T-cells also show reactivity to the lipoic acid domain, with both cell types enriched in the liver and hiliar lymph nodes[6]. The key histological characteristic of PBC is the florid duct lesion, an intense inflammatory infiltrate with granuloma formation, located proximally to the small interloboluar and septal bile ducts[1]. It is thought that this breakdown in immune tolerance relates to the so-called “mitochondrial phenotype” characterized by elevated expression and abnormal localization of PDC-E2-like protein on the cell surface of bile duct, lymph node and salivary tissue[7].

Currently the etiology of PBC is not known; however there is consensus that PBC is a complex disease, where genetically susceptible individuals are exposed to an unknown environmental trigger that induces the breakdown of self-tolerance to mitochondrial proteins.

Targeted Complex	Specific Subunit(s) Targeted (Frequency of autoantibodies in PBC)	Primary Function
Pyruvate Dehydrogenase Complex (PDC)	PDC-E2 (95%) PDC-E1α (41-66%) PDC-E3BP (95%)	Facilitates the decarboxylation of pyruvate to acetyl-CoA in the mitochondria[8]
Oxoglutarate dehydrogenase complex (OGDC)	OGDC-E2 (39-88%)	A citric acid cycle enzyme that catalyzes the conversion of α-ketoglutarate to succinyl-CoA in the mitochondria[9]
Branched-Chain Oxoacid dehydrogenase complex (BCOADC)	BCOADC-E2 (53-55%)	Functions in branched-chain amino acid catabolism by facilitating the decarboxylation of branched-chain keto acids in the mitochondria[10]

Table 1.1. Characteristics of mitochondrial antigens in PBC [Adapted from Gershwin *et al.,* 2000][11]

1.3 Genetic predisposition to PBC

Epidemiological studies strongly support a genetic component to PBC. Prevalence of PBC has been shown to be highly elevated in first-degree relatives with a sibling relative risk of 10.5 in the UK and 10.7 in the US[12,13]. Higher concordance rates are also observed in monozygotic twins compared to dizygotic twins, further supporting the role of a genetic component in PBC[14]. The evidence for a genetic component led to the assessment of risk loci associated with PBC through genome wide association studies (GWAS). The majority of PBC implicated loci are involved with the adaptive immune system, including HLA gene variants and immune regulatory pathways such as the IL-12, Jak-STAT, NF-KB and TNF-α networks[15]. These studies support the hypothesis that PBC may occur as a result of a dysfunctional immune response to an environmental trigger.

To date, knowledge of immune dysfunction in PBC has not translated to any beneficial therapy for patients. No animal models with these genetic abnormalities have been shown to recapitulate the components of PBC, and clinical trials of immunosuppressive therapies have proved to have low efficacy or toxic side effects[16,17]. A recent study assessing the cumulative risk of implicated loci, suggests that only ~5% of variance is explained by the current association studies[18]. The unexplained variance may be attributed, in part, to heritable epigenetic traits, which are not assessed with these methods[17]. Thus, further work is still required to continue to characterize genetic associations with PBC and assess how these risk loci play a causative role in the development of PBC.

1.4 Environmental factors in PBC

Epidemiological studies have proposed numerous environmental associations with PBC. Currently there are several triggers hypothesized to induce the breach of tolerance in PBC but a single causative agent has yet to be established. Current investigations assessing the environmental trigger focus either on chemical compounds or infectious agents.

Geographical clustering of PBC cases around superfund toxic waste sites, as well as associations with the frequent use of cosmetic products in PBC patients, support a role for chemical compounds in the development of PBC.[13,19] It is proposed that chemical agents may induce PBC through a mechanism of molecular mimicry. This theory suggests that as chemicals are excreted into bile they react or complex with the lipoic acid domain of the 2-OADC complexes, which creates novel antigens that induce an immune response. Self-proteins are then targeted by the immune system due to the structural similarity between self-antigens and the molecular mimic[20].

As a mechanistic proof of principle for the xenobiotic hypothesis, it has been established that the lipoylation pathway, which normally conjugates the lipoic acid group to the 2-OADC complexes, is capable of incorporating xenobiotic groups on to PDC-E2

in vitro[21]. Elaborating on this mechanism, Amano *et al.* (2005) used a protein microarray to assess the reactivity of over a hundred xenobiotics, conjugated to the lipoic domain of PDC-E2, with PBC patient sera. Of these candidates, 9 showed higher reactivity to sera compared to the native PDC-E2. These findings support that xenobiotic modification of PDC-E2 may make it more immunogenic in immunosusceptible hosts[22]. However, a critical issue with the xenobiotic hypothesis is the lack of an association with the mitochondrial phenotype, or how an excessive amount of modified PDC-E2 is presented on the cell surface to the immune system to induce the breach in tolerance.

Currently, two candidate compounds, 2-octynoic acid (2-OA, a chemical compound used in cosmetics and food additives) and 6-bromohexoanate (6-BH) have been used to induce hepatic and bile ducts lesions in animal models. C57BL/6 and NOD.1101 mice immunized with 2-OA conjugated to bovine serum albumin both develop high-titer AMA and liver lesions [23,24]. Although the reproducibility of these models is high, the histological damage observed is different than that observed in patients with PBC. Thus, the xenobiotic hypothesis requires further evaluation[25].

Infectious agents have also been implicated in PBC and agents can be separated into two main groups, bacterial and viral infections. Infectious agents are implicated in PBC with epidemiological studies showing that cases cluster in geographic regions and unrelated family members develop disease[26]. Furthermore, certain immunosuppressive therapies may also accelerate the onset and severity of recurrent disease in transplant patients. This raises the possibility that an inadequate immune response in PBC patients prevents them from fighting off infectious triggers of disease[27].

A role for bacterial infection began with the observation that there is an elevated prevalence of bacteriuria and an increased history of urinary tract infections (UTI) in PBC patients[28]. Bacterial induction of PBC is also hypothesized to work through a mechanism of molecular mimicry. This theory suggests that conserved mitochondrial antigens, present on bacterial cell membranes, will stimulate an immune response that leads to the breakdown of immune-tolerance to the similar endogenous mitochondrial

proteins[29]. Similar to xenobiotics, PDC-E2 homologues from a wide range of bacterial species have been shown to cross-react with AMA [29]. Out of this long list of bacterial candidates two bacterial species, *N. aromaticivorans* and *E. coli*, have been shown to induce host PDC-E2 specific antibodies and the development of histological liver lesions similar to PBC in infected mice[30,31]. However, these bacteria have not been localized to the liver in patients with PBC.

A role for viral infection was first proposed following the observation that a significant number of PBC patients showed seroreactivity with retroviral proteins[2]. Soon after, a human betaretroviral (HBRV) genome, that shared high sequence similarity to mouse mammary tumour virus (MMTV), was cloned from a PBC BEC cDNA library and PBC lymph node tissue[32,33]. In order to verify that there was a higher prevalence of HBRV infection in PBC patients, next generation sequencing was used assess for the presence of pro-viral integrations. These studies showed that 58% of PBC patient' BEC show evidence of integration compared to 7% of liver disease controls, supporting that there is an elevated levels of HBRV infection at the site of disease in PBC[34]. Elevated levels of betaretroviral transcripts are also observed in liver and lymph node tissue from multiple spontaneous PBC mouse models (NOD.c3c4, dnTGFβRII, and IL2$\alpha^{-/-}$), relative to control strains[35]. Furthermore, anti-retroviral treatment in the NOD.c3c4 PBC mouse model was found to induce significant improvements in biochemical and histological markers of disease[36]. These findings raise the possibility that the NOD.c3c4 strain is actually an infectious model of PBC induced by betaretroviral infection; however, further work is required to establish whether virus directly triggers the development of cholangitis.

1.5 The mitochondrial phenotype in PBC

Although mitochondrial proteins are ubiquitously expressed in all cells, the bile ducts are the main target of autoimmune-mediated destruction in PBC. It is suspected that the loss of immune tolerance in the bile ducts may be, in part, explained by the "mitochondrial phenotype" observed in PBC BEC, *in vitro* and *in vivo*[37–39]. The mitochondrial phenotype is defined by the increased expression and aberrant localization of PDC-E2-like protein to the luminal surface of PBC BEC (Figure 1.1). The cell surface expression of E2-like protein in both intact and damaged intrahepatic BEC occurs during early-stage disease in almost all PBC patients and recurs following transplant in a significant number of PBC liver allografts[40,41]. The early occurrence of the mitochondrial phenotype in PBC patients' BEC suggests that it may be involved in disease pathogenesis. The mitochondrial phenotype is not limited to the bile ducts in PBC patients. Surface expression of PDC-E2-like protein is also observed in the salivary epithelia[42]. Salivary tissue also shows evidence of pathology with lymphoid cell infiltration and ductular destruction[43]. Based on these findings, it has been suggested that the mitochondrial phenotype could also play a role in the immune-mediated damage of epithelia outside of the liver[11]. However, even though the mitochondrial phenotype is a well-established characteristic of PBC, its existence raises several questions that remain unanswered.

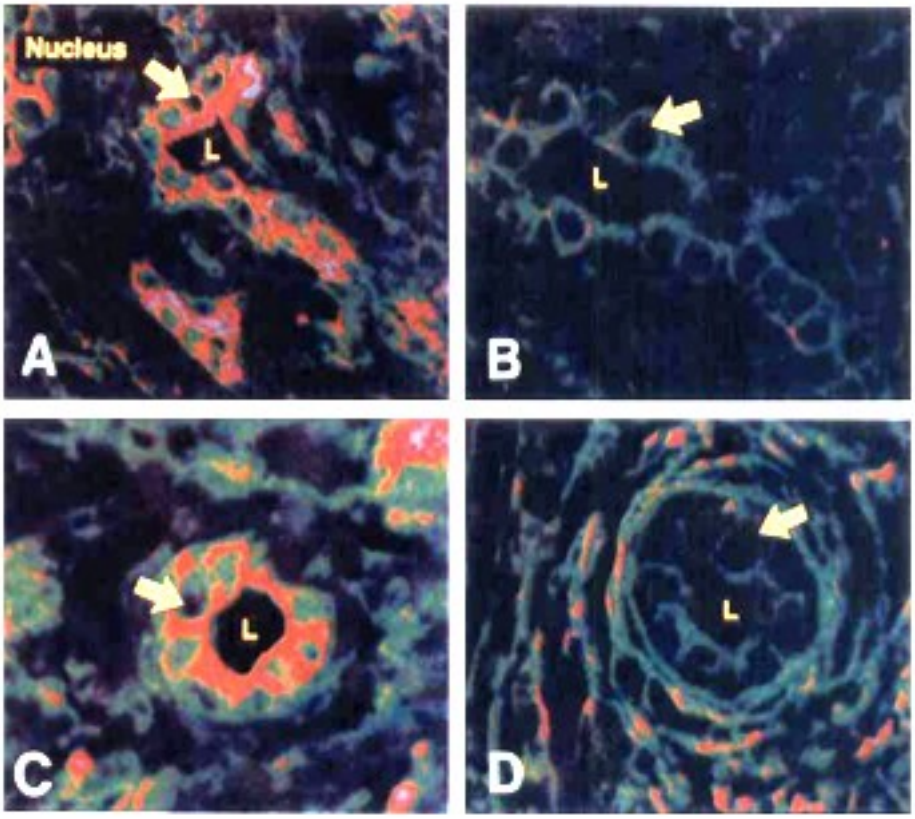

Figure 1.1 Aberrant localization of PDC-E2 in PBC bile ducts. Confocal micrographs of patient liver sections show the aberrant localization of PDC-E2-like protein to the apical surface of primary biliary cholangitis (PBC) (A and C) but not primary sclerosing cholangitis (PSC) bile ducts (B and D). Two combinatorial monoclonal antibodies, SP1 (A and B) and SP4 (C and D) specific for PDC-E2 were used for these studies. [Modified from Cha *et al.,* 1994][44]

The biggest question with the mitochondrial phenotype is in regards to the identity of the E2-like protein localizing to the cell-surface. Opinions are divided whether the protein is endogenous or exogenous in origin. When PBC liver sections were examined with a panel of monoclonal antibodies against various regions of PDC-E2, only two antibodies, that were specific for the lipoic acid domain, were able to show cell-surface staining in BEC. The remaining antibodies only showed the expected mitochondrial staining, leading the authors to propose that the molecule localizing to the

cell-surface differs from mitochondrial PDC-E2. This raises the possibility that the E2-like protein is a modified form of PDC-E2 or a cross-reactive mimic[45].

In order to further assess the identity of the PDC-E2-like protein Joplin and colleagues isolated the plasma membrane protein fraction of BEC extracted from explanted PBC livers and performed western blot with a PDC-specific antibody[46]. Their results unexpectedly showed little to no reactivity towards PDC-E2; however a lower molecular weight protein, corresponding to the E3BP subunit of the PDC, was present in the membrane fraction. This study supports that the PDC-E2-like protein is endogenous but surprisingly is not PDC-E2; however, the authors do suggest this finding requires further validation. In contrast, *in situ* studies assessing transcript levels of the 2-OADC complex subunits, including PDC-E3BP, in patient liver sections showed that expression of these genes are not elevated in the interlobular bile ducts of PBC patients[47,48]. These *in situ* studies suggest that continuous synthesis of the 2-OADC complexes is not occurring in PBC BEC and argues against theories that elevated synthesis of protein leads to the abnormal spill over of endogenous proteins to the apical surface. Still, the cell surface phenotype could be attributed to the abnormal targeting of endogenous protein to the luminal surface of BEC.

To date, limited work has been done assessing mechanisms behind the aberrant localization of E2-like protein. Factors present in lymph nodes have been implicated in inducing the mitochondrial phenotype. This was suggested by *in vitro* studies showing that PBC patient lymph node homogenates (PBC-LN) induce elevated expression of PDC-E2/E3BP and membrane localization of E2-like protein in cultured BEC extracted from non-PBC human liver tissue[49]. Xu and colleagues elaborated on these experiments by assessing for evidence of viral infection in non-PBC BEC following the treatment with PBC-LN[32]. These studies showed significantly higher levels of viral transcripts and proteins in BEC samples incubated with PBC LN compared to non-PBC LN. Furthermore, treatment of non-PBC BEC with supernatant extracted from an MMTV producing cell line induced elevated expression of AMA reactive proteins. Co-localization of betaretroviral capsid protein and PDC-E2-like protein are also observed in

both BEC and spleen tissue in NOD.c3c4 mice, and in PBC lymph node sections[32,50]. In combination, these studies support that betaretroviruses can induce the mitochondrial phenotype in normal BEC *in vitro.*

Apoptosis has also been suggested as a mechanism for cell-surface expression of PDC-E2-like protein. *In vitro* studies have shown that the induction of apoptosis with staurosporine treatment in Jurkat, L929 and HepG2 cell lines stimulates cell surface expression of a PDC-E2 like protein as assessed by fluorescence activated cell sorting[51]. It has also been shown that PDC-E2 remains immunologically intact and is recognizable by AMA in BEC but not control cell lines following the induction of apoptosis[52]. It was reported that the epitope retains its immunogenicity due to an absence of glutathiolation and that this epitope is present in BEC apoptotic bodies[53]. It is proposed that the recognition of the epiptope in apoptotic bodies by antigen-presenting cells may stimulate an innate immune response at the biliary epithelium in patients with a susceptible genetic background[54].

Although the mitochondrial phenotype is an established feature of PBC BEC both *in vitro* and *in vivo*, its relationship to disease pathogenesis is still largely enigmatic. Given the early development and high prevalence of the phenotype it appears to be an important feature of disease that requires further characterization.

1.6 Altered mitochondrial and metabolic function in PBC

One of the well-established functions of the mitochondria is the role it plays in energy metabolism. Mitochondrial pathways are involved in the catabolism of a variety of substrates to produce ATP through oxidative phosphorylation. Mitochondrial PDC plays a critical role in these processes by acting as the "mitochondrial gatekeeper". The PDC functions to convert pyruvate into acetyl-CoA, which can then be used as a substrate for the citric acid cycle (TCA) (Figure 1.2). In turn, the TCA reduces electron donors (NADH and $FADH_2$), which fuel the electron transport chain (ETC). The ETC then establishes a proton gradient across the inner mitochondrial membrane which fuels

ATP synthase-mediated production of ATP. Thus, if the PDC-E2-like protein is in fact endogenous PDC-E2, a question is raised as to how increased expression and aberrant localization affect mitochondrial function in PBC BEC.

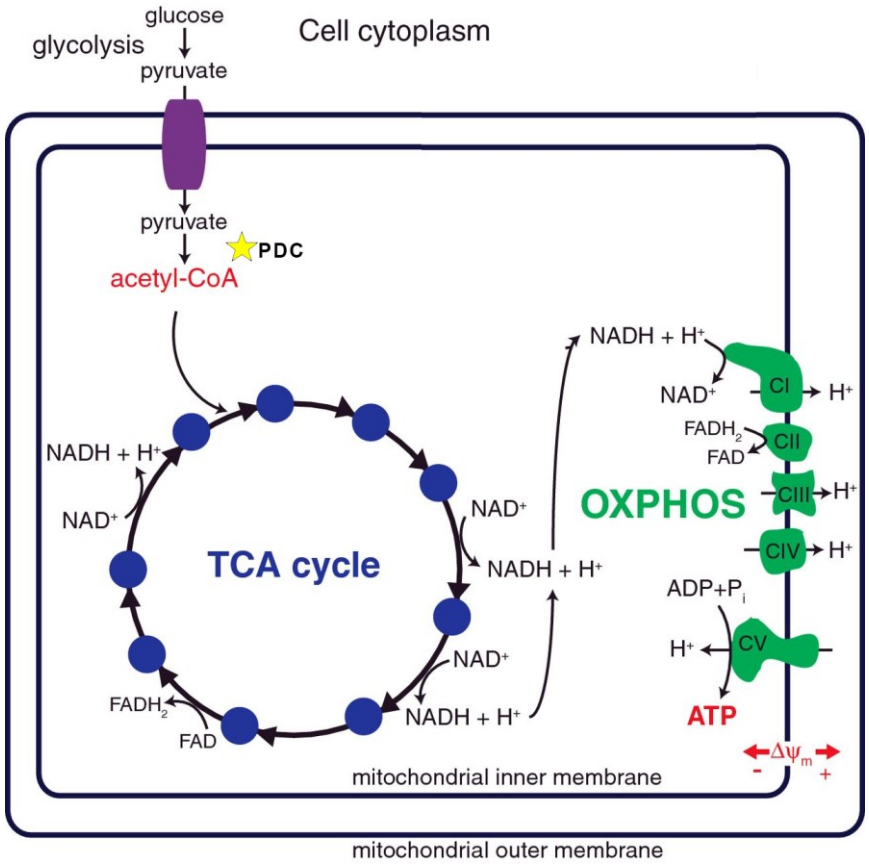

Figure 1.2. Glucose oxidation. Glucose is broken down to pyruvate by glycolysis in the cell cytoplasm. After pyruvate is imported into the mitochondrial matrix, the pyruvate dehydrogenase complex (PDC) facilitates its conversion into acetyl-CoA. Acetyl-CoA is then broken down in the citric acid cycle (TCA), which also reduces NAD+ to NADH. OXPHOS then begins by using NADH to reduce the electron transport chain (ETC) complexes, which facilitates the pumping of protons into the intermembrane space. ATP-synthase then uses the electrochemical gradient produced by the ETC to phosphorylate ADP to ATP, completing the OXPHOS cycle. [Adapted from Nsiah-Sefaa and McKenzie (2016)][55]

In terms of general mitochondrial morphology and number, past electron microscopy (EM) studies have shown that mitochondria are altered in a subset of PBC BEC that show elevated numbers of mitochondria and mitochondria that are swollen with abnormal cristae[56,57]. These EM studies are suggestive of mitochondrial dysfunction. However, elevated levels of mitochondria in PBC BEC were contested in a study done by Joplin and colleagues that showed no significant increase in mitochondria in PBC BEC as assessed by immunohistochemistry for a mitochondrial marker on liver tissue sections[38].

Given its fundamental importance, mitochondrial metabolism and overall function is tightly regulated through several pathways that respond to inputs such as oxygen levels, substrate availability, and cellular stress. Harada *et al.* (2014), examined the PPAR-γ coactivator-1α (PGC-1α) and estrogen related receptor-α (ERRα) axis in BEC *in vivo* to assess for an association between energy metabolism and the pathogenesis of PBC[58]. The PGC-1α–ERRα axis plays a key role in energy metabolism regulating the expression of nuclear genes involved in mitochondrial biogenesis and the metabolic shift to fatty-acid oxidation (Figure 1.3)[59]. Although typically expressed at low levels in liver tissue, it was observed that PGC-1α and ERRα were specifically activated in the damaged inter-lobular bile ducts of PBC patients and PGC-1α activation showed a positive correlation with the degree of chronic cholangitis. They also observed an elevated activation of PDK4 in interlobular bile ducts, an enzyme that phosphorylates and inhibits the pyruvate dehydrogenase complex. Given that fatty acid oxidation is a major producer of ROS, the authors suggest that the shift away from glycolysis may increase susceptibility of PBC BEC to apoptosis. However, PGC-1α is also known to induce the expression of anti-oxidants to alleviate oxidative stress meaning this hypothesis requires further study (Figure 1.3)[60].

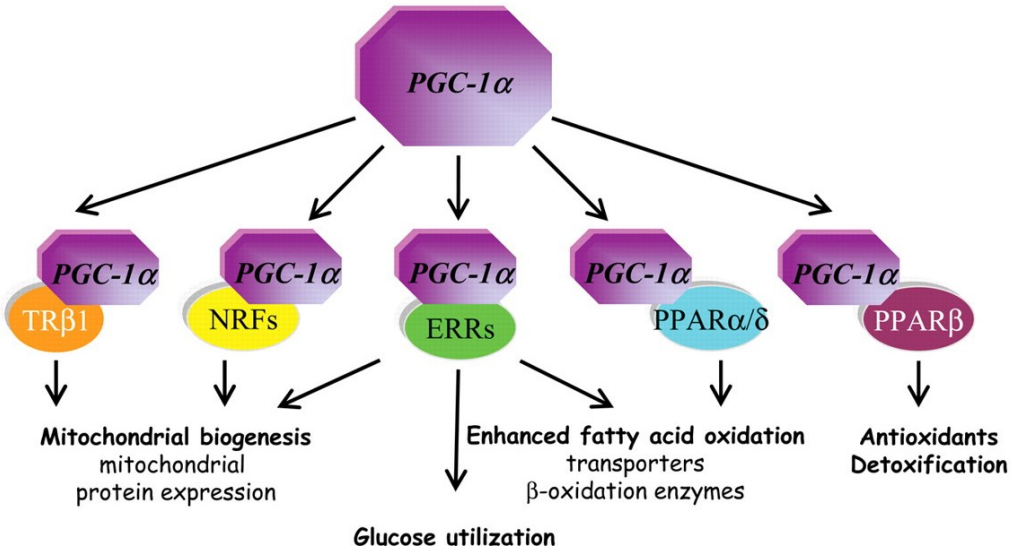

Figure 1.3 Downstream effects of PGC-1α activation. PGC-1α activates transcription factors related to mitochondrial function and cellular energy metabolism. Potential downstream affects of PGC-1α activation include transcription of genes related to mitochondrial biogenesis, glucose utilization, and fatty acid oxidation and anti-oxidant defenses. [Adapted from Vetura-Clapier *et al.,* 2008][61]

1.7 Altered redox homeostasis in PBC

Although mitochondria are typically thought of as the "cellular powerhouse", they also play critical roles in sensing environmental cues and mounting signalling responses relating to metabolism, autophagy, local inflammation, apoptosis, and redox homeostasis[62]. An unavoidable by-product of oxidative phosphorylation is the leakage of electrons from the electron transport chain (ETC), making the mitochondria a leading producer of reactive oxygen species (ROS). These free radicals can readily react with and damage endogenous proteins and lipids; however, a variety of cellular mechanisms are in place to scavenge ROS and prevent them from doing significant harm. When the levels of ROS exceed the cell's ability to regulate them a condition referred to as oxidative stress occurs, where free radicals begin to damage or alter cellular components. Although, ROS can prove to be harmful in excess, in homeostatic conditions ROS also play an important role in mitochondrial cell signalling[63].

Oxidative stress has been implicated in the pathogenesis of several cholestatic diseases [64,65]. In PBC specifically, patients show significantly elevated levels of urine and blood markers of oxidative stress, as well as significant alterations in levels of serum antioxidants and antioxidant capacity[66–68]. These studies provide support that PBC patients are in a systemic state of oxidative stress, however it does not speak directly to a specific site of stress. Interestingly, oxidative stress has been shown to alter mitochondrial morphology *in vitro,* with ultrastructural changes in the mitochondrial cristae similar to those observed in BEC by Tobe *et al.* (1982).[64]

In vivo examination of liver sections further suggest that PBC bile ducts specifically have an altered redox status. Damaged interlobular bile ducts and hepatocytes both show elevated expression of Mn-superoxide dismutase, a mitochondrial oxidant scavenger, in PBC patient liver biopsies[68]. Furthermore, oxidative lipid and DNA modifications are only present in the inter-lobular bile ducts of PBC patients but not extra-hepatic cholestatic liver disease[69–71]. This finding implicates that oxidative modifications in PBC BEC are not mediated by cholestasis and the retention of bile. Lipid peroxidation is also observed in intact bile ducts in early-stage PBC patients, suggesting that altered redox homeostasis may be an early event in bile duct injury[70,71]. It has also been shown that UDCA reduces oxidative stress both *in vitro* and in *in vivo,* and it has been suggested that these antioxidant properties could play a role in UDCA's therapeutic effects in PBC[72–75].

Together these findings implicate that PBC BEC may have abnormal mitochondrial function with altered redox homeostasis and cellular metabolism; thus, at this time it is not clear whether this is a secondary symptom of PBC or plays an active role in pathogenesis.

1.8 Hypothesis

Although the mitochondrial phenotype is a distinguishing characteristic of PBC and is thought to play a critical role in the breakdown of immune tolerance, the mechanism by which it manifests and its relationship to disease pathogenesis remain largely uncharacterized. Given that several lines of evidence implicate mitochondrial changes and modified metabolism in PBC BEC *in vivo*, we hypothesize that the mitochondrial phenotype in PBC BEC may relate to altered mitochondrial function and cellular metabolism. Thus, our aim is to characterize mitochondrial and metabolic aberrations in PBC BEC using an *in vitro* model relying on primary BEC cell lines extracted from the explanted livers of PBC and liver-disease control patients.

1.9 Implications and importance of investigation

Characterization of the mitochondrial phenotype and aberrant metabolism in PBC BEC will provide further insight into disease pathology at the specific site of the autoimmune reaction. As mentioned earlier, the development of PBC seems to circle around mitochondrial enzymes, as they are key epitopes targeted by the autoimmune response, and appear to show elevated expression and cell-surface localization in PBC BEC. It is thought that the cell-surface localization may be involved in the presentation of mitochondrial antigens and breakdown of immune tolerance in PBC. More recent studies also implicate altered metabolism in PBC BEC specifically with modified redox homeostasis, and differences in the expression of key metabolic regulators. At this point in time, it is not clear whether these modifications in PBC BEC are actively involved in the development/perpetuation of disease or are secondary phenomena. Thus, further research characterizing mitochondrial function and cellular metabolism in PBC BEC may provide novel insight into pathogenic mechanisms.

Currently, the majority of research characterizing metabolism in BEC relies on immunohistochemical (IHC) studies that assess enzyme expression or markers of cell stress. Although these studies have provided insight into candidate metabolic pathways

that may be deregulated in PBC BEC, they do not have the power to assess how these changes functionally alter BEC metabolism. Furthermore, these studies are often semi-quantitative or qualitative in nature making the results more challenging to interpret. The high use of IHC for studying BEC can be attributed to their relative prevalence in the liver. Parenchymal hepatocytes constitute 80% of the liver's volume and 60% of the total number of cells, while the remaining 40% of cells are a mixture of non-parenchymal cells[76]. These include endothelial cells, kupffer cells, hepatic stellate cells and BEC. Thus, BEC represent a minute portion (3%) of total liver content [77]. This means that total liver tissue cannot be used to assess for functional changes in metabolic pathways in BEC specifically, making *in vivo* characterization of BEC a challenging task.

For this reason we have elected to use an *in vitro* model of BEC, allowing the use of techniques that are not available with *in vivo* models. These techniques permit us to characterize mitochondrial function and metabolism in BEC with greater depth. These studies rely on primary BEC extracted from the explanted livers of end-stage PBC and liver disease patients using an established immuno-magnetic isolation protocol[78]. The use of an *in vitro* model comes with several challenges in replicating the state of PBC BEC *in vivo.* As previously described, PBC is a complex disease, resulting from an interaction between genetics and environment that leads to the immune system perversely targeting intra-hepatic BEC. With our *in vitro* model we are examining the metabolic properties of BEC without any immune interaction. This means the model is not fully representative of the complex state of disease *in vivo*. However, it is has been previously established that BEC show cell surface staining of PDC-E2-like protein *in vitro* supporting this phenotype is retained in culture[39]. Therefore, we have deemed this an acceptable model for the study of alterations in energy metabolism and mitochondrial function in PBC BEC.

Chapter 2: Materials and Methods

2.1 Cell culture

2.1.1 Biliary epithelial cell (BEC) culture

BEC were cultured in BEC growth media (BGM) composed of Dulbecco's Modified Eagle Medium/Nutrient Mixture F-12 (DMEM/F12, *ThermoFisher Scientific, Waltham, MA, USA*) supplemented with 5% heat-inactivated fetal bovine serum (HI-FBS, *Gibco***,** *Waltham, MA, USA*), epithelial growth factor (10 ng/mL, *R&D Systems, Minneapolis, MN, USA*), insulin (0.4 µg/mL, *Sigma-Aldrich, Oakville, ON, Canada*), hepatocyte growth factor (10 ng/mL, *R&D Systems, Minneapolis, MN, USA*) and primocin (100 µg/mL, *Invivogen, San Diego, CA, USA*). Media was changed every 3-4 days. Cells were grown in incubators set at 37°C and 5% CO_2. For passaging, cells were washed with phosphate buffered saline (PBS, *Gibco***,** *Waltham, MA, USA*) and incubated with 0.25% Trypsin-EDTA (*Gibco***,** *Waltham, MA, USA*) for 1-2 minutes. Typsin was

deactivated with an equal volume of HI-FBS then spun down in unsupplemented DMEM/F12 at 200 g for 5 minutes at room temperature. Cells were then resuspended in BGM and plated at dilutions of 1:2-1:5. When freezing cells, cells were split following the standard protocol above and 2-10 x 10^5 cells were resuspended in 500-1000 µL of Freezing Media (*Gibco*, *Waltham, MA, USA*), gradually cooled to -80°C and stored in liquid nitrogen for future use. Cells were grown on flasks coated with rat tail type I collagen (*ThermoFisher Scientific, Waltham, MA, USA*).

Collagen-coated flasks were prepared by incubating the plates with collagen-plating solution (0.02 M Acetic Acid and 30 µg/mL rat tail type I collagen in PBS) for 1 hour at room temperature. Plates were then washed three times with PBS and left to dry at room temperature overnight. Plates were then stored at 4°C for future use.

2.1.2 BEC isolation

Using a protocol modified from established methods, BEC were extracted from liver tissue obtained from the explanted livers of end-stage liver disease transplant patients[78]. 50-150g of liver tissue was excised from explanted whole liver and submerged in RPMI media (*Gibco*, *Waltham, MA, USA*). Tissue was either immediately used or stored at 4°C for up to 24 hours before performing cell extractions. Liver tissue was diced into a paste with scalpels and then digested enzymatically with collagenase from *Clostridium histolyticum* (1-2 mg/mL, *Sigma-Aldrich, Oakville, ON, Canada*) for 20-30 min. at 37 °C. The tissue slurry was then strained over a sterile mesh screen (*Sigma-Aldrich, Oakville, ON, Canada)* to isolate detached cells. The cell containing flow-through was then distributed to 50 mL Falcon tubes (*ThermoFisher Scientific, Waltham, MA, USA*) and centrifuged (2000 RPM, 5 min., 4 °C). Supernatants were then decanted and pellets were resuspended in PBS before combing two pellets into one tube. Tubes were then centrifuged (2000 RPM, 5 min., 4 °C) and the process was repeated until only two pellets remained. Cells were then semi-purified by density gradient centrifugation (2000 RPM, 30 min., no brake, room temperature) on a 33%/77% Percoll column (*ThermoFisher Scientific, Waltham, MA, USA*). Columns were made by underlaying 3-

4mL of 77% Percoll underneath 3-4 mL of 33% Percoll and then topped with 3-4 mL of cells resuspended in PBS. The BEC-containing interphase was collected, brought up to a volume of 50 mL with autoMACS running buffer (*Miletenyi Biotec, Auburn, CA, USA*) and centrifuged (2000 RPM, 5 min, 4 °C). The pellet was then resuspended in 500uL of autoMACS running buffer supplemented with 60 μL of magnetically labelled antibodies that bind to the BEC specific cell surface marker, CD326 (*Miletenyi Biotec, Auburn, CA, USA*). Cells were left to incubate with antibody at 4°C for 20-30 minutes. During this incubation, MACS columns were prepared by running 3 mL of autoMACS running buffer over the column. The cell-antibody mixture was then put through a 30 μM pre-separation (*Miletenyi Biotec, Auburn, CA, USA*) or a 40 μM cell strainer (*ThermoFisher Scientific, Waltham, MA, USA*) prior to being added to the MACS column. The column was then washed three times with autoMACS buffer. 5 mL of autoMACS buffer was then added to the column and the cells were plunged onto a second MACS column. The column was again washed three times with autoMACS buffer. Finally, 3 mL of BGM was added to the column and cells were plunged into a collagen-coated T-25 flask and stored in a cell incubator (37°C, 5% CO_2).

2.2 Akt quantitative real-time PCR (qRT-PCR)

BEC that were derived from PBC (n=6) and non-PBC (n=9) livers were grown and harvested when they reached 80% confluency in T-150 flasks. Total RNA was extracted using Trizol reagent (Invitrogen). Complementary DNA (cDNA) was synthesized using random primers and RT superscript II (Invitrogen) and amplified as described[79]. 1 μL of 1:80 diluted amplified cDNA, 12.5 μL of 2X SYBR Master Mix (SA Biosciences), 10.5 μL of UltraPure DNase-RNase-free water (Gibco), and 0.5 μL of commercially available Akt1 or Akt3 primer (SA Biosciences) were added to each well in a 96-well plate (Applied BioSystems). The reaction was run at 50°C for 2 min and 95°C for 10 min, followed by 40 cycles at 95°C for 15 sec, 60 °C for 1 min, and an extension phase of 1 cycle at 95°C for 15 sec, 60°C for 30 sec and 95°C for 15 sec in the Applied Biosystem 7300 Real Time PCR System. The cycle threshold (C_t) values were normalized using ACTB as an internal gene expression control. Fold-changes in Akt

expression were expressed as the ratio in PBC BECs to non-PBC BECs. Mean fold-change was then compared between PBC and non-PBC control BEC using a 2-tailed T-test in Excel.

2.3 Lactate secretion assay

PBC (n=5) and non-PBC (n=5) BECs were seeded at concentrations of $4X10^5$ cells per well in 24-well plates and allowed to attached overnight. Fresh BEC media was added to each well the next day and marked as time 0 hour. At each hour, 100 μL of supernatant was collected and frozen at -80°C immediately. Concentrations of lactate were determined by a commercially available colorimetric lactate assay kit that was commercially available (Eton Bioscience Inc.) Briefly, diluted samples or lactate standards were added to a 96-well transparent, flat bottom microplate. Lactate assay solution was added to each well and the mixtures were agitated at 37°C. The reactions were stopped by the addition of 0.5M acetic acid. The absorbance at 490nm (A_{490}) was measured using a microplate reader SpectraMax Plus384. Lactate production was normalized to cell number. Mean lactate production was then compared between PBC and non-PBC control BEC using a 2-tailed t-test in Excel

Diagnosis	Patient Number	Passage Number
Primary Biliary Cholangitis	120	N/A
Primary Biliary Cholangitis	145	N/A
Primary Biliary Cholangitis	183	N/A
Primary Biliary Cholangitis	187	N/A
Primary Biliary Cholangitis	201	N/A
Alcoholic Liver Disease/ Hepatocellular Carcinoma	129	N/A
Alcoholic Liver Disease	155	N/A
Sarcoidosis	178	N/A
Alcoholic Liver Disease	179	N/A
Autoimmune Hepatitis	196	N/A

Table 2.1 Biliary epithelial cell samples used for lactate secretion assay.

2.4 Glucose tracing

Jasper Bitner performed cell culture and extraction steps for these studies. BEC were incubated with DMEM containing 25 mM [U-^{13}C] glucose, followed by extraction of cell lysates and collection of cell incubation media. Incubation media was subsequently lyophilized. Samples were then shipped to Dr. Claudia Zwingmann's (University of Montreal) who performed 1H-NMR and subsequent NMR analysis based on previous methods[80]. Average ^{13}C-enrichment for lactate was compared between PBC and non-PBC BEC using a 2-tailed student's T-test in Excel. Shown are means +/- SE. [Studies performed by Dr. Claudia Zwingmann and Jasper Bitner]

Diagnosis	Patient Number	Cell Lysate	Cell Supernatant	Passage Number
Primary Biliary Cholangitis	183	X	X	N/A
Primary Biliary Cholangitis	185	X	X	N/A
Primary Biliary Cholangitis	120	X	X	N/A
Primary Biliary Cholangitis	32	X	N/A	N/A
Normal Cadaveric Liver	25	X	X	N/A
Focal Nodule Hyperplasia	27	X	X	N/A
Normal Tissue around Hemangioma	28	X	X	N/A

Table 2.2 Biliary epithelial cell samples used for glucose tracing

2.5 Comparative shotgun proteomics

2.5.1 Liquid chromatography tandem mass spectrometry (LC-MS/MS)

Dr. B Meng performed lysate extractions. Cultured BEC were washed four times with PBS prior to the addition of 400 µL of 2D lysis Buffer (7M urea, 2M thiourea, 4%

chaps, 30mM Trish-HCl pH 8.8, 1M PMSF, 0.5mM EDTA, 1mM DTT, EDTA-free Halt protease inhibitor cocktail, (*ThermoFisher Scientific, Waltham, MA, USA*). Cells were scraped off the plate on ice followed by rigorous pipetting to help facilitate lysis. Lysates were spun at 12 000 g for 10 min and stored at -80°C. Protein concentration was quantified using a Bradford Assay. 25 µg of protein was loaded for PAGE separation. Gels were then given to the University of Alberta Proteomics Core (Dr. R. Fahlman) at the University of Alberta for LC-MS/MS. A total of 3 PBC and 4 non-PBC disease control BEC were collected and run on LC-MS/MS in duplicate.

Diagnosis	Patient Number	Passage Number
Primary Biliary Cholangitis	239	N/A
Primary Biliary Cholangitis	261	N/A
Primary Biliary Cholangitis	263	N/A
Cryptogenic Cirrhosis	101	N/A
Autoimmune Hepatitis	197	N/A
Alcoholic Liver Disease	252	N/A
Cryptogenic Cirrhosis	271	N/A

Table 2.3 Biliary epithelial cell samples used for LC-MS/MS.

2.5.2 LC-MS/MS analysis

Primary analysis of LC-MS/MS was performed by the Fahlman group to determine peptide spectral counts as a quantitative measure of protein expression. Dr. W. Wang and Dr. B. Meng performed normalization and statistical analysis using the DanteR software package. For statistical analysis, normalized spectral counts were compared between PBC and non-PBC BEC[81]. P-values less than 0.05 were considered significant. In order to compare overlap between significant candidates in the microarray and proteomic datasets, both Uniprot accession numbers and Affymetrix IDs were converted to official gene symbols using the online Gene ID Conversion tool offered by the DAVID bioinformatics database[82]. Lists were then compared and figures were produced using the online Venn Diagram tool offered by Bioinformatics Gent (http://bioinformatics.psb.ugent.be/webtools/Venn/).

Proteins found to be differentially expressed were then separated into upregulated and downregulated lists of uniprot accession numbers. These lists were then separately analyzed using the functional enrichment analysis tool through the online STRING database under default settings[83,84]. The Bioinformatics Gent Venn Diagram tool was also used to assess for any protein overlap in terms related to cellular energy-metabolism. PRISM 7 software was used to produce bar graphs showing normalized peptide spectral counts of proteins related to energy metabolism.

2.6 Oxygen biosensor assay

PBC (n=5) and non-PBC (n=5) BECs were seeded at densities of $4x10^5$ cells per well in a 96-well Oxygen Biosensor System (BD Bioscience). Antimycin A (Sigma) was added in concentration of 0.1 μM to each cell line in a paired study as a negative control. Plates were read at 485 nm (excitation) and 590 nm (emission) in a BioTek Gen5 Synergy HT plate reader. Aerobic respiration signals were detected every 15 min for one hour at 37°C and oxygen consumption was calculated as normalized relative fluorescence units (NRFU).

Diagnosis	Patient Number	Passage Number
Primary Biliary Cholangitis	120	N/A
Primary Biliary Cholangitis	145	N/A
Primary Biliary Cholangitis	183	N/A
Primary Biliary Cholangitis	187	N/A
Primary Biliary Cholangitis	201	N/A
Alcoholic Liver Disease/ Hepatocellular Carcinoma	129	N/A
Alcoholic Liver Disease	155	N/A
Sarcoidosis	178	N/A
Alcoholic Liver Disease	179	N/A
Alpha-1 Anti-Trypsin Deficiency	196	N/A

Table 2.4 Biliary epithelial cell samples used for oxygen consumption assay.

2.7 Seahorse XF24 assay

12-16 hours prior to running the Seahorse assay, 10 000/15 000 BEC were seeded to XF24 cell culture microplates (*Agilent Technologies, Santa Clara, CA, USA*) in 100 µL of BGM (Table 2.3). Cells were allowed to adhere to the plate for 1 hour at room temperature before another 150 µL of BGM was added. Each sample was seeded as 5 replicates with a total of 4 samples assessed per plate. 4 wells were seeded with media only for background normalization. The XF24 sensor cartridge was also hydrated at this point by adding 1 mL of Seahorse XF calibrant per well and stored in a non-CO_2 37°C incubator overnight. The following day cells were washed with PBS followed by the addition of 525 µL of Seahorse XF Base Medium (pH 7.35, *Agilent Technologies, Santa Clara, CA, USA)* supplemented with 17.5mM Glucose (*Sigma-Aldrich, Oakville, ON, Canada*), 2.5mM L-Glutamine (*Gibco***,** *Waltham, MA, USA*) and 0.5 mM Sodium Pyruvate (*Gibco***,** *Waltham, MA, USA*). Measurement of cellular oxygen consumption rate (OCR) and extracellular acidification rate (ECAR) was performed during 8-min intervals over 1.5 hours using the Seahorse XF24 analyzer. Basal conditions were first measured 3 times without any drug added, followed by 3 measurements after injection of the mitochondrial uncoupler CCCP (0/10/100 µM, *Immunohistochemistry*), and finally 3 measurements with the electron transport chain inhibitor antimycin A (1 µM, *Sigma-Aldrich, Oakville, ON, Canada*).

Following the assay, media was poured off and 100 µL of Lysis buffer (NP40 lysis buffer (*Invitrogen, Carlsbad, CA, USA*), 1 mM PMSF (*Sigma-Aldrich, Oakville, ON, Canada)*, 1x protease inhibitor cocktail (*Sigma-Aldrich, Oakville, ON, Canada*) was immediately added to each well of the plate followed by incubation on ice for 30 minutes. Protein content of each well was then determined using a Pierce BCA assay (*ThermoFisher Scientific, Waltham, MA, USA*) following the manufacturers instructions. OCR and ECAR values were then imported into Microsoft Excel (14.4.7) for normalization to protein content and technical replicates were then averaged. If a sample was run across multiple plates the median value was used for analysis. Normalized values were then exported into Prism 7 software for further analysis. Using the Grubbs test

(α=0.05) one control sample (BEC 334 p3) was determined to be a significant outlier and was removed from further analysis. The median OCR/ECAR was then compared between PBC and Non-PBC control BEC using a 1-tailed Mann Whitney test.

Diagnosis	**Patient Number**	**Passage Number**
Primary Biliary Cholangitis	188	6
Primary Biliary Cholangitis	185	5
Primary Biliary Cholangitis	258	6
Primary Biliary Cholangitis	263	4
Primary Biliary Cholangitis	329	3
Primary Biliary Cholangitis	358	3
Primary Biliary Cholangitis	330	5
Primary Sclerosing Cholangitis	159	3
Alcoholic Liver Disease	309	5
Alpha-1 Antitrypsin Deficiency	339	5
Cryptogenic Cirrhosis	101	6
Alcoholic liver disease	334	3

Table 2.5 Biliary epithelial cell samples used for Seahorse XF24 assay.

2.8 Mitochondrial DNA quantitative PCR

2.8.1 DNA extraction

Chelsea McDougall cultured BEC and snap-froze samples in liquid nitrogen, followed by immediate storage at -80°C. DNA extractions were performed on frozen pellets by Tracy Jordan using a DNeasy Blood and Tissue kit (*Qiagen, Toronto, ON, Can*) following the manufacturers instructions and stored at -80°C. DNA concentration and quality were assessed using a Nanodrop 1000 prior to performing experiments

(Appendix Table 1.1) DNA Samples that showed a 260/280 ratio less than 1.6 or 260/230 less than 1, were precipitated and reconstituted using a standard ethanol precipitation protocol. For ethanol precipitation, sodium acetate (3M, pH 5.2, *ThermoFisher Scientific, Waltham, MA, USA*) was added such that it was 1/10 of the total DNA sample volume. Samples were then thoroughly mixed followed by addition of 2 volumes of one hundred percent ethanol. Samples were again mixed then left at -20°C for 25 minutes or overnight. Samples were then spun at max speed for 25 to 30 minutes at max speed at 4°C. Supernatant was then eluted and pellets were left to air dry. Samples were then resuspended in DNeasy AE Elution Buffer (*Qiagen, Toronto, ON, Can*).

2.8.2 Quantitative PCR (qPCR) for mtDNA copy number

Relative abundance of mitochondrial DNA (mtDNA) was assessed using real-time quantitative polymerase chain reaction (qPCR). A pre-designed singleplex FAM-MGB TaqMan assay was used to assess the copy number of the mitochondrial D-loop region (Hs02596861_s1, *ThermoFisher Scientific, Waltham, MA, USA*). Nuclear DNA was used for normalization and was assessed using SYBR Green with previously validated primers for the single copy gene, beta-2-microglobulin (B2M) (Table 2.6)[85]. All reactions were run on MicroAmp Optical 96-well reaction plates (*ThermoFisher Scientific, Waltham, MA, USA*). The D-loop assay was carried out in 20 µL reaction volumes consisting of the following: 10uL TaqMan Universal PCR Master Mix (*ThermoFisher Scientific, Waltham, MA, USA*), 1 µL TaqMan D-loop Expression Assay, and 9 µL DNA diluted in commercial Ultrapure RNase/DNase free water (*Gibco***,** *Waltham, MA, USA)*. After samples had been loaded, plates were covered with MicroAmp Optical Adhesive Film (*ThermoFisher Scientific, Waltham, MA, USA*) and spun at 300 g for 3 minutes. Reactions were run in the ABI 7300 Real-Time PCR System, which continuously monitored fluorescence spectra. The cycling condition included an initial phase of 2 min at 50 °C, followed by 10 min at 95 °C, then 40 cycles of 15 s at 95 °C and 1 min at 60 °C. The B2M assay was carried out in 20 µL reaction volumes consisting of the following: 10 µL SYBR Green PCR Master Mix (*ThermoFisher Scientific, Waltham, MA, USA*), 1250nM FB2M/RB2M primers, and 9 µL DNA diluted

in commercial Ultrapure RNase/DNase free water (*Gibco***,** *Waltham, MA, USA)*. Each sample was assayed in duplicate and two wells were used as no template controls (NTC) with only water added. The cycling condition included an initial phase of 10 min at 95 °C, 40 cycles of 15 s at 95 °C, 15s at 55°C and 1 min at 60 °C, followed by a disassociation step to assess for primer specificity.

A preliminary trial for each assay was performed using serial dilutions from one BEC DNA sample in order to determine PCR efficiency, correlation coefficients, threshold settings and optimal DNA concentration. 25 ng/well of DNA was used for the TaqMan D-loop assay and 10 ng/ well was used for the SybrGreen B2M assay. Primer specificity was confirmed for the B2M assay by assessing the presence of a single peak in disassociation curves and an agarose gel of amplified product to confirm the presence of a single band. 2% Agarose gels were prepared by boiling 1g of agarose (*EM Science, Gibbstown, NJ, USA*) in 50 mL of TAE buffer using microwave under high power. 5 μL of SYBR© safe DNA gel stain (*Invitrogen, Carlsbad, CA, USA*) was added once the solution had cooled. Samples were diluted in 6X loading dye (*ThermoFisher Scientific, Waltham, MA, USA)* before loading the gel and a Gene Ruler 1KB (*ThermoFisher Scientific, Waltham, MA, USA)* ladder was used for sizing. The gel was run at 107V until the ladder bands had separated distinctly. Threshold and baseline settings for cycle threshold (C_t) determinations were manually set based on this initial trial and kept consistent throughout the remaining experiments.

Gene Name	Sequence
B2M	Forward: 5'-GCTGGGTAGCTCTAAACAATGTATTCA-3'
	Reverse: 5'-CCATGTACTAACAAATGTCTAAAATGGT-3'

Table 2.6. Beta-2-microglobulin (B2M) primer sequences

2.8.3 qPCR analysis

For the optimization plates C_t values were exported from the ABI7300 software and further analyzed using Prism 7 software. NTCs did not show significant C_t values on any plates run. Disassociation curves were also checked to ensure primer specificity. Samples with replicates showing a standard deviation greater than 0.5 C_t were removed from analysis. The non-linear regression analysis tool in PRISM 7 was used to produce a line of best fit to determine slope and correlation values. PCR efficiency was then calculated from the slope of the line of best fit using the online qPCR efficiency calculator from ThermoFisher Scientific (*Waltham, MA, USA*).

For experimental plates C_t values were imported into Microsoft Excel (14.4.7) for initial analysis. Samples with replicates showing a standard deviation greater than 0.5 C_t were either run a second time or discarded from further analysis. Duplicate C_t values were averaged prior to housekeeping normalization.

D-loop levels were normalized to B2M levels using the $\Delta\Delta C_t$ method[86]:

1. Avg. $C_t^{D\text{-}loop}$ - Avg. $C_t^{B2M} = \Delta C_t$
2. Sample ΔC_t – Interplate Calibrator $\Delta C_t = \Delta\Delta C_t$
3. $2^{-\Delta\Delta Ct}$ = Fold Difference

Samples were then grouped based on clinical diagnosis being placed into PBC or non-PBC control. These values were then imported into Prism 7 for graphing and statistical analysis. Using a Grubbs Test (α=0.0001), one sample was determined to be an outlier (BEC 245p2) and removed from further analysis. Median fold difference for mtDNA copy number was compared between PBC and non-PBC control BEC using a two-tailed Mann Whitney-test in Prism 7.

Chapter 3: Results

Section 1: Elevated levels of aerobic glycolysis in PBC BEC

3.1 Prior work showing elevated glycolysis in PBC BEC

Dr. I. Wong, Dr. S. Wasilenko and Dr. L Xu began the assessment of global metabolic disturbances in PBC BEC *in vitro* with an Affymetrix plus 2.0-microarray chip. The microarray was used to characterize differences in messenger RNA (mRNA) expression between cultured biliary epithelial cells (BEC) extracted from the explanted livers of patients with either primary biliary cholangitis (PBC) or control end-stage liver diseases. The microarray studies showed a total of 1921 genes with significantly different levels of expression in PBC BEC compared to liver-disease controls (784 downregulated and 1137 upregulated genes).

In order to assess for biological meaning within the list of differentially expressed proteins, the online STRING statistical enrichment analysis tool was used to characterize functional interactions between candidate genes. In summary, enrichment analysis works by assessing how lists of candidate genes relate to annotation terms present in available databases such as Gene Ontology or KEGG pathways. It can then be established whether gene lists show statistically significant enrichment in specific terms

relative to what is expected in the genetic background. These term enrichments then provide a larger picture of what general biological functions may be altered in an experiment. Specifically, the STRING enrichment analysis tool used with these studies assesses term enrichment in a variety of databases including Gene Ontology, KEGG, Pfam and InterPro[83,84].

For the microarray dataset, separate analyses of upregulated and downregulated proteins using STRING enrichment analysis both showed significant interaction enrichment. Significant enrichment in the "pathways in cancer" term was observed for both the upregulated (34 genes) and downregulated gene groups (21 genes). Significant enrichment in genes related to the phosphoinositide 3-kinase (PI3K) / serine/threonine kinase (Akt) axis signalling pathway (37 genes upregulated and 21 genes downregulated in PBC BEC) was also observed. These findings are interesting given that one of the distinguishing characteristics of cancer is the Warburg phenotype, where cells shift from mitochondrial oxidative phosphorylation to aerobic glycolysis as the primary source of ATP even in the presence of oxygen[87]. It has also been proposed that the PI3K/Akt signalling axis is a key player in this phenotype as it is an important regulator of glycolytic metabolism, cell proliferation and cell survival[88]. Given the enrichment in these cancer-related terms, the group went on to assess how expression of glycolytic genes was altered in this dataset. It was found that the glycolytic gene ENO1 is significantly increased in PBC BEC and there are trends for elevated expression of several other glycolytic genes (Appendix Figure 5.1). FBP1, a rate-limiting enzyme involved in gluconeogenesis, was found to be significantly decreased in PBC BEC.

Following completion of these experiments, the group realized that not all samples had been treated in the same fashion. A few samples had been grown without hepatocyte growth factor (HGF) supplemented to the media. HGF has been shown to alter pathways related to energy metabolism, which in turn raises questions as to how valid these results actually are[89,90]. Accordingly, other methods were employed to validate these results.

To begin, Dr. I. Wong and Dr. S. Wasilenko used qPCR to validate differential expression of significant candidate genes from the microarray study. These studies showed that mRNA expression of one microarray candidate, Akt3, was significantly upregulated in PBC BEC compared to end-stage liver disease controls (Figure 3.1). Significantly higher levels of Akt1 expression were also observed in these qPCR studies but not in the microarray dataset.

Given the evidence suggesting that glycolytic metabolism may be elevated in PBC BEC, Dr. Wong also went on to assess whether glycolysis was functionally altered in PBC BEC *in vitro.* She began by examining glycolytic activity indirectly by assessing the levels of lactate secretion from PBC BEC *in vitro.* As cells are undergoing aerobic glycolysis pyruvate is converted into lactate in the cytosol rather than being imported into the mitochondria for aerobic respiration. Lactate is then exported into the extracellular space by monocarboxylate transporters[91]. Therefore, the levels of extracellular lactate in the supernatant of cultured cells can be used as a surrogate measure of glycolytic activity. Thus, Dr. Wong went on to characterize the rate of lactate secretion from cultured BEC in cell supernatant. These studies showed a significant increase in the rate of lactate secretion in cultured PBC BEC compared to end-stage liver-disease controls using a commercial assay (Figure 3.2). This study supports that glycolytic activity in PBC BEC is functionally elevated *in vitro*.

In collaboration with Dr. Claudia Zwingmann (U Montreal), PBC and control BEC were investigated for glucose metabolism using a method of glucose tracing. For these studies ^{13}C-labeled glucose was added to the media of cells 24 hours prior to collecting intracellular and extracellular metabolites. The metabolites were then quantified using ^{1}H-NMR, which can distinguish between unlabelled (^{12}C) and labelled carbons (^{13}C) by spectral analysis. These studies showed enrichment of ^{13}C carbon in both intracellular and extracellular lactate, which suggests that there is an increased flux of glucose carbon through the glycolytic pathway (Figure 3.3). These studies provide further support for increased aerobic glycolytic activity in PBC BEC *in vitro.*

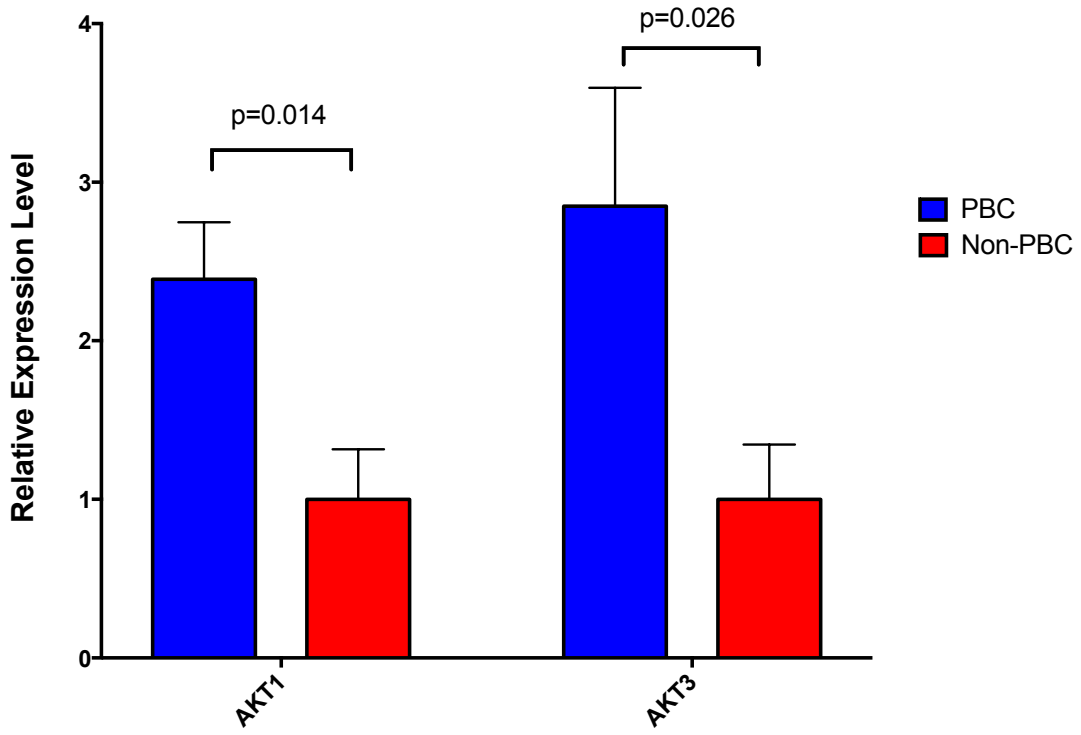

Figure 3.1. Cultured biliary epithelial cells (BEC) from patients with Primary Biliary Cholangitis (PBC) show elevated RNA expression of the serine/threonine kinase genes (Akt1 and Akt3). Real-time quantitative PCR (qPCR) shows greater than 2-fold differences in RNA expression of both Akt1 and Akt3 in PBC patients' cultured BEC relative to end-stage disease controls. QPCR was performed on amplified cDNA obtained from end-stage liver disease controls (n=9) and PBC (n=6) BEC. RNA was extracted using Trizol reagent, and cDNA was synthesized using random primers and RT superscript II. QPCR was performed using commercially available primers (SA Biosciences) and SYBR master mix following the manufacturers protocol. C_t values were normalized using β–actin as an internal gene expression control. Fold-changes in the expression of Akt were expressed as the ratio in PBC BECs to non-PBC BECs. Bar graphs were made using PRISM 7 software. Shown are mean relative expression levels +/- SE. Relative expression in PBC BEC was compared to non-PBC BEC using a two-tailed T-test in Excel. [Studies performed by Isabella Wong and Shawn Wasilenko]

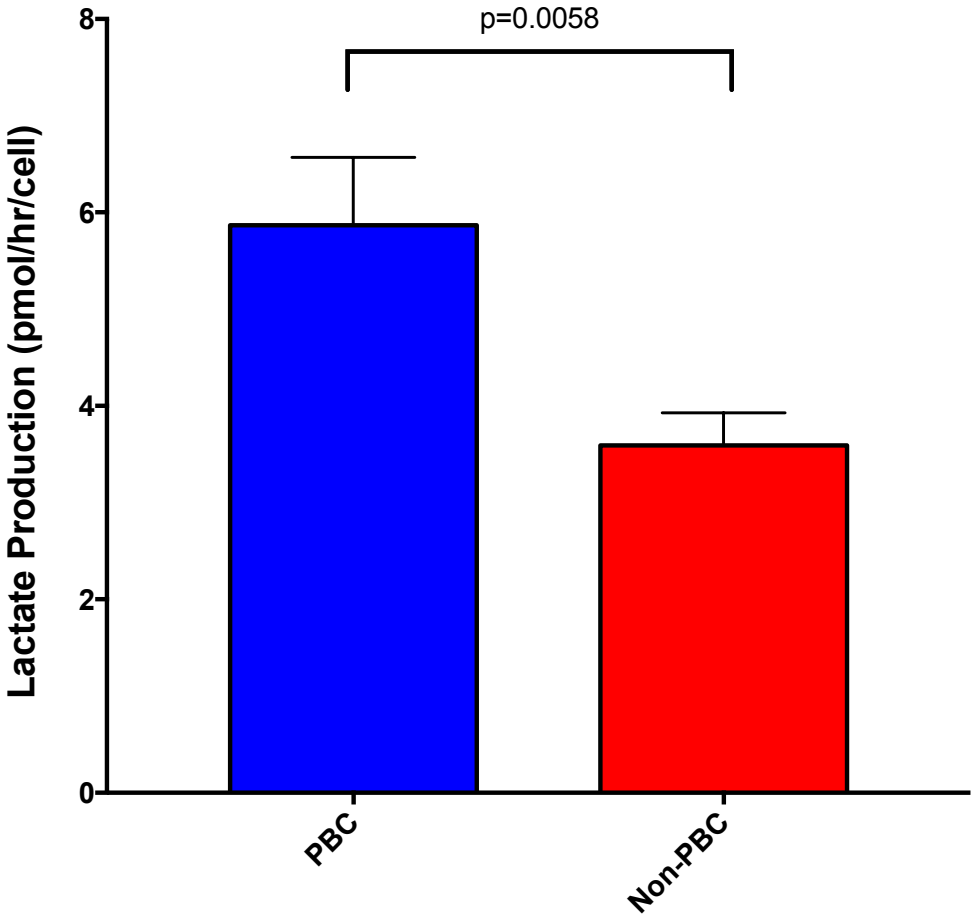

Figure 3.2. Cultured biliary epithelial cells (BEC) from patients with Primary Biliary Cholangitis (PBC) show elevated levels of lactate production. PBC (n=5) and non-PBC (n=5) BEC were seeded at concentrations of $4x10^5$ cells per well in 24-well plates and allowed to attach overnight. Fresh BEC media was added to each well the next day and marked as time 0 hour. At each hour, 100 µL of supernatant was collected and frozen at -80°C immediately. An Eton Bioscience lactate assay kit was used to determine the concentrations of lactate in supernatants following the manufacturer's instructions. Absorbance was read at 490nm (A_{490}) using a microplate reader SpectraMax Plus384. Lactate production was normalized to cell number. Mean +/- SE rate of lactate production are shown here. Statistical analysis was performed using a 2-tailed t-test in Excel. [Studies performed by Dr. Isabella Wong]

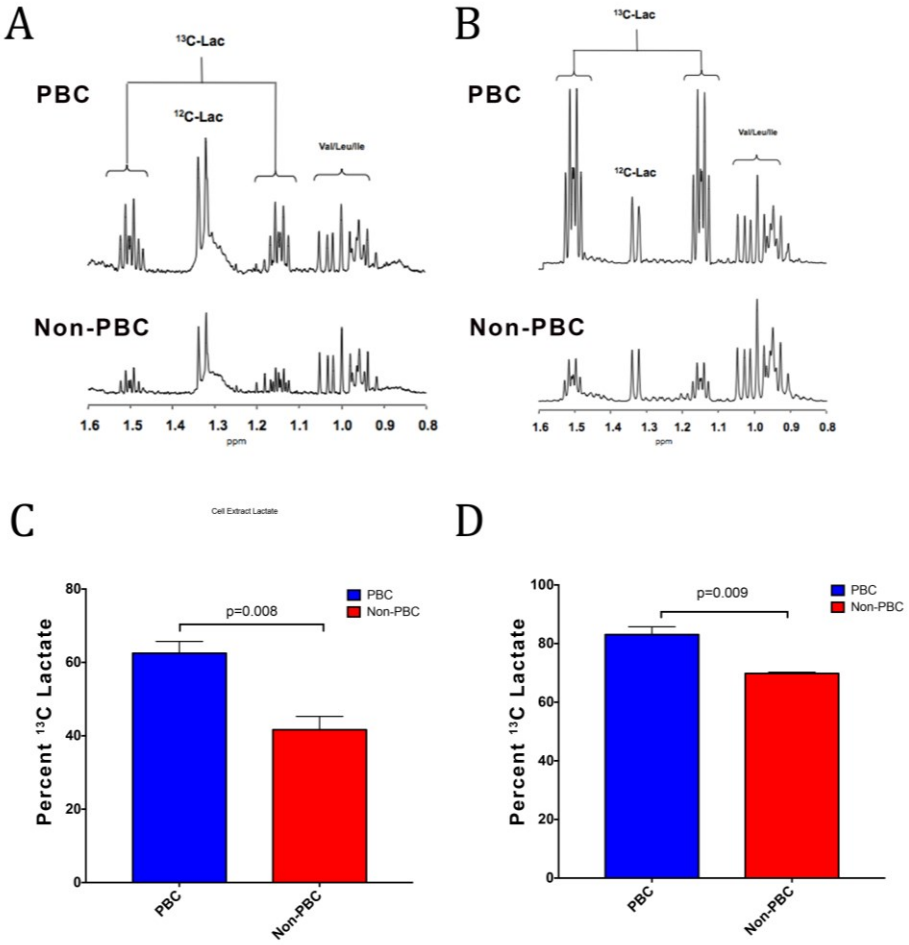

Figure 3.3. Cultured biliary epithelial cells (BEC) from patients with Primary Biliary Cholangitis (PBC) show elevated levels of intracellular and excreted lactate in ^{13}C glucose tracer studies. Representative sections of ^{1}H NMR spectra of cell extracts (A) and lyophilized incubation media (B) after a 24-h incubation with DMEM containing 25 mM [U-^{13}C] show elevated levels of intra- and extracellular lactate, respectively, in PBC BEC compared to end-stage liver disease controls. The expanded spectra show the methyl resonances of unlabeled lactate (^{12}C-Lac) as well as its satellites arising from ^{1}H-^{13}C coupling. The ^{13}C-Lac isotopomer has been synthesized through glycolysis; its changes reflect changes in glycolytic flux. Valine, leucine, and isoleucine were consistent between the samples. C, D. Significantly higher enrichment of intracellular (C) and extracellular (D) U-^{13}C in lactate in PBC BEC (cell lysates n=4; cell supernatant n=3) compared to end-stage liver disease controls (cell lysates and cell supernatant n=3) suggest glycolysis-mediated breakdown of glucose is elevated in PBC BEC. Statistical analysis was performed using a 2-tailed student's T-test in Excel. Shown are means +/- SE. [Studies performed by Dr. Claudia Zwingmann and Jasper Bitner]

3.2 Proteomic studies show glycolytic signature in PBC BEC

To derive additional supportive data, label-free shotgun-proteomics was used as a second OMICs method to assess for global metabolic disturbances between PBC versus liver disease control BEC *in vitro*. For these studies, Dr. B. Meng extracted protein lysates from cultured BEC followed by size separation of proteins with polyacrylamide gel electrophoresis. Protein quantification was performed in collaboration with the proteomics core laboratory (Dr. R. Fahlman, University of Alberta), which performed liquid chromatography tandem-mass spectrometry (LC-MS/MS) and assisted with primary data processing. Using spectral counts obtained from LC-MS/MS, proteins were compared between 3 PBC and 4 end-stage liver disease control BEC. A total of 99 proteins were found to be significantly different between the two groups, with 53 candidates upregulated and 46 candidates downregulated in PBC BEC (Appendix Table 5.2). 8% of the proteomic candidates were found to be significantly upregulated at the protein and transcript level when compared with our microarray dataset (Figure 3.4). These candidates included the metabolism-related enzymes alpha-enolase (ENO1, a glycolytic enzyme that facilitates the conversion of 2-phosphoglycerate to phosphoenol pyruvate) and the transferrin receptor (TFRC, a protein involved in the uptake of iron and the regulation of mitochondrial biogenesis). 5% of proteomic candidate's proteins showed opposite trends at the protein and transcript level (Figure 3.4).

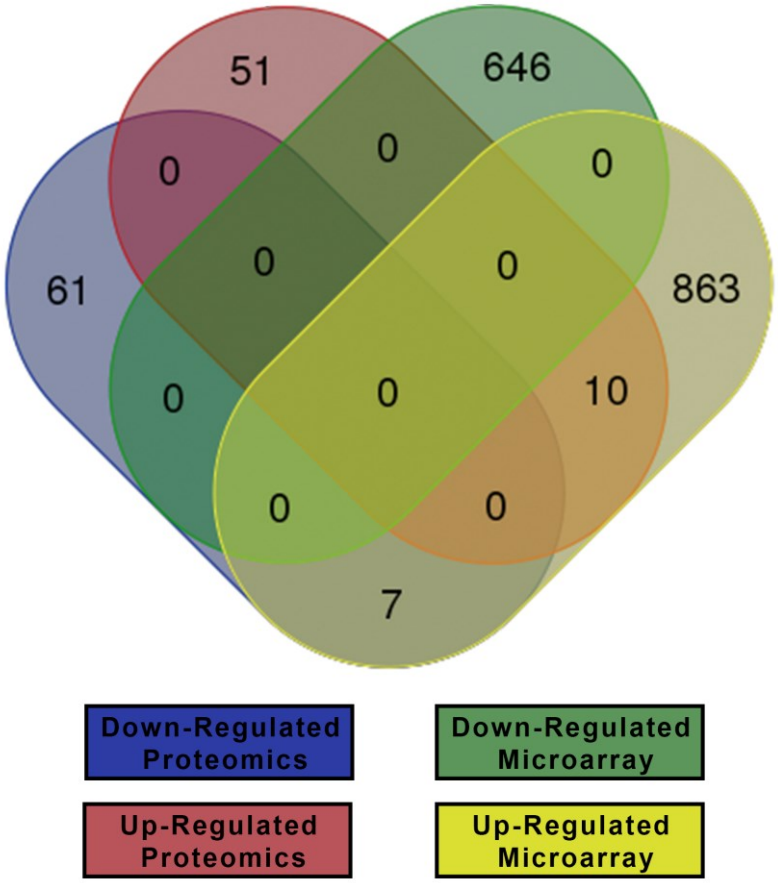

Groups	Count	Gene Symbols
Up regulated in Microarray AND Proteomics	10	CD44, CDH13, PTRF, ENO1, FN1, TFRC, ENG, NID2, DNAJB4, HADHA
Up regulated in Microarray AND Down-regulated in Proteomics	7	MATR3, DPYSL3, LMNB1, PTBP1, THOC4, DHX9, SHMT2

Figure 3.4. Overlap of differentially regulated genes between microarray and shotgun proteomic studies. Lists of differentially expressed candidates from the proteomic and microarray datasets were converted to official gene symbols using the DAVID gene ID conversion tool for consistency in nomenclature when comparing groups. The online Venn Diagram tool from bioinformatics GENT was used to assess for overlap between microarray and proteomic candidates and to produce figures.

Functional enrichment analysis of protein candidates was performed using a similar method to our microarray experiments. Candidates were separated into either upregulated or downregulated groups, followed by functional enrichment using the online STRING functional enrichment tool. In the upregulated group, KEGG pathway enrichment showed that 30% of candidates are involved in metabolic pathways. 9.4% of upregulated candidates are involved in the KEGG glycolysis/gluconeogenesis pathway and 17% are related to glucose metabolism further implicating glycolytic activation in PBC BEC. 5.6% of upregulated proteins are also shown to be involved in the KEGG fatty acid degradation pathway (Table 3.1, Figure 3.5 and 3.6). Together these data, suggest that catabolic processes involved in energy metabolism may be altered in PBC BEC *in vitro.* This is illustrated in in Figure 3.6, where it can be observed that catabolic enzymes involved in the breakdown of glucose, glycogen and fatty acids are significantly upregulated while PCK2, an enzyme involved in the anabolic process of gluconeogenesis, is significantly downregulated. PDHB, a subunit of the E1 component of the pyruvate dehydrogenase complex (PDC), is also significantly downregulated. As previously mentioned, The PDC acts as the "mitochondrial gatekeeper" connecting glycolysis to the citric acid cycle by converting pyruvate into acetyl-CoA.

Interestingly, 32% of upregulated proteins were also found to relate to the mitochondrial compartment (Table 3.1). Several of these mitochondrial proteins are involved in the above-mentioned metabolic pathways or are related to antioxidant activity (Figure 3.5). Other differentially expressed candidates classified as mitochondrial proteins include SLC25A1, a solute carrier protein that exports mitochondrial citrate in exchange for cytosolic malate; DNM1L, a GTPase that functions in mitochondrial and peroxisomal division; and TFRC, the transferrin receptor which is necessary for cellular iron uptake and is a regulator of mitochondrial biogenesis. A total of 43% of the upregulated proteins were related to either energy metabolism or mitochondrial processes (Table 3.1, Figure 3.5a and b). Together these data further support that PBC BEC may be in a hyper-metabolic state with elevated levels of glycolysis, fatty acid-metabolism and altered redox.

STRING analysis of downregulated protein candidates also showed significant interaction enrichment. KEGG pathway enrichment showed that 17% of these proteins are a part of the spliceosomal pathway (Table 3.1). Altered expression of proteins involved in mRNA processing is further illustrated as 50% of downregulated proteins are found to have a function in RNA-binding and 37% are involved in the biological process of RNA splicing (Table 3.1).

ENRICHMENT OF UP-REGULATED PROTEINS			ENRICHMENT OF DOWN-REGULATED PROTEINS		
Cellular Component			**Cellular Component**		
Description	Number	FDR Value	Description	Number	FDR Value
Extracellular Exosome	40	1.35E-22	Ribonucleoprotein complex	16	4.49E-11
Extracellular Region Part	40	3.16E-18	Nucleoplasm	26	1.55E-10
Membrane-Bounded Vesicle	39	3.41E-18	Spliceosomal complex	9	7.93E-09
Extracellular Region	40	1.15E-15	Membrane-enclosed lumen	27	6.18E-08
Cytosol	29	2.17E-09	Catalytic step 2 spliceosome	7	6.43E-08
Focal Adhesion	10	3.59E-06	Intracellular organelle lumen	26	1.59E-07
Mitochondrion	17	1.63E-05	Nuclear part	24	7.60E-07
Molecular Function			**Molecular Function**		
Description	Number	FDR Value	Description	Number	FDR Value
Protein binding	30	5.60E-05	Poly (A) RNA binding	23	5.02E-15
Binding	43	0.000451	RNA binding	23	1.03E-12
Catalytic activity	29	0.00147	Small molecule binding	27	3.35E-12
Long-chain-3-hydroxyacyl-CoA dehydrogenase activity	2	0.00677	Nucleotide binding	25	2.37E-11
Calcium-dependent cysteine-type endopeptidase activity	3	0.0166	mRNA binding	7	3.51E-06
Antioxidant activity	4	0.0166	Nucleic acid binding	23	2.15E-05
KEGG Pathways			**KEGG Pathways**		
Description	Number	FDR Value	Description	Number	FDR Value
Metabolic pathways	16	6.07E-06	Spliceosome	6	5.53E-05
Glycolysis / Gluconeogenesis	5	6.77E-05			
Carbon metabolism	5	0.000499			
HIF-1 signaling pathway	5	0.000499			
Shigellosis	4	0.000822			
Biosynthesis of amino acids	4	0.00155			
Bacterial invasion of epithelial cells	4	0.00157			
Fatty acid degradation	3	0.00676			
Biological Process			**Biological Process**		
Description	Number	FDR Value	Description	Number	FDR Value
ADP metabolic process	8	5.10E-09	RNA splicing	16	1.55E-14
Nucleoside diphosphate phosphorylation	8	6.46E-09	RNA splicing, via transesterification reactions	14	2.82E-14
single-organism carbohydrate catabolic process	9	7.11E-09	mRNA processing	16	8.20E-14
Glycolytic process	7	1.56E-08	mRNA splicing, via spliceosome	13	4.62E-13
Glucose metabolic process	9	9.39E-08	mRNA metabolic process	15	1.94E-10
Small molecule metabolic process	22	7.51E-07	mRNA stabilization	6	3.63E-08

= Terms related to energy metabolism

Table 3.1. Enriched terms for upregulated and downregulated proteins in Primary Biliary Cholangitis Biliary Epithelial cells as assessed by STRING functional enrichment.

A

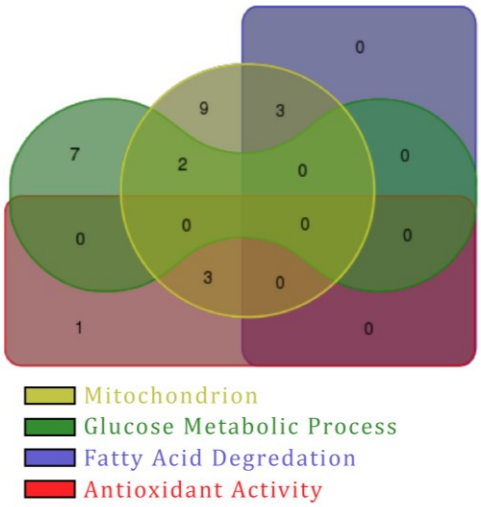

B

Term(s)	Number Of Proteins	Gene Names
Glucose Metabolic Process AND Mitochondria	2	SLC25A1, PKM
Fatty Acid Degredation AND Mitochondria	3	HADHB, HADHA, ACADVL
Antioxidant Activity AND Mitochondria	3	SOD1, PRDX4, TXNRD1
Glucose Metabolic Process	7	PYGB, ALDOA, ENO1, PGM1, ENO2, GAPDH, GBE1
Mitochondria	9	CAV1, TFRC, GARS, P4HA1, LDHA, CAPN1, DNM1L, AK4, PTRF
Antioxidant Activity	1	PRDX6
Total	25	

C

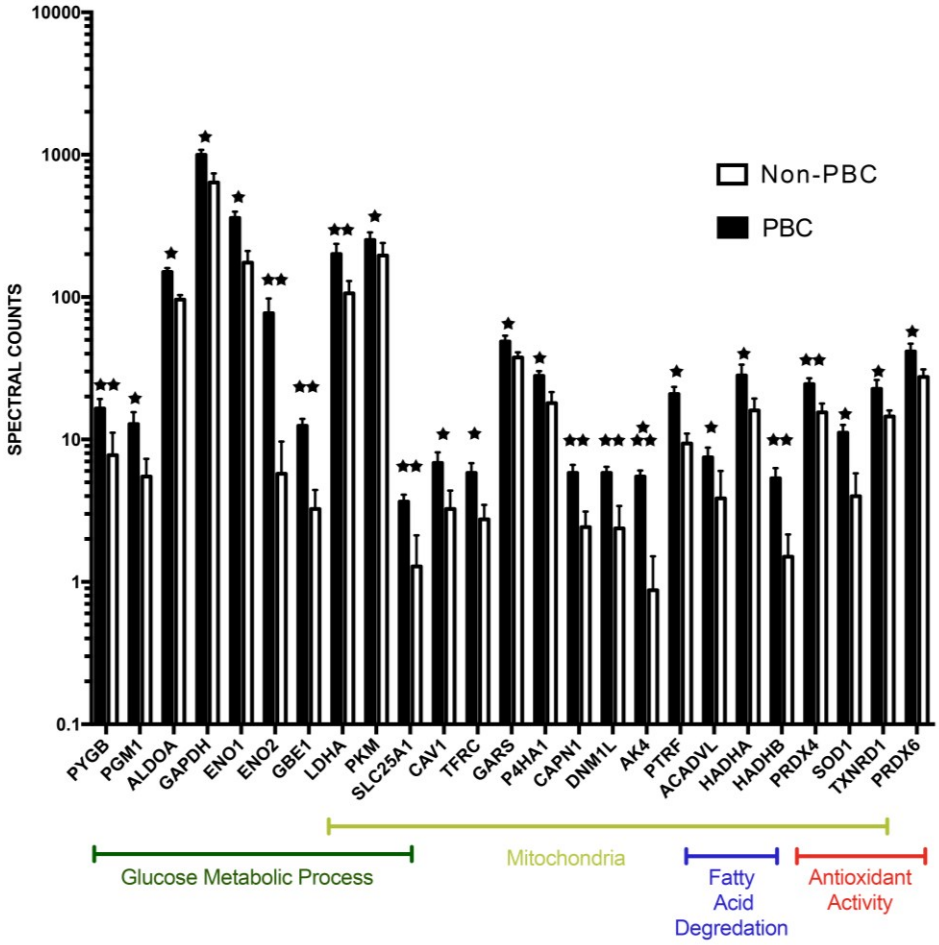

Figure 3.5. Upregulated proteins in Primary Biliary Cholangitis (PBC) biliary epithelial cells (BEC) are enriched in pathways related to cellular energy metabolism. A. Venn Diagram comparing how the upregulated protein candidates from shotgun-proteomics are distributed within terms related to cellular energy metabolism. B. Table listing gene symbols and how each protein candidate was grouped in the Venn Diagram. C. Bar chart showing normalized peptide spectral counts for each candidate protein examined in the venn diagram. Proteins found to be differentially expressed between PBC and liver disease control BEC show enrichment in terms related to several aspects of cellular metabolism. Several terms are suggestive of increased expression of enzymes related to the catabolic pathways of glycolysis and fatty acid degradation. There also appears to be increased expression of proteins related to mitochondrial compartment and proteins with antioxidant activity. For shotgun-proteomic studies, cultured PBC BEC (n=3) extracted from explanted livers were compared to end-stage liver disease BEC (n=4) using liquid chromatography tandem mass-spectrometry (LC-MS/MS) in collaboration with the Fahlman group. Protein was extracted using 2D lysis buffer, followed by band separation using polyacrylamide gel electrophoresis. Gel bands were then excised and given to the Fahlman group for liquid chromatography tandem mass-spectrometry (LC-MS/MS) who performed primary analysis. For quantification, protein spectral counts were normalized and statistically analyzed using DanteR software. Differentially expressed proteins were separated into upregulated or downregulated groups before being used for functional enrichment analysis with the online STRING database enrichment tool. STRING analysis was performed using default settings with Uniprot accession numbers as protein IDs. Term enrichments are separated into the following groups: cellular component, molecular function, KEGG pathways and biological process. Only a few of the top terms for each group were included in this table for the sake of simplicity. Terms that we deemed related to cellular metabolism are highlighted in yellow. [Sample collection performed by Dr. Bo Meng, LC-MS/MS and primary analysis performed by the University of Alberta Proteomics Core (Dr. R. Fahlman), statistical analysis and normalization performed by Dr. B Meng and Dr. W. Wang] Venn diagram was produced using the online Venn Diagram tool from bioinformatics Gent. Bar graphs were produced using PRISM 7 software and shown are means +/- SE. Normalized spectral counts and p-values were determined using DanteR software. One star represents $p<0.05$, two stars represent $p<0.01$ and three stars represent $p<0.001$.

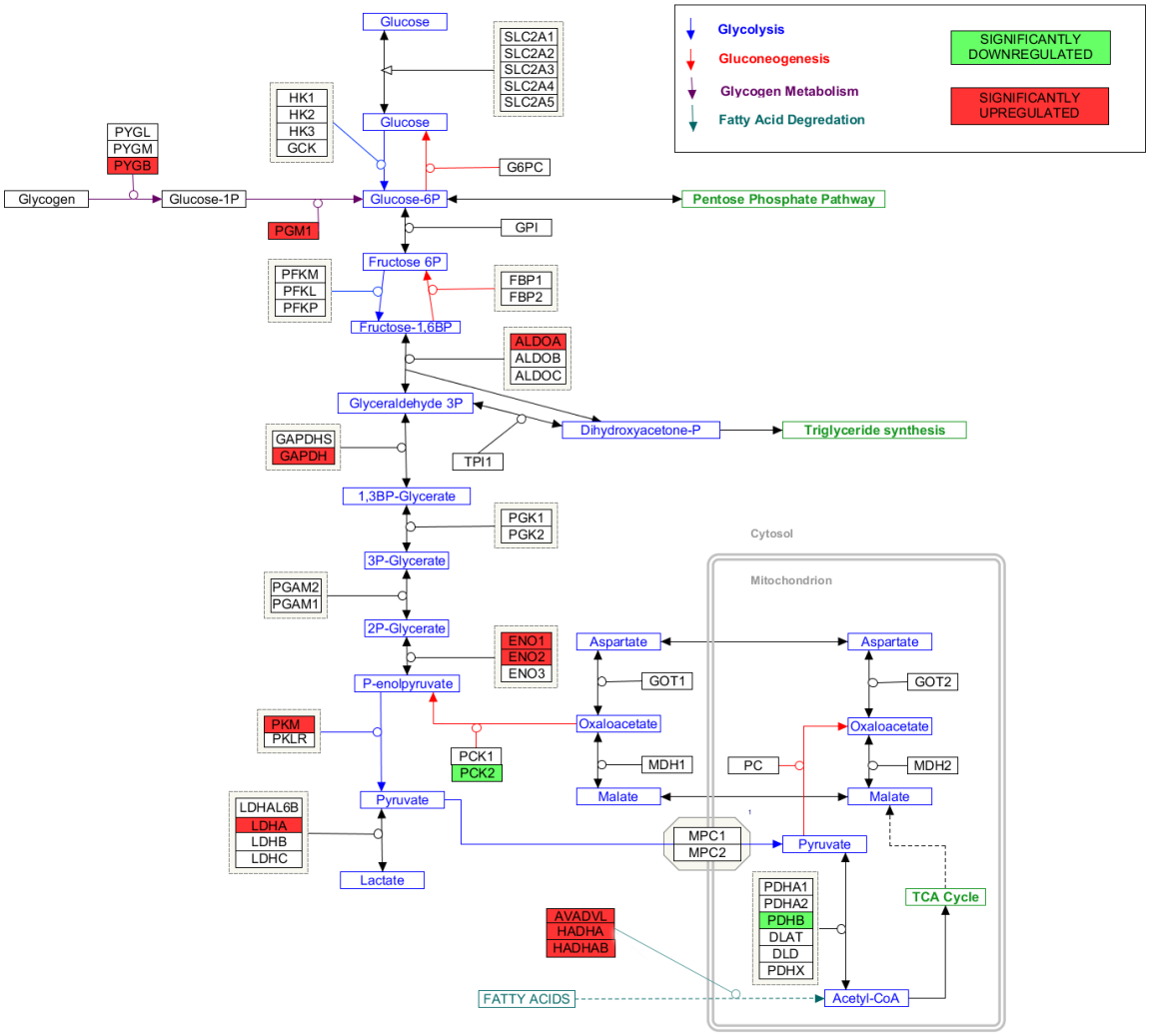

Figure 3.6. Pathway map highlighting differentially expressed proteins related to cellular energy metabolism in Primary Biliary Cholangitis (PBC) biliary epithelial cells (BEC). Pathway map modified from wikipathways map WP534 (Glycolysis/Gluconeogenesis (Homo Sapiens)) using Pathovisio software. Significantly upregulated proteins are highlighted in red and significantly downregulated proteins are highlighted in green. Different pathways are represent by the coloured arrows: Blue=Glycolysis, Red=Gluconeogenesis, Purple=Glycogen metabolism, Teal=Fatty acid degradation. The dotted line for fatty acid degradation is meant to represent that several steps and proteins involved in this pathway that have been left out for the sake of simplicity.

Section 2: Elevated levels of oxidative phosphorylation in PBC BEC *in vitro*

3.3 Previous work studying oxidative phosphorylation in PBC BEC

Given the evidence supportive of PBC BEC taking on a hyper-metabolic phenotype with elevated levels of glycolysis, Dr. Isabella Wong carried on to assess how oxidative phosphorylation (OXPHOS) is altered in PBC BEC *in vitro.* Elevated levels of glycolysis observed are typically accompanied by a subsequent decrease in mitochondrial ATP production via OXPHOS[91]. Mechanistically, this can be explained by reduced levels of pyruvate available for mitochondrial metabolism due to the increased glycolytic breakdown of pyruvate into lactate.

The group began by characterizing how oxygen consumption rate (OCR) is functionally altered in PBC BEC *in vitro* as a method to assess for electron transport chain (ETC) activity. The ETC is an essential step in oxidative phosphorylation since it establishes the proton gradient necessary for ATP Synthase to function.
The ETC accepts electrons from donors (NADH, $FADH_2$), which are subsequently transferred through various complexes before reaching oxygen, the final electron acceptor. Since oxygen is consumed in this reaction, OCR can be used as indirect measure of electron transport chain activity.

To assess OCR Dr. Wong used a 96-well BD oxygen biosensor system that measures relative oxygen levels in the supernatant of living cells[92]. For these studies, cells are incubated in media containing a fluorophore that is quenched by oxygen. As the cells consume oxygen the intensity of fluorescence increases and is used as a surrogate marker for relative oxygen consumption (Figure 3.7). These studies unexpectedly showed a significantly higher rate of oxygen consumption in PBC BEC compared to end-stage liver disease controls *in vitro* (Figure 3.7). Surprisingly, these results suggest that PBC BEC show elevated levels of both glycolysis and oxidative phosphorylation *in vitro.* These results are counter-intuitive given the competitive nature between aerobic

glycolysis and OXPHOS, where an increase in glycolysis normally leads to a subsequent decrease in oxidative phosphorylation.

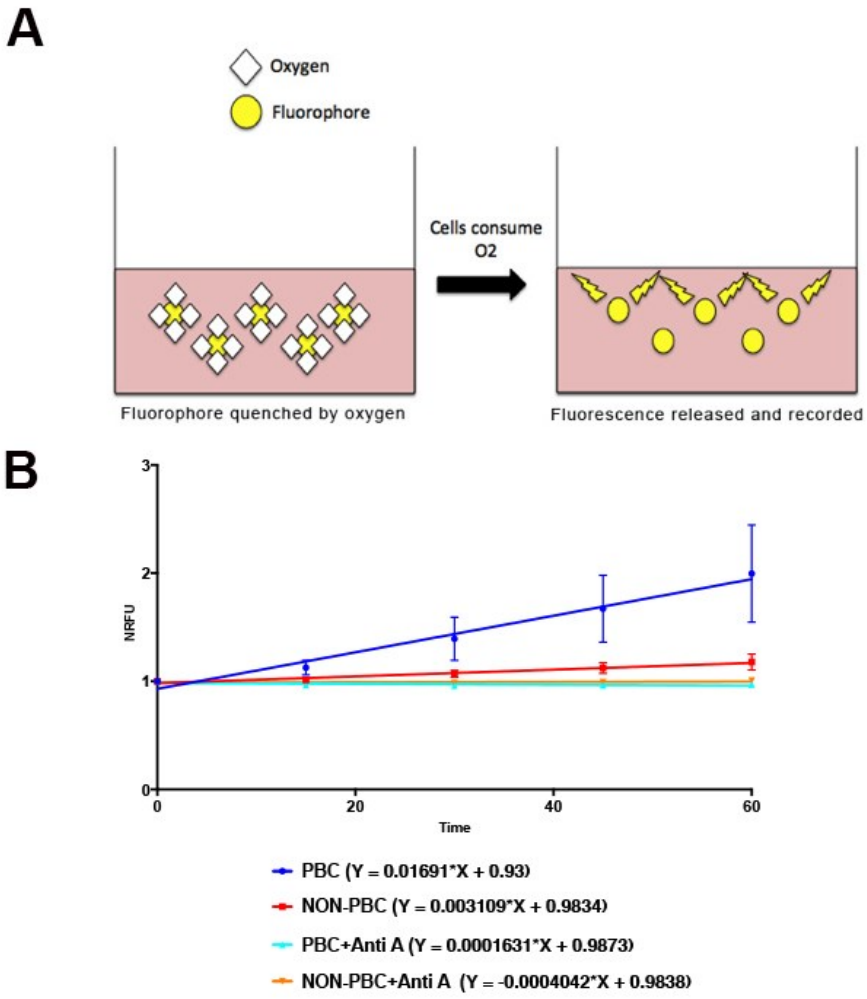

	0 minutes	15 minutes	30 minutes	45 minutes	60 minutes
2-Way ANOVA P-Value (PBC v Non-PBC)	>0.9999	0.9302	0.3184	0.0229	0.0002

	Slope +/- SE	95% CI	F	P-Value
PBC	0.01691 ± 0.005168	0.00622 to 0.0276	6.498	0.0114
Non-PBC	0.003109 ± 0.000843	0.001365 to 0.004853		

Figure 3.7. Cultured biliary epithelial cells (BEC) from patients with Primary Biliary Cholangitis (PBC) show elevated levels of oxygen consumption. A. Simplified diagram illustrating how the Oxygen Biosensor system works. Cells are incubated with media containing a fluorophore (yellow circle) that is quenched by oxygen (white diamond). As cells consume oxygen, fluorophore quenching is reduced and the intensity of fluorescent signal increases which in turn can be used as a surrogate marker for oxygen consumption. B. Assessment of oxygen consumption by an Oxygen Biosensor system shows an increased oxygen consumption rate in PBC BEC compared to end-stage disease control BEC *in vitro*. PBC (n=5) and end-stage liver disease control BEC (n=5) were seeded at densities of $4x10^5$ cells per well in a 96-well BD Oxygen Biosensor System plate. Antimycin A, an electron transport chain inhibitor, was added at a concentration of 0.1 μM to each cell line in a paired study as a negative control Fluorescence was read in a Biotek Synergy HT plate reader where ex=485nm and em=590nm. Aerobic respiration signals were detected every 15 min for one hour at 37 °C and oxygen consumption was calculated as normalized relative fluorescence units (NRFU). 2-way ANOVA with a Sidak's multiple comparison test was performed with Prism 7 software comparing NRFU values between PBC and Non-PBC BEC at each time point showed that there was a significant increase in NRFU at 60 minutes (p=0.0012). Linear regression analysis was also performed using PRISM 7 to produce a line of best fit modelling the oxygen consumption rate. Line equation is included in brackets in the legend. Comparison of slopes between PBC and Non-PBC BEC showed that they are significantly different (p=0.011). Shown are means +/- SE. The table below the graph shows the results of the linear regression analysis. [Studies performed by Isabella Wong]

3.4 Seahorse validation of the hyper-metabolic phenotype

Given the surprising nature of our findings, that both aerobic glycolysis and OXPHOS are elevated in PBC BEC *in vitro,* we went on to validate these findings with the Seahorse XF24 platform. The Seahorse assay simultaneously measures both electron transport chain and glycolytic activity in live cells over several time points. The Seahorse assay indirectly measures glycolytic activity by quantifying the extracellular acidification rate (ECAR). As lactate is secreted it is co-exported with a proton into the extracellular fluid which reduces the media's pH and is measured as ECAR by the Seahorse XF. Similar to the oxygen biosensor system previously mentioned, the Seahorse XF quantifies oxygen consumption rate (OCR) as an indirect measure of electron transport chain activity.

For these studies measurements of OCR and ECAR were performed every 8 minutes over a course of 25 minutes in cells grown in Seahorse XF base media supplemented with glucose, glutamine and pyruvate. Upon initial analysis no difference was observed between PBC and non-PBC BEC (Appendix figure 5.2); however using a Grubbs test (α=0.05) one significant outlier was found. When the outlier was removed PBC BEC showed significantly higher levels of extracellular acidification (42% increase, p=0.0364) and a strong trend for an increase in oxygen consumption (41% increase, p=0.0818) relative to liver disease control BEC *in vitro* (Figure 3.8). These data supports our previous finding that aerobic glycolysis is elevated in PBC BEC. Although the OCR is not significantly increased with this sample size, a strong trend is observed supporting that oxygen consumption is elevated in PBC BEC.

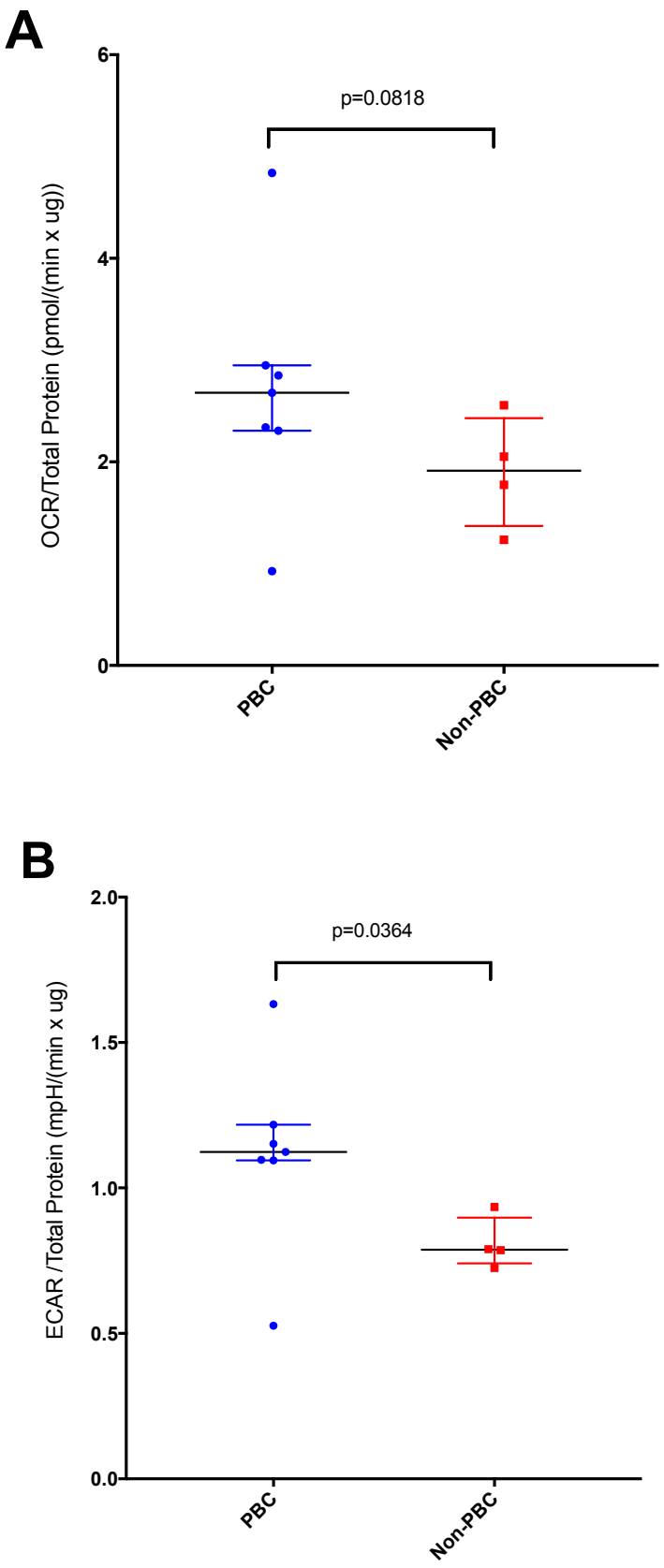
A
p=0.0818
OCR/Total Protein (pmol/(min x ug))
6
4
2
0
PBC
Non-PBC
B
p=0.0364
ECAR /Total Protein (mpH/(min x ug)
2.0
1.5
1.0
0.5
0.0
PBC
Non-PBC

Figure 3.8. Significantly increased levels of extracellular acidification rate (ECAR) and trend for elevated oxygen consumption rate (OCR) in Primary Biliary Cholangitis (PBC) patients' biliary epithelial cells (BEC). A trend for elevated oxygen consumption rate (OCR; A) is observed between cultured PBC (n=7) and end-stage liver control BEC (n=4), while no difference is observed in extracellular acidification rate (ECAR; B), as measured by the Seahorse XF24 platform. $1.0/1.5x10^4$ cells were seeded to each well of Seahorse XF24 cell culture plates 16-24 hours prior to running the assay. Each sample was seeded as 5 replicates with 4 blank wells for background normalization. OCR and ECAR were assessed every 8 minutes over 3 time points. Following the run, protein concentration was assessed in each well using a commercial BCA assay kit following the manufacturers instructions. OCR and ECAR values were normalized to total protein content in Excel. Samples run on multiple plates were also averaged in Excel then imported into Prism 7. Using a Grubbs Test (α=0.05), one outlier was found and removed from further analysis. Statistical analysis was performed the same for both ECAR and OCR using a 1-tailed Mann Whitney Test comparing the median values for PBC and non-PBC with Prism 7 Software. Values were graphed using Prism 7 software. Shown are medians +/- IQR.

3.5 Elevated mtDNA copy number in PBC BEC

The mitochondria are an intriguing organelle given that they have their own circular double-stranded DNA genome that undergoes replication, transcription, and translation separately from the nuclear genome. Mitochondrial DNA (mtDNA) codes 11 mRNAs that are translated into 13 proteins that code for subunits of the electron transport chain and are essential to the function of OXPHOS. Therefore, cells require continuous replication of mtDNA for the generation of ATP through OXPHOS and mtDNA copy number can be modulated depending on energy demands[93]. Cells with high-energy requirements, such as neurons, maintain high numbers of mtDNA copies while low-energy cells, such as endothelial cells, have fewer copies[94].

Given that PBC BEC show elevated levels of OXPHOS *in vitro* we went on to assess whether this relates to changes in mtDNA copy number. To assess for mtDNA copy number, a TaqMan assay specific to the non-coding D-loop region of mtDNA was used. A SybrGreen assay specific for beta-2-microglobulin (B2M) was used for housekeeping normalization since it is a single-copy gene with low-inter patient variation[85]. Prior to running patient samples, quality control was performed with both our D-loop TaqMan and B2M SybrGreen assays as suggested by the MIQE guidelines[95]. For these tests serial dilutions of one BEC DNA sample were run with both assays. Both assays showed acceptable values for PCR efficiency (between 96 and 106%) and correlation values (R^2>.99) (Appendix Figure 5.3).

Using these qPCR assays we observed a strong trend for increased mtDNA copy number in PBC BEC; however, there was a significant outlier present in the dataset (Appendix figure 5.4). Following removal of the outlier we observed that PBC BEC have significantly increased levels (39% increase, p=0.0271) of mtDNA copy number compared to non-PBC liver disease controls *in vitro* (Figure 3.9). This suggests that elevated mitochondrial respiration observed in PBC BEC may be related, in part, to increased levels of mtDNA.

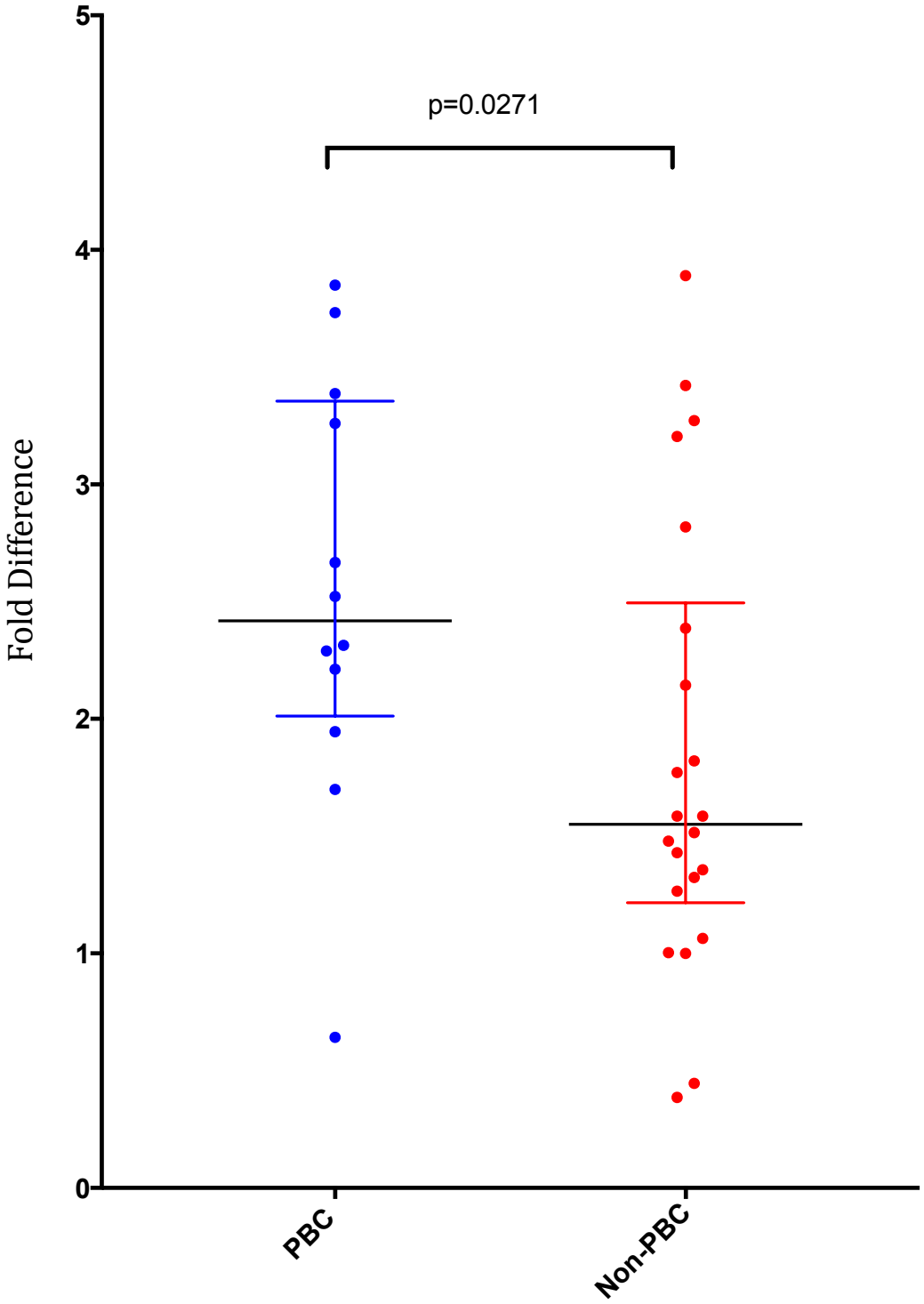
p=0.0271
Fold Difference
5
4
3
2
1
0
PBC
Non-PBC

Figure 3.9. Significantly higher levels of mitochondrial DNA (mtDNA) in Primary Biliary Cholangitis (PBC) patients' biliary epithelial cells (BEC). Cultured PBC BEC (n=12) extracted from explanted livers show significantly higher levels of mtDNA compared to liver disease controls (n=22) as assessed by quantitative PCR (qPCR). Relative mtDNA copy number was assessed with qPCR using a commercial TaqMan assay for the mitochondrial D-loop region (D-loop) with 25 ng of DNA used per reaction. Beta-2-microglobulin (B2M) relative copy number was assessed in the same samples as a single-copy, low variation housekeeping gene for normalization. B2M relative copy number was assessed using a SybrGreen assay with 10 ng of DNA per reaction. Samples were run as duplicates for each assay and fluorescence spectra were monitored by the ABI7300 Real-Time PCR system. D-loop C_t values were normalized to B2M C_t in Excel using the $\Delta\Delta C_t$ method. Values were then exported into Prism 7 software. Using a Grubbs test (α=0.0001) one outlier was detected and removed from further analysis. Normalized values were then compared using a 2-tailed Man Whitney Test. Statistical analysis and graphing was performed with Prism 7 software. Shown are medians +/- IQR.

Chapter 4: Discussion

4.1 Introduction

Given the uncharacterized nature of the mitochondrial phenotype in primary biliary cholangitis (PBC), we sought to further characterize how metabolic and mitochondrial function are altered in primary biliary cholangitis (PBC) patients' biliary epithelial cells (BEC). The present study provides the most comprehensive characterization of metabolic function in PBC patients' BEC *in vitro.* Given that BEC represent a minute population of cells in total liver tissue, an *in vitro* model of primary BEC extracted from explanted liver tissue was used. This allowed for the use of assays to characterize metabolic function in BEC specifically.

Herein, we provide evidence suggesting that PBC BEC take on a hyper-metabolic phenotype, with evidence of increased levels of oxidative phosphorylation (OXPHOS) and aerobic glycolysis relative to end-stage liver disease controls *in vitro.* The key findings of this study are:

a) PBC BEC show elevated levels of Akt gene expression
b) Shotgun proteomics shows increased expression of proteins related to the mitochondrial compartment, anti-oxidant activity, glycolysis and fatty acid oxidation in PBC BEC.

c) PBC BEC show elevated levels of aerobic glycolysis as suggested by three separate methods.
d) PBC BEC show elevated levels of oxygen consumption as suggested by two separate methods.
e) PBC BEC show elevated levels of mtDNA copy number.

In the following sections I will describe the significance of these findings in relation to previous studies. I will also examine caveats of our studies, as well as provide potential explanations for unexpected results. Furthermore, I will discuss the implications of this study for future research.

4.2 Is Akt involved with the observed increase in aerobic glycolysis?

Characterization of mitochondrial and metabolic function began with a microarray to assess for differences in the transcriptome of PBC and liver disease control BEC. This study was meant to act as a method of hypothesis-discovery to elucidate pathways that may be altered and could be focused on for future experiments. Functional enrichment of the significantly different gene candidates from our microarray dataset showed that pathways related to cancer and the phosphoinositide 3-kinase (PI3K) / serine/threonine kinase (Akt) axis may be dysregulated in PBC BEC. Furthermore, genes throughout the glycolytic pathway showed trends for elevated expression in PBC BEC. Given that Akt is a well-established regulator of cellular metabolism, these findings suggested that PBC BEC may have elevated glycolytic activity and Akt function; however, it was later found that BEC were not cultured in a consistent manner and these findings required further validation.

Characterization of protein expression using shotgun-proteomics also showed increased levels of glycolytic enzymes, supporting the initial microarray finding that glycolytic gene expression is elevated. Furthermore, functional assessment of aerobic glycolysis through two separate methods was suggestive of increased glycolytic function in PBC BEC *in vitro*. Initial studies assessed for lactate levels in BEC culture supernatant

with a commercial kit and were followed by a more robust metabolomics method that characterized the carbon flux of glucose. These studies provide strong support that aerobic glycolysis is upregulated in PBC BEC *in vitro*.

Quantitative-PCR (qPCR) validation of differentially regulated candidate genes from the microarray studies showed elevated mRNA expression of both AKT1 and AKT3 in PBC BEC supporting that Akt may play a role in stimulating glycolysis. A caveat with these findings is the lack of Akt protein expression in PBC BEC *in vitro* as assessed by shotgun-proteomics. However, this may be attributed to the fact that MS-based protein identification is biased toward detecting abundant proteins, and Akt simply falls below the dynamic range of the assay[96]. *In vivo* characterization of phosphorylated-Akt (active form, p-Akt) with immunohistochemistry (IHC) has shown that 30% of early-stage interlobular PBC BEC express p-Akt compared to less than 1% in normal liver tissue. The percentage of p-Akt positive BEC was also found to increase to 70% in end-stage PBC patients[97]. Given that our *in vitro* model relies on BEC extracted from end-stage patients' livers, these findings support that Akt may be active in PBC BEC *in vitro;* however, Akt activation in PBC still requires further validation with our *in vitro* model.

4.3 Unexpected elevation of mitochondrial respiration in PBC BEC

The evidence that aerobic glycolytic activity is elevated in PBC BEC *in vitro* led us to characterize how mitochondrial oxidative phosphorylation (OXPHOS) is affected. In a typical cellular setting glycolysis mediates the breakdown of glucose into pyruvate, which can then be used for the production of lactate or shuttled into the mitochondria where it will fuel the tricarboxylic acid cycle (TCA) and OXPHOS (Figure 4.1). Given the competitive nature between glycolysis and OXPHOS, we expected to see reduced levels of mitochondrial respiration in PBC BEC. Surprisingly, increased levels of oxygen consumption (an indirect measure of electron transport chain (ETC) activity) were observed in PBC BEC as assessed by an oxygen biosensor. Validation of the simultaneous elevation in OXPHOS and aerobic glycolysis with the Seahorse XF24 assay showed significant increases in extracellular acidification rate (a surrogate marker for

glycolysis) and a strong trend for elevated oxygen consumption. These findings suggest that OXPHOS activity is also increased in PBC BEC. Elevated levels of oxygen consumption were further supported by the observation that PBC BEC have 39% higher levels of mtDNA relative to end-stage liver disease controls, which is indicative of mitochondrial biogenesis. Since mtDNA codes for the essential ETC subunits, increased oxygen consumption could be explained, in part, by an increased capacity to perform OXPHOS[98]. In combination, these results support that PBC BEC are taking on a hyper-metabolic phenotype where both OXPHOS and aerobic glycolysis are simultaneously elevated in PBC BEC *in vitro.*

Although this phenotype deviates from the usual principles of energy metabolism, it is not entirely novel. Recently it has been shown that TC mice (a systemic lupus erythematosus model (SLE)) and SLE patients' CD4+ T-cells show simultaneous activation of aerobic glycolysis and mitochondrial metabolism relative to controls. The elevated levels in TC mice were associated with increased mammalian target of rapamycin complex 1 (mTORC1) activity. Treatment with rapamycin, an mTOR inhibitor, reduced the function of both pathways[99]. MTORC1 is a critical regulator of cellular energy metabolism capable of stimulating both mitochondrial biogenesis (by stimulating the transcription factor PGC-1α) and glycolysis (by stimulating transcription factors c-Myc or HIF1α, Figure 4.2)[100,101].

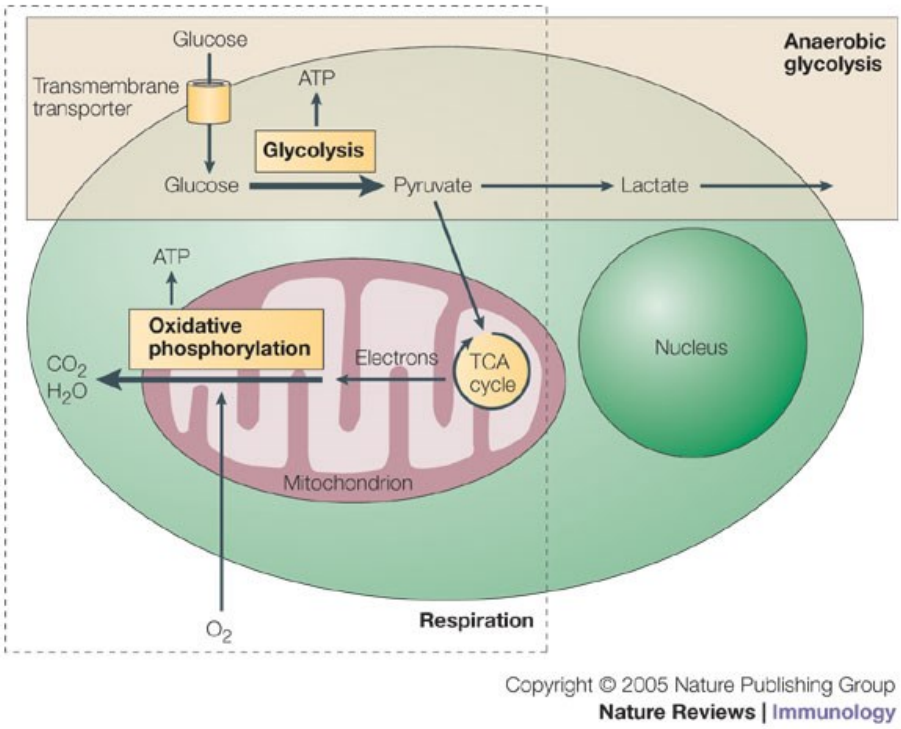

Figure 4.1. Simplified map of glycolysis and oxidative phosphorylation. Glucose is converted to pyruvate during glycolysis, which produces ATP. In conditions of low oxygen, pyruvate is converted to lactate and transported out of the cell (anaerobic glycolysis). When oxygen levels are high, pyruvate is transported into the mitochondria and is used as fuel for the tricarboxylic acid cycle (TCA). The TCA produces reducing agents, which will donate electrons to the electron transport chain. The electron transport chain then facilitates the movement of protons into the intermembrane space, consuming oxygen in the process. The electrochemical gradient produced is then used to fuel ATP production through oxidative phosphorylation. [Adapted from Sitkovsky and Lukashev, 2005][102]

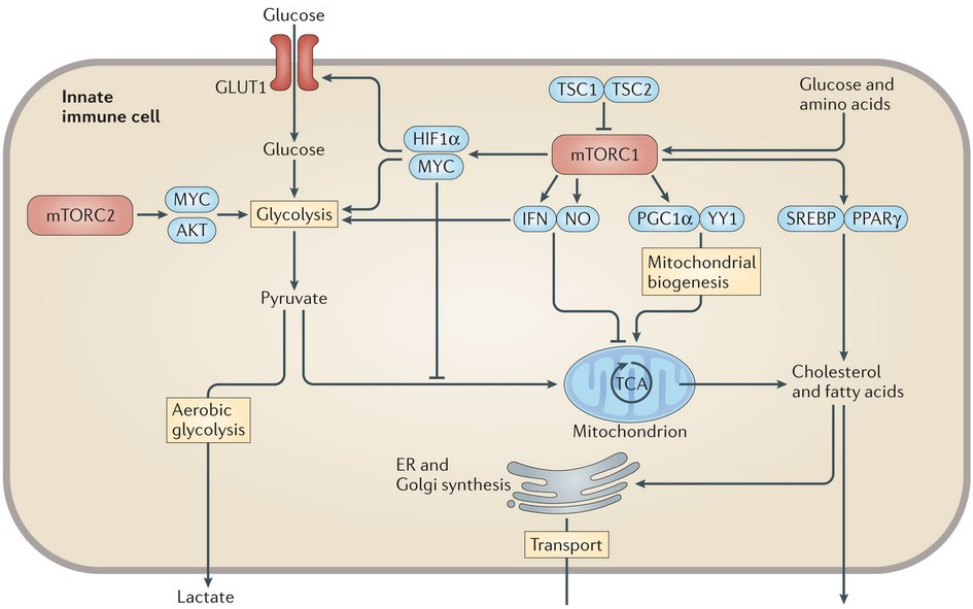

Figure 4.2. MTOR mediated regulation of cellular metabolism. The mammalian target of rapamycin complex 1 (mTORC1) induces the activation of the transcription factors, hypoxia inducible factor 1α (HIF1α) and Myc. Both of these factors stimulate glycolysis by increasing expression of glycolytic genes and the surface translocation of glucose transporter 1 (GLUT1). MTORC1 also induces mitochondrial biogenesis through the transcription factors PPARγ co-activator 1α (PGC1α), and yin and yang 1 (YY1). Furthermore, mTORC1 also stimulates cholesterol and fatty acid synthesis through interactions with sterol regulatory element-bindings proteins (SREBPs) and peroxisome proliferator-activated receptor-γ (PPARγ). [Adapted from Weichart *et al.* 2015][101]

Another enzyme that is capable of simultaneously increasing oxygen consumption and aerobic glycolysis is the oncogene C-Myc. C-Myc is a transcription factor that plays a key role in regulating the expression of genes related to cell cycle progression and metabolism (Figure 4.3)[103]. The overexpression of Myc has been shown to increase lactate production by stimulating increased transcription of glycolytic genes (LDHA, ENO1, PFKM)[104,105]. Myc also regulates genes involved in mitochondrial replication and its expression has been shown to induce mitochondrial biogenesis[106,107]. Furthermore, *in vitro* studies have shown that Myc-mediated progression through the cell cycle requires a simultaneous increase in OXPHOS and aerobic glycolysis[108].

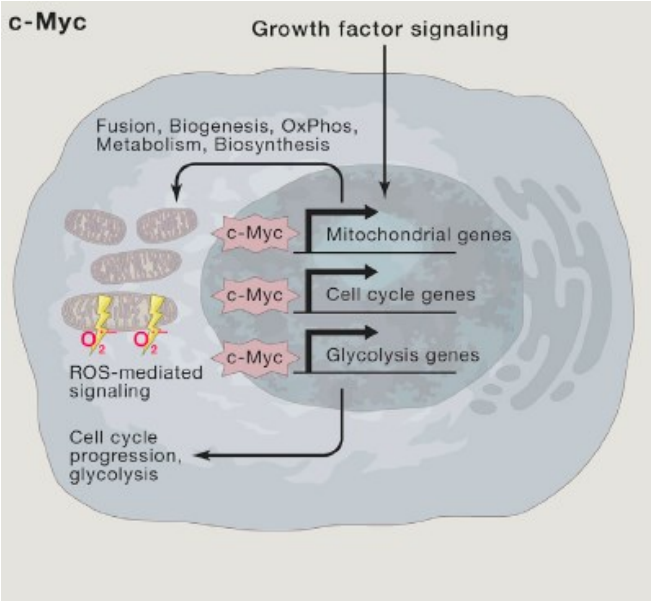

Figure 4.3. Myc mediated regulation of cellular metabolism. As a transcription factor, c-Myc can induce mitochondrial biogenesis, metabolism, cell-cycle progression, and glycolysis. C-Myc induces the transcription of genes related to mitochondrial biogenesis, fusion and metabolism. This may lead to the production of reactive oxygen species (ROS) and oxidative signalling. [Adapted from Vyas *et al.,* 2016][109]

It has been proposed that Akt is also capable of elevating both OXPHOS and glycolysis through the coupling of HKII to the mitochondrial VDAC (Figure 4.4)[88]. HKII functions in the initial step of glycolysis, phosphorylating glucose to glucose-6-phosphate. The physical association of HKII with the mitochondria is thought to increase the efficiency of this process due to the close proximity of ATP produced through OXPHOS. This further increases the efficiency of oxidative phosphorylation given that HKII produces ADP that can immediately be returned to the mitochondria for ATP production. Knockout of Akt/2 in mouse embryonic fibroblasts has been shown to reduce cellular oxygen consumption, and is elevated in Rat1a cells expressing activated Akt[110]. However, the expression of activated Akt in mouse pre-B cells has been shown to induce

aerobic glycolysis without any effects on oxygen consumption[111]. Thus, the effect of Akt on oxygen consumption may vary depending on the cellular context. Akt has also been shown to induce both mTORC1 and Myc activity[112,113]. Induction of mTORC1 is well-documented, and functions to stimulate protein translation and cell growth[112]. The PI3K/Akt/mTORC pathway has been shown to facilitate Myc activity by inhibiting transcriptional repressors[113].

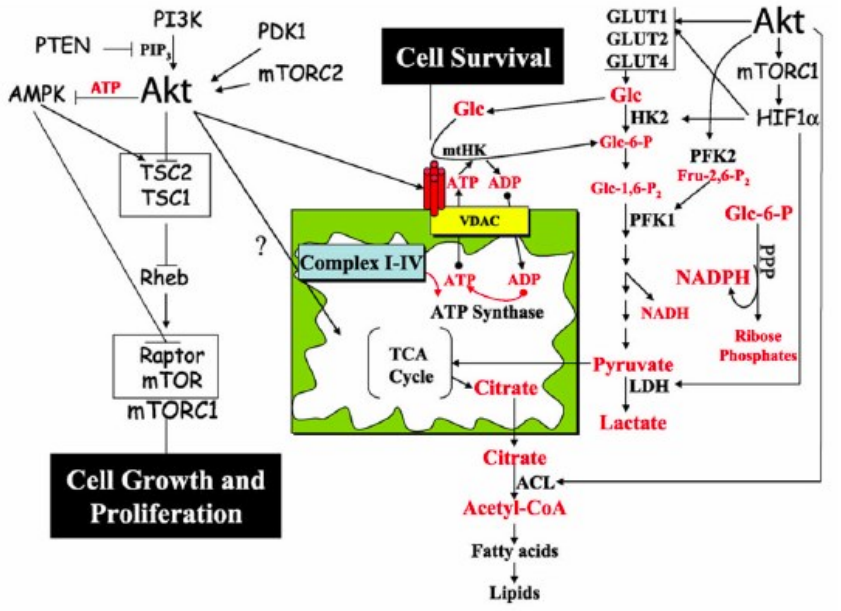

Figure 4.4 Akt mediated regulation of cellular metabolism. Akt regulates cellular energy metabolism, cell survival and proliferation. Akt stimulates both aerobic glycolysis and oxidative phosphorylation by promoting an enhanced association between hexokinase (HK), VDAC and mitochondria. This facilitates a coupling that allows for the rapid exchange of mitochondrial derived ATP and HK derived ADP. [Adapted from Robey and Hay, 2009[114]]

Thus, the simultaneous elevation of aerobic glycolysis and OXPHOS may be a normal cellular process and its deregulation may lead to pathological conditions. Currently, only Akt activation has been associated with PBC; however, given the connected nature of these pathways any of the above-mentioned metabolic regulators could be involved with the Warburg-like phenotype and it is worthwhile to further characterize their activity with our *in vitro* model.

4.4 Are increases in mitochondrial respiration fuelled by fatty acid β-oxidation?

Our studies show that lactate production is elevated in PBC BEC, suggesting that there is a decreased flux of pyruvate into the TCA to fuel the ETC. This corresponds with IHC studies showing that 65% of BEC in PBC patient liver sections are positive for pyruvate dehydrogenase kinase 4 (PDK4) expression compared to only 33% of controls[58]. PDK4 is known to phosphorylate and inhibit the pyruvate dehydrogenase complex (PDC) from producing mitochondrial acetyl-CoA. Thus, questions are raised as to what is fuelling oxidative phosphorylation in PBC BEC?

Although glycolysis-mediated production of pyruvate is an important source of carbon for the TCA, it is not the only contributor. Glutaminolysis and fatty acid oxidation (FAO), can both provide alternative sources of substrate[115]. In recent years, these pathways have become of greater interest in cancer research as it is becoming apparent that both aerobic glycolysis and mitochondrial metabolism are of critical importance in oncogenesis[116]. The hyper-metabolic phenotype observed in SLE CD4+ T-cells was associated with increased expression of FAO enzymes, increased uptake of fatty acids and genes associated with amino acid metabolism; thus the authors propose that glycolysis, FAO, and glutaminolysis may all contribute to the elevated levels of OXPHOS and aerobic glycolysis[99]. Elevated levels of glutaminolysis, lactate production and oxygen consumption have also been shown to be stimulated by the activation of Myc in Myc-inducible B-cell lines[117]. In another study, induction of Myc in mouse pre-B cell lines stimulated increases in oxygen consumption, lactate production, mtDNA copy number and fatty acid oxidation rate[111].

Currently there is not any evidence that glutaminolysis is upregulated in PBC BEC, although with ^{1}H NMR we observed that there is a significant reduction in steady state glutamate and glutamine levels in PBC BEC (Data not shown). Our shotgun-proteomic study showed significantly increased expression of enzymes that play a role in mitochondrial FAO. This pathway mediates the breakdown of fatty acids into acetyl-CoA, which can be used to fuel the TCA and OXPHOS[115]. Three mitochondrial proteins involved in FAO (very long-chain specific acyl-CoA dehydrogenase and both subunits of the mitochondrial trifunctional protein) were specifically found to be upregulated in PBC BEC with our shotgun-proteomic study. These results raise the possibility that elevated levels of FAO could sustain elevated OXPHOS in PBC BEC; however further characterization of FAO enzyme activity is required.

As previously mentioned, activation of the PPAR-γ coactivator-1α (PGC-1α) and estrogen related receptor-α (ERRα) axis, a well-established regulator of FAO and mitochondrial biogenesis, has been implicated in PBC BEC *in vivo*[58]. Thus, it is tempting to suggest that PGC-1α activation could be involved with the observed increases in mtDNA content, oxidative phosphorylation, and FAO enzyme expression we observe here. However, we did not detect PGC-1α *in vitro* with our proteomic dataset as was observed *in vivo* by Harada and colleagues (2014). Similar to Akt, this may be attributed to the fact that PGC-1α falls below the dynamic range of the assay[96]. Therefore, further characterization of PGC-1α expression in PBC BEC with our *in vitro* model is worthwhile.

It is also important to mention that although we see increased expression of FAO enzymes with our proteomic study, more work is necessary to show that FAO is functionally active [118,119]. Consequently, it is of great interest to assess how fatty acid and glutamine carbon are metabolized in PBC BEC.

4.5 Does altered metabolism in PBC BEC relate to redox regulation?

Another interesting finding with our proteomic dataset is the observation that several antioxidant enzymes are elevated in PBC BEC relative to liver disease controls, suggesting that redox status may be dysregulated in PBC BEC. This coincides with *in vivo* data showing evidence of lipid peroxidation and oxidative DNA damage in PBC BEC, in 100% or 91.7% of patients, respectively[70,120]. Assessment of blood and urine markers also shows that oxidative stress is a feature of early-stage PBC and could involved in disease progression[121]. Given the close relationship between ROS generation and mitochondrial metabolism, it is possible that the observed metabolic reprogramming could relate to altered redox regulation.

Oxidative phosphorylation is one of the major producers of endogenous reactive oxygen species (ROS) due to electron leak from the ETC, suggesting elevated oxygen consumption in PBC BEC could be contributing to the production of ROS[122]. Harada *et al.* (2014) suggest that elevated levels of PGC-1α induced FAO could enhance oxidative stress by elevating ROS levels which will increase the susceptibility of PBC BEC to apoptosis[123]. It has also been shown that Akt mediated increases in oxygen consumption stimulates elevated levels of ROS rendering mouse embryonic fibroblasts more susceptible to premature senescence[124].

However, Onori and colleagues (2007) showed that the increase in PBC BEC positive for p-Akt with disease stage coincided with reduced markers of apoptosis. They suggest that the activation of Akt may actually provide a selective advantage that allows them to survive until the latter stages of disease.[125] It is possible that the Akt-mediated association of HKII to the mitochondria could also reduce ROS by maintaining the ETC in an oxidized state. When ADP is absent, the ETC is highly reduced leading to an increase in electron leak and ROS formation. A mtHKII facilitated increase in mitochondrial ADP may accelerate electron flux and oxygen consumption, leading to a more oxidized ETC and reduced ROS formation[122]. This is supported by *in vitro* work

showing that mtHK activity in rat embryonic cortical neurons is important in sustaining ADP levels in the mitochondria, and leads to a decrease in ROS formation[126].

The reduction of ROS production is not the only mechanism of alleviating oxidative stress, as there are several endogenous mechanisms to scavenge free radicals. Although glycolysis and the TCA are generally thought of as energy-producing pathways, both play important roles in producing substrates that participate in cell signalling, feed anabolic pathways and act as reducing agents to combat oxidative stress (Figure 4.5)[127,128]. Both glycolysis and TCA intermediates can be shunted into separate pathways in order to produce anabolic precursors and NADPH. NADPH plays a role as a cofactor in several enzymatic reactions and has an important role regenerating reduced glutathione (GSH), a critical free radical scavenger[129]. Interestingly, our ^{1}H-NMR studies also showed significantly elevated levels of intracellular GSH in PBC BEC (Data not shown). In our proteomic dataset we also observed increased levels of the SLC25A1, a mitochondrial carrier protein that exchanges mitochondrial citrate for cytosolic malate. Mitochondrial citrate is an intermediate metabolite in the TCA, which can be exported into the cytosol where it is used as a substrate for anabolic pathways (e.g. lipogenesis), the production of acetyl-CoA for protein acetylation, and the production of cytosolic NADPH (Figure 4.5)[130,131]. Thus, another potential explanation for the elevated levels of glycolysis and oxygen consumption could be that it is an adaptive mechanism to increase NADPH levels to help combat oxidative stress or provide substrates for anabolic pathways

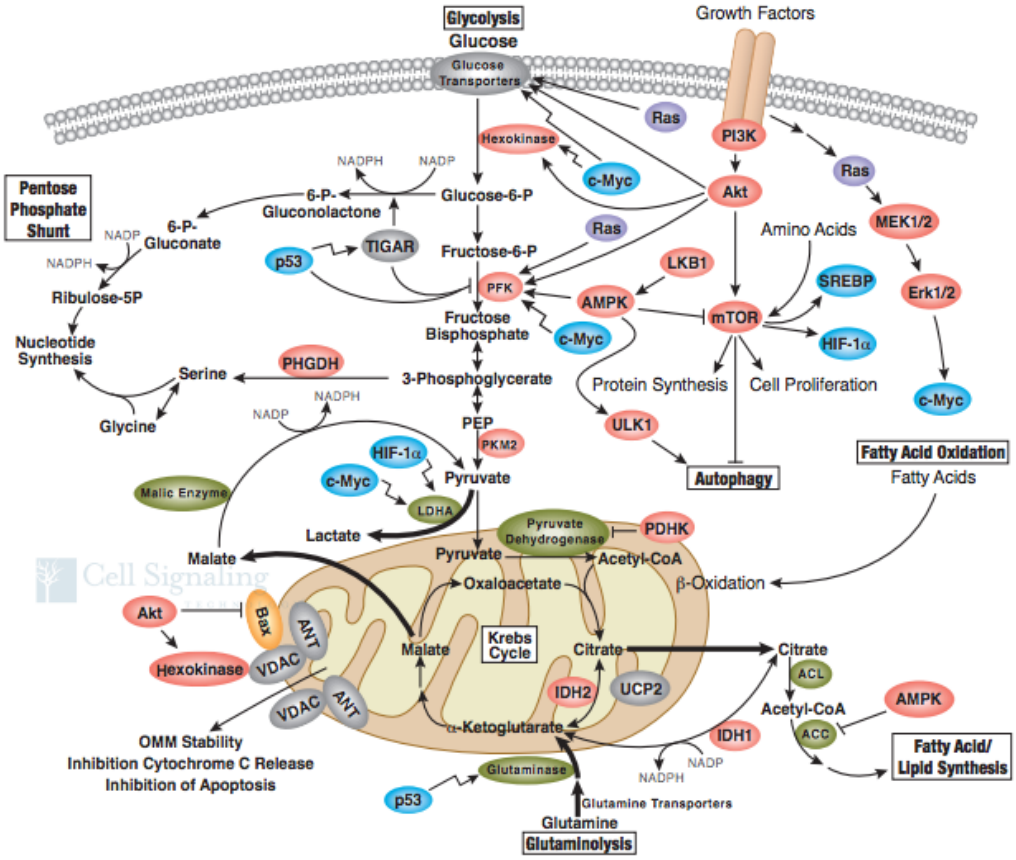

Figure 4.5. **Glycolysis and tricarboxylic acid metabolites can be used for multiple pathways.** Glucose-6-phosphate can be used in the pentose phosphate shunt to produce substrates for nucleotide synthesis and NADPH. 3-phophosphoglycerate can also be used in the serine/glycine biosynthesis pathway to produce precursors for nucleotide synthesis. Citrate can be shunted away from the tricarboxylic acid/Krebs cycle to produce acetyl-CoA for lipid synthesis or to produce NADPH. Malate can also be exported into the cytoplasm to produce NADPH and regenerate pyruvate. [Illustration reproduced courtesy of Cell Signaling Technology, Inc. (www.cellsignal.com)]

4.6 Potential implications of metabolic modifications in PBC BEC

Although there are several lines of evidence implicating mitochondrial and metabolic dysfunction in PBC BEC, how this relates to disease pathogenesis is still unclear. Mitochondria play a critical role both as an environmental sensor and active signalling platform[62]. Through these functions they are actively involved in the regulation of various cellular processes including metabolism, redox homeostasis, autophagy, local inflammation, and apoptosis. Thus, the observed mitochondrial reprogramming in PBC BEC could have several downstream effects on cellular health and the inflammatory milieu observed in the portal tract in PBC.

A relationship between redox regulation and the mitochondrial phenotype is a relatively novel connection that has not yet been characterized. ROS-mediated translocation of auto-antigens have been implicated in SLE, as it has been shown that *in vitro* exposure of keratinocytes to ultraviolet light induces ROS formation, and the localization of La and Sm antigens to the cell membrane[132]. Interestingly, recent studies have also shown that PDC is not limited to the mitochondrial compartment and may translocate to different organelles in response to ROS. Treatment of 786-O cells with rotenone (an established inducer of ROS production) has been shown to prompt increased levels of nuclear PDC[133]. It has also been shown that PDC-E2 and E3BP subunits are found in ROS-induced mitochondrial derived vesicles (MDVs) directed towards lysosomes[134]. Furthermore, it has been shown that MDVs are involved in the trafficking and presentation of oxoglutarate dehydrogenase, a known AMA antigen, on MHC class I molecules in response to infectious stimuli[135]. Thus, the observed metabolic aberrations in PBC BEC could relate to the presentation of mitochondrial antigens to the immune system and the bile-duct specific breakdown of immune-tolerance.

Another interesting possibility is that metabolic reprogramming relates to innate immune function in BEC. It is well established that BEC have the capacity to sense pathogen-associated molecular patterns (PAMPs) through the expression of toll-like receptors (TLRs) and secrete pro-inflammatory cytokines[136]. However, opinions are

divided in regards to whether BEC take an active role in the perpetuation of biliary inflammation in PBC, or are simply an "innocent victim" of disease[137]. Although we did not specifically look at cytokine production here, it has been reported that PBC BEC show elevated expression of IL-6 and TNF alpha *in situ*[138]. Furthermore, preliminary studies also suggest that cultured PBC BEC show elevated cytokine secretion in response to LPS, a bacterial membrane component[139]. A similar observation is also observed in PBC monocytes, which show an elevated cytokine secretion in response to various TLR ligands, including poly I:C, a viral RNA mimic, and LPS[140]. Combined, these findings suggest that the innate immune system is overactive in PBC patients.

A similar phenotype is observed in TNFR1-associated periodic syndrome (TRAPS) monocytes, which is associated with elevated baseline levels of ROS and oxygen consumption[141]. Furthermore, inhibition of mitochondrial ROS (mROS) reduced cytokine secretion in response to LPS, implicating that dysregulated mROS production leads to an increase in innate immune responsiveness. Thus, it is possible that metabolic reprogramming in PBC BEC may relate to altered regulation of the innate immune system.

4.7 Future directions

Given the relatively novel nature of the hyper-metabolic phenotype we have observed in PBC BEC, where glycolysis and mitochondrial metabolism are simultaneously elevated, the first step is to characterize these processes with greater depth. As mentioned previously, PBC BEC show elevated levels of lactate production, implicating that there is a reduction in the amount of pyruvate being converted to acetyl-CoA via PDC. Thus, it is of interest to further characterize PDC function either by quantifying the levels of phosphorylated-PDC with western blot or assessing its activity using functional immuno-capture assays. These studies will tell us whether glucose oxidation is in fact reduced in PBC BEC.

Our proteomic dataset also implicated that FAO enzyme expression is upregulated in PBC BEC, implicating that fatty acids may be an alternate fuel source fuelling elevated mitochondrial respiration. An important first step in verifying this hypothesis is to validate elevated FAO enzyme expression using an alternative method such as western blot. Once validated, future metabolomic studies can be pursued using isotopically labelled palmitate in order to characterize how fatty acid carbon is metabolized in PBC BEC.

It is also of interest to further define which regulatory enzymes may be involved in the regulation of this phenotype. Akt, PGC-1α, and Myc would be ideal to characterize first given that they all regulate cellular metabolism, and have been associated with similar metabolic phenotypes or PBC. A preliminary western blot screen assessing for the relative expression of the activated forms of these enzymes would allow us to determine candidate regulators of the Warburg-like phenotype. Following these studies specific inhibitors can be used on BEC followed by assessment of OCR and ECAR with the Seahorse platform to characterize which enzymes are involved in the induction of the hyper-metabolic phenotype. Finally, is worthwhile to characterize whether metabolic reprogramming relates to altered redox regulation in PBC BEC. For these studies, ROS levels could be assessed using commercial dyes to characterize whether elevated mitochondrial respiration is associated with increased ROS.

4.8 Conclusions

Given the evidence implicating mitochondrial dysfunction in primary biliary cholangitis patients' biliary epithelial cells, this project was undertaken with the intention to further characterize mitochondrial function and cellular metabolism in PBC BEC *in vitro*. Through these studies we have observed that PBC BEC have an altered metabolic profile relative to end-stage liver disease control BEC *in vitro.* In general, this phenotype is characterized by increases in aerobic glycolysis, oxygen consumption, and mitochondrial DNA copy number. Elevated levels of fatty acid oxidation and oxidative stress are also implicated in our proteomic dataset; however, further study is required to

validate that elevated expression of FAO enzymes has a functional impact in PBC BEC. Although further is work required, the current study provides the most comprehensive characterization of cellular metabolism in PBC BEC *in vitro* to date. Given the central role of mitochondria in cellular energy production, cell signalling and immunity, the observed metabolic reprogramming in PBC BEC here further supports that mitochondrial dysfunction may play a role in disease pathogenesis. These studies may provide groundwork for future studies assessing how mitochondrial function is altered in PBC BEC and how this phenotype relates to disease pathogenesis.

Bibliography

1. Carey, E. J., Ali, A. H. & Lindor, K. D. Primary biliary cirrhosis. *Lancet (London, England)* **386,** 1565–1575 (2015).

2. Mason, A. L. *et al.* Detection of retroviral antibodies in primary biliary cirrhosis and other idiopathic biliary disorders. *Lancet (London, England)* **351,** 1620–1624 (1998).

3. Boonstra, K., Beuers, U. & Ponsioen, C. Y. Epidemiology of primary sclerosing cholangitis and primary biliary cirrhosis: a systematic review. *J. Hepatol.* **56,** 1181–1188 (2012).

4. Baum, H. & Palmer, C. The PBC-specific antigen. *Mol. Aspects Med.* **8,** 201–234 (1985).

5. Yeaman, S. J., Kirby, J. A. & Jones, D. E. Autoreactive responses to pyruvate dehydrogenase complex in the pathogenesis of primary biliary cirrhosis. *Immunol. Rev.* **174,** 238–249 (2000).

6. Hirschfield, G. M. & Gershwin, M. E. The immunobiology and pathophysiology of primary biliary cirrhosis. *Annu. Rev. Pathol.* **8,** 303–330 (2013).

7. Wasilenko, S. T., Mason, G. E. & Mason, A. L. Primary biliary cirrhosis, bacteria and molecular mimicry: What's the molecule and where's the mimic? *Liver Int.* **29,** 779–782 (2009).

8. Saunier, E., Benelli, C. & Bortoli, S. The pyruvate dehydrogenase complex in cancer: An old metabolic gatekeeper regulated by new pathways and pharmacological agents. *Int. J. cancer* **138,** 809–817 (2016).

9. McLain, A. L., Szweda, P. A. & Szweda, L. I. alpha-Ketoglutarate dehydrogenase: a mitochondrial redox sensor. *Free Radic. Res.* **45,** 29–36 (2011).

10. Harris, R. A., Joshi, M., Jeoung, N. H. & Obayashi, M. Overview of the molecular and biochemical basis of branched-chain amino acid catabolism. *J. Nutr.* **135,** 1527S–30S (2005).

11. Gershwin, M. E. *et al.* Primary biliary cirrhosis: an orchestrated immune response against epithelial cells. *Immunol. Rev.* **174,** 210–225 (2000).

12. Jones, D. E. J., Watt, F. E., Metcalf, J. V, Bassendine, M. F. & James, O. F. W. Familial primary biliary cirrhosis reassessed: a geographically-based population study. *J. Hepatol.* **30,** 402–407 (2016).

13. Gershwin, M. E. *et al.* Risk Factors and Comorbidities in Primary Biliary Cirrhosis: A Controlled Interview-Based Study of 1032 Patients. *Hepatology (Baltimore, Md.)* **42,** 1194–1202 (2005).

14. Selmi, C. *et al.* Primary biliary cirrhosis in monozygotic and dizygotic twins: genetics, epigenetics, and environment. *Gastroenterology* **127,** 485–492 (2004).

15. Gulamhusein, A. F., Juran, B. D. & Lazaridis, K. N. GWAS in Primary Biliary Cirrhosis. *Seminars in liver disease* **35,** 392–401 (2015).

16. Mason, A. L. & Wasilenko, S. T. Other potential medical therapies: the use of antiviral agents to investigate and treat primary ciliary cirrhosis. *Clin. Liver Dis.* **12,** 445–60; xi (2008).

17. Webb, G. J. & Hirschfield, G. M. Using GWAS to identify genetic predisposition in hepatic autoimmunity. *J. Autoimmun.* **66,** 25–39 (2016).

18. Tang, R. *et al.* The cumulative effects of known susceptibility variants to predict primary biliary cirrhosis risk. *Genes Immun.* **16,** 193–198 (2015).

19. Ala, A. *et al.* Increased Prevalence of Primary Biliary Cirrhosis Near Superfund Toxic Waste Sites. *Hepatology.* **43,** 525-531 (2006).

20. Wang, J. *et al.* Xenobiotics and loss of tolerance in primary biliary cholangitis. *World J Gastroenterol.* **22,** 338–348 (2016).

21. Walden, H. R. *et al.* Xenobiotic incorporation into pyruvate dehydrogenase complex can occur via the exogenous lipoylation pathway. *Hepatology* **48,** 1874–1884 (2008).

22. Amano, K. *et al.* Chemical xenobiotics and mitochondrial autoantigens in primary biliary cirrhosis: identification of antibodies against a common environmental, cosmetic, and food additive, 2-octynoic acid. *J. Immunol.* **174,** 5874–5883 (2005).

23. Wakabayashi, K. *et al.* Loss of tolerance in C57BL/6 mice to the autoantigen E2 subunit of pyruvate dehydrogenase by a xenobiotic with ensuing biliary ductular disease. *Hepatology* **48,** 531–540 (2008).

24. Wakabayashi, K. *et al.* Induction of autoimmune cholangitis in non-obese diabetic (NOD).1101 mice following a chemical xenobiotic immunization. *Clinical and Experimental Immunology* **155,** 577–586 (2009).

25. Tsuneyama, K., Moritoki, Y., Kikuchi, K. & Nakanuma, Y. Pathological Features of New Animal Models for Primary Biliary Cirrhosis. *International Journal of Hepatology* **2012,** (2012).

26. Sharon, D. & Mason, A. L. Role of Novel Retroviruses in Chronic Liver Disease: Assessing the Link of Human Betaretrovirus with Primary Biliary Cirrhosis. *Curr. Infect. Dis. Rep.* **17,** 1–10 (2015).

26. Sharon, D. & Mason, A. L. Role of Novel Retroviruses in Chronic Liver Disease: Assessing the Link of Human Betaretrovirus with Primary Biliary Cirrhosis. *Curr. Infect. Dis. Rep.* **17,** 1–10 (2015).

27. Sasaki, M., Hsu, M., Yeh, M. M. & Nakanuma, Y. In recurrent primary biliary cirrhosis after liver transplantation, biliary epithelial cells show increased expression of mitochondrial proteins. *Virchows Arch.* **467,** 417–425 (2015).

28. Hirschfield, G. M. & Gershwin, M. E. The immunobiology and pathophysiology of primary biliary cirrhosis. *Annu. Rev. Pathol.* **8,** 303–330 (2013).

29. Ortega-Hernandez, O.-D., Levin, N.-A., Altman, A. & Shoenfeld, Y. Infectious agents in the pathogenesis of primary biliary cirrhosis. *Dis. Markers* **29,** 277–286 (2010).

30. I Wang, J. J. *et al.* Escherichia coli infection induces autoimmune cholangitis and anti-mitochondrial antibodies in non-obese diabetic (NOD).B6 (Idd10/Idd18) mice. *Clin. Exp. Immunol.* **175,** 192–201 (2014).

31. Mattner, J. *et al.* Liver autoimmunity triggered by microbial activation of natural killer T cells. *Cell Host Microbe* **3,** 304–315 (2008).

32. Xu, L. *et al.* Does a betaretrovirus infection trigger primary biliary cirrhosis? *Proc. Natl. Acad. Sci. U. S. A.* **100,** 8454–8459 (2003).

33. Xu, L. *et al.* Cloning the human betaretrovirus proviral genome from patients with primary biliary cirrhosis. *Hepatology* **39,** 151–156 (2004).

34. Wang, W. *et al.* Frequent proviral integration of the human betaretrovirus in biliary epithelium of patients with autoimmune and idiopathic liver disease. *Aliment. Pharmacol. Ther.* **41,** 393–405 (2015).

35. Zhang, G. *et al.* Mouse mammary tumor virus in anti-mitochondrial antibody producing mouse models. *J. Hepatol.* **55,** 876–84 (2011).

36. Sharon, D. *et al.* Impact of combination antiretroviral therapy in the NOD.c3c4 mouse model of autoimmune biliary disease. *Liver Int.* **35,** 1442–1450 (2015).

37. Tsuneyama, K. *et al.* Human combinatorial autoantibodies and mouse monoclonal antibodies to PDC-E2 produce abnormal apical staining of salivary glands in patients with coexistent primary biliary cirrhosis and Sjogren's syndrome. *Hepatology* **20,** 893–898 (1994).

38. Joplin, R. E. *et al.* Distribution of pyruvate dehydrogenase dihydrolipoamide acetyltransferase (PDC-E2) and another mitochondrial marker in salivary gland and biliary epithelium from patients with primary biliary cirrhosis. *Hepatology* **19,** 1375–1380 (1994).

39. Joplin, R. *et al.* Subcellular localization of pyruvate dehydrogenase dihydrolipoamide acetyltransferase in human intrahepatic biliary epithelial cells. *J. Pathol.* **176,** 381–390 (1995).

40. Tsuneyama, K. *et al.* Abnormal expression of the E2 component of the pyruvate dehydrogenase complex on the luminal surface of biliary epithelium occurs before major histocompatibility complex class II and BB1/B7 expression. *Hepatology* **21,** 1031–1037 (1995).

41. Van de Water, J. *et al.* Immunohistochemical evidence of disease recurrence after liver transplantation for primary biliary cirrhosis. *Hepatology* **24,** 1079–1084 (1996).

42. Tsuneyama, K. *et al.* Primary biliary cirrhosis an epithelitis: evidence of abnormal salivary gland immunohistochemistry. *Autoimmunity* **26,** 23–31 (1997).

43. Epstein, O., Thomas, H. C. & Sherlock, S. Primary biliary cirrhosis is a dry gland syndrome with features of chronic graft-versus-host disease. *Lancet (London, England)* **1,** 1166–1168 (1980).

44. Cha, S. *et al.* Heterogeneity of combinatorial human autoantibodies against PDC-E2 and biliary epithelial cells in patients with primary biliary cirrhosis. *Hepatology* **20,** 574–583 (1994).

45. Van de Water, J. *et al.* Molecular mimicry in primary biliary cirrhosis. Evidence for biliary epithelial expression of a molecule cross-reactive with pyruvate dehydrogenase complex-E2. *Journal of Clinical Investigation* **91,** 2653–2664 (1993).

46. Joplin, R. E. *et al.* The human biliary epithelial cell plasma membrane antigen in primary biliary cirrhosis: pyruvate dehydrogenase X? *Gastroenterology* **113,** 1727–1733 (1997).

47. Harada, K. *et al.* In situ nucleic acid detection of PDC-E2, BCOADC-E2, OGDC-E2, PDC-E1alpha, BCOADC-E1alpha, OGDC-E1, and the E3 binding protein (protein X) in primary biliary cirrhosis. *Hepatology* **30,** 36–45 (1999).

48. Harada, K. *et al.* In situ nucleic acid hybridization of pyruvate dehydrogenase complex-E2 in primary biliary cirrhosis: pyruvate dehydrogenase complex-E2 messenger RNA is expressed in hepatocytes but not in biliary epithelium. *Hepatology* **25,** 27–32 (1997).

49. Sadamoto, T. *et al.* Expression of pyruvate-dehydrogenase complex PDC-E_2 on biliary epithelial cells induced by lymph nodes from primary biliary cirrhosis. *Lancet* **352,** 1595–1596 (1998).

50. Zhang, G. *et al.* Mouse mammary tumor virus in anti-mitochondrial antibody producing mouse models. *J. Hepatol.* **55,** 876–84 (2011).

51. Macdonald, P., Palmer, J., Kirby, J. a & Jones, D. E. J. Apoptosis as a mechanism for cell surface expression of the autoantigen pyruvate dehydrogenase complex. *Clin. Exp. Immunol.* **136,** 559–67 (2004).

52. Odin, J. A., Huebert, R. C., Casciola-Rosen, L., LaRusso, N. F. & Rosen, A. Bcl-2–dependent oxidation of pyruvate dehydrogenase-E2, a primary biliary cirrhosis autoantigen, during apoptosis. *Journal of Clinical Investigation* **108,** 223–232 (2001).

53. Lleo, A. *et al.* Apotopes and the biliary specificity of primary biliary cirrhosis. *Hepatology* **49,** 871–879 (2009).

54. Lleo, A. & Invernizzi, P. Apotopes and innate immune system : Novel players in the primary biliary cirrhosis scenario. *Dig. Liver Dis.* **45,** 630–636 (2013).

55. Nsiah-Sefaa, A. & McKenzie, M. Combined defects in oxidative phosphorylation and fatty acid beta-oxidation in mitochondrial disease. *Biosci. Rep.* **36,** (2016).

56. Yu-hui, X. & Zhong-bi, W. The ultrastructure of intrahepatic bile ducts in primary biliary cirrhosis. *J. Tongji Med. Univ.* **6,** 37–42 (1986).

57. Tobe, K. Electron microscopy of liver lesions in primary biliary cirrhosis. I. Intrahepatic bile duct oncocytes. *Acta Pathol. Jpn.* **32,** 57–70 (1982).

58. Harada, K. *et al.* Alteration of energy metabolism in the pathogenesis of bile duct lesions in primary biliary cirrhosis. *J. Clin. Pathol.* **67,** 396–402 (2014).

59. Tan, Z. *et al.* The Role of PGC1alpha in Cancer Metabolism and its Therapeutic Implications. *Mol. Cancer Ther.* **15,** 774–782 (2016).

60. St-Pierre, J. *et al.* Suppression of reactive oxygen species and neurodegeneration by the PGC-1 transcriptional coactivators. *Cell* **127,** 397–408 (2006).

61. Ventura-Clapier, R., Garnier, A. & Veksler, V. Transcriptional control of mitochondrial biogenesis: the central role of PGC-1alpha. *Cardiovasc. Res.* **79,** 208–217 (2008).

62. Dromparis, P. & Michelakis, E. D. Mitochondria in vascular health and disease. *Annual review of physiology* **75,** (2013).

63. Finkel, T. Signal transduction by reactive oxygen species. *J. Cell Biol.* **194,** 7–15 (2011).

64. Jendrach, M., Mai, S., Pohl, S., Voth, M. & Bereiter-Hahn, J. Short- and long-term alterations of mitochondrial morphology, dynamics and mtDNA after transient oxidative stress. *Mitochondrion* **8,** 293–304 (2008).

65. Copple, B. L., Jaeschke, H. & Klaassen, C. D. Oxidative stress and the pathogenesis of cholestasis. *Semin. Liver Dis.* **30,** 195–204 (2010).

66. Aboutwerat, A. *et al.* Oxidant stress is a significant feature of primary biliary cirrhosis. *Biochim. Biophys. Acta* **1637,** 142–150 (2003).

67. Notas, G. *et al.* Patients with primary biliary cirrhosis have increased serum total antioxidant capacity measured with the crocin bleaching assay. *World J. Gastroenterol.* **11,** 4194–8 (2005).

68. Ono, M. *et al.* Elevated level of serum Mn-superoxide dismutase in patients with primary biliary cirrhosis: possible involvement of free radicals in the pathogenesis in primary biliary cirrhosis. *J. Lab. Clin. Med.* **118,** 476–483 (1991).

69. Kitada, T. *et al.* In situ detection of oxidative DNA damage, 8-hydroxydeoxyguanosine, in chronic human liver disease. *J. Hepatol.* **35,** 613–8 (2001).

70. Paradis, V. *et al.* In situ detection of lipid peroxidation by-products in chronic liver diseases. *Hepatology* **26,** 135–142 (1997).

71. Kawamura, K. *et al.* Enhanced hepatic lipid peroxidation in patients with primary biliary cirrhosis. *Am. J. Gastroenterol.* **95,** 3596–3601 (2000).

72. Kouroumalis, E. & Notas, G. Primary biliary cirrhosis: From bench to bedside. *World J. Gastrointest. Pharmacol. Ther.* **6,** 32–58 (2015).

73. Lapenna, D. *et al.* Antioxidant properties of ursodeoxycholic acid. *Biochem. Pharmacol.* **64,** 1661–1667 (2002).

74. Mitsuyoshi, H. *et al.* Ursodeoxycholic acid protects hepatocytes against oxidative injury via induction of antioxidants. *Biochem. Biophys. Res. Commun.* **263,** 537–542 (1999).

75. Sokolovic, D. *et al.* The effect of ursodeoxycholic acid on oxidative stress level and DNase activity in rat liver after bile duct ligation. *Drug Chem. Toxicol.* **36,** 141–148 (2013).

76. Kmiec, Z. Cooperation of liver cells in health and disease. *Adv. Anat. Embryol. Cell Biol.* **161,** III–XIII, 1–151 (2001).

77. Tabibian, J. H. *et al.* Characterization of cultured cholangiocytes isolated from livers of patients with primary sclerosing cholangitis. *Lab. Invest.* **94,** 1126–1133 (2014).

78. Joplin, R. & Kachilele, S. Human intrahepatic biliary epithelial cell lineages: studies in vitro. *Methods Mol. Biol.* **481,** 193–206 (2009).

79. Cox-Foster, D. L. *et al.* A metagenomic survey of microbes in honey bee colony collapse disorder. *Science* **318,** 283–287 (2007).

80. Zwingmann, C., Richter-Landsberg, C. & Leibfritz, D. 13C isotopomer analysis of glucose and alanine metabolism reveals cytosolic pyruvate compartmentation as part of energy metabolism in astrocytes. *Glia* **34,** 200–212 (2001).

81. Polpitiya, A. D. *et al.* DAnTE: a statistical tool for quantitative analysis of -omics data. *Bioinformatics* **24,** 1556–1558 (2008).

82. Dennis, G. J. *et al.* DAVID: Database for Annotation, Visualization, and Integrated Discovery. *Genome Biol.* **4,** P3 (2003).

83. Szklarczyk, D. *et al.* STRING v10: protein-protein interaction networks, integrated over the tree of life. *Nucleic Acids Res.* **43,** D447–52 (2015).

84. Franceschini, A. *et al.* STRING v9.1: protein-protein interaction networks, with increased coverage and integration. *Nucleic Acids Res.* **41,** D808–15 (2013).

85. Phillips, N. R., Sprouse, M. L. & Roby, R. K. Simultaneous quantification of mitochondrial DNA copy number and deletion ratio: a multiplex real-time PCR assay. *Sci. Rep.* **4,** 3887 (2014).

86. Ajaz, S., Czajka, A. & Malik, A. Accurate measurement of circulating mitochondrial DNA content from human blood samples using real-time quantitative PCR. *Methods Mol. Biol.* **1264,** 117–131 (2015).

87. Palsson-McDermott, E. M. & O'Neill, L. A. J. The Warburg effect then and now: from cancer to inflammatory diseases. *Bioessays* **35,** 965–973 (2013).

88. Robey, R. B. & Hay, N. Is Akt the 'Warburg kinase'?-Akt-energy metabolism interactions and oncogenesis. *Semin. Cancer Biol.* **19,** 25–31 (2009).

89. Okano, J. *et al.* Hepatocyte growth factor exerts a proliferative effect on oval cells through the PI3K/Akt signaling pathway. *Biochem. Biophys. Res. Commun.* **309,** 298–304 (2003).

90. Perdomo, G. *et al.* Hepatocyte growth factor is a novel stimulator of glucose uptake and metabolism in skeletal muscle cells. *J. Biol. Chem.* **283,** 13700–13706 (2008).

91. Bayley, J.-P. & Devilee, P. The Warburg effect in 2012. *Curr. Opin. Oncol.* **24,** 62–67 (2012).

92. Wang, W., Upshaw, L., Strong, D. M., Robertson, R. P. & Reems, J. Increased oxygen consumption rates in response to high glucose detected by a novel oxygen biosensor system in non-human primate and human islets. *J. Endocrinol.* **185,** 445–455 (2005).

93. Lee, H.-C. & Wei, Y.-H. Mitochondrial biogenesis and mitochondrial DNA maintenance of mammalian cells under oxidative stress. *Int. J. Biochem. Cell Biol.* **37,** 822–834 (2005).

94. Dickinson, A. *et al.* The regulation of mitochondrial DNA copy number in glioblastoma cells. *Cell Death Differ.* **20,** 1644–1653 (2013).

95. Bustin, S. A. *et al.* The MIQE guidelines: minimum information for publication of quantitative real-time PCR experiments. *Clin. Chem.* **55,** 611–622 (2009).

96. Ghaemmaghami, S. *et al.* Global analysis of protein expression in yeast. *Nature* **425,** 737–741 (2003).

97. Onori, P. *et al.* Activation of the IGF1 System Characterizes Cholangiocyte Survival During Progression of Primary Biliary Cirrhosis. *J. Histochem. Cytochem.* **55,** 327–334 (2006).

98. Reznik, E. *et al.* Mitochondrial DNA copy number variation across human cancers. *Elife* **5,** (2016).

99. Yin, Y. *et al.* Normalization of CD4+ T cell metabolism reverses lupus. *Sci. Transl. Med.* **7,** 274ra18 (2015).

100. Schieke, S. M. *et al.* The mammalian target of rapamycin (mTOR) pathway regulates mitochondrial oxygen consumption and oxidative capacity. *J. Biol. Chem.* **281,** 27643–27652 (2006).

101. Weichhart, T., Hengstschläger, M. & Linke, M. Regulation of innate immune cell. *Nat. Publ. Gr.* **15,** 599–614 (2015).

102. Sitkovsky, M. & Lukashev, D. Regulation of immune cells by local-tissue oxygen tension: HIF1 alpha and adenosine receptors. *Nat. Rev. Immunol.* **5,** 712–721 (2005).

103. Stine, Z. E., Walton, Z. E., Altman, B. J., Hsieh, A. L. & Dang, C. V. Myc, Metabolism, and Cancer. *Cancer Discov.* **5,** 1024–1039 (2015).

104. Shim, H. *et al.* c-Myc transactivation of LDH-A: implications for tumor metabolism and growth. *Proc. Natl. Acad. Sci. U. S. A.* **94,** 6658–6663 (1997).

105. Osthus, R. C. *et al.* Deregulation of glucose transporter 1 and glycolytic gene expression by c-Myc. *J. Biol. Chem.* **275,** 21797–21800 (2000).

106. Ahuja, P. *et al.* Myc controls transcriptional regulation of cardiac metabolism and mitochondrial biogenesis in response to pathological stress in mice. *J. Clin. Invest.* **120,** 1494–1505 (2010).

107. Li, F. *et al.* Myc stimulates nuclearly encoded mitochondrial genes and mitochondrial biogenesis. *Mol. Cell. Biol.* **25,** 6225–6234 (2005).

108. Morrish, F., Neretti, N., Sedivy, J. M. & Hockenbery, D. M. The oncogene c-Myc coordinates regulation of metabolic networks to enable rapid cell cycle entry. *Cell Cycle* **7,** 1054–1066 (2008).

109. Vyas, S., Zaganjor, E. & Haigis, M. C. Review Mitochondria and Cancer. *Cell* **166,** 555–566 (2016).

110. Nogueira, V. *et al.* Akt determines replicative senescence and oxidative or oncogenic premature senescence and sensitizes cells to oxidative apoptosis. *Cancer Cell* **14,** 458–470 (2008).

111. Fan, Y., Dickman, K. G. & Zong, W.-X. Akt and c-Myc differentially activate cellular metabolic programs and prime cells to bioenergetic inhibition. *J. Biol. Chem.* **285,** 7324–7333 (2010).

112. Memmott, R. M. & Dennis, P. A. Akt-dependent and -independent mechanisms of mTOR regulation in cancer. *Cell. Signal.* **21,** 656–664 (2009).

113. Zhu, J., Blenis, J. & Yuan, J. Activation of PI3K/Akt and MAPK pathways regulates Myc-mediated transcription by phosphorylating and promoting the degradation of Mad1. *Proc. Natl. Acad. Sci. U. S. A.* **105,** 6584–6589 (2008).

114. Robey, R. B. & Hay, N. Is Akt the 'Warburg kinase'?-Akt-energy metabolism interactions and oncogenesis. *Semin. Cancer Biol.* **19,** 25–31 (2009).

115. Ralph, S. J., Rodríguez-enríquez, S., Neuzil, J. & Moreno-sánchez, R. Molecular Aspects of Medicine Bioenergetic pathways in tumor mitochondria as targets for cancer therapy and the importance of the ROS-induced apoptotic trigger. *Mol. Aspects Med.* **31,** 29–59 (2010).

116. Ward, P. S. & Thompson, C. B. Metabolic reprogramming: a cancer hallmark even warburg did not anticipate. *Cancer Cell* **21,** 297–308 (2012).

117. Le, A. *et al.* Metabolism via TCA Cycling for Proliferation and Survival in B Cells. *Cell Metab.* **15,** 110–121 (2012).

118. Carracedo, A., Cantley, L. C. & Pandolfi, P. P. Cancer metabolism : fatty acid oxidation in the limelight. (2013). at <http://dx.doi.org/10.1038/nrc3483>

119. Pike, L. S., Smift, A. L., Croteau, N. J., Ferrick, D. A. & Wu, M. Biochimica et Biophysica Acta Inhibition of fatty acid oxidation by etomoxir impairs NADPH production and increases reactive oxygen species resulting in ATP depletion and cell death in human glioblastoma cells ☆. *BBA - Bioenerg.* **1807,** 726–734 (2011).

120. Kitada, T. *et al.* In situ detection of oxidative DNA damage , 8-hydroxydeoxyguanosine , in chronic human liver disease. **35,** 613–618 (2001).

121. Aboutwerat, A. *et al.* Oxidant stress is a significant feature of primary biliary cirrhosis. *Biochim. Biophys. Acta - Mol. Basis Dis.* **1637,** 142–150 (2003).

122. Nickel, A., Kohlhaas, M. & Maack, C. Journal of Molecular and Cellular Cardiology Mitochondrial reactive oxygen species production and elimination. *J. Mol. Cell. Cardiol.* **73,** 26–33 (2014).

123. Harada, K. *et al.* Alteration of energy metabolism in the pathogenesis of bile duct lesions in primary biliary cirrhosis. 396–402 (2014). doi:10.1136/jclinpath-2013-201815

124. Nogueira, V. *et al.* Akt Determines Replicative Senescence and Oxidative or Oncogenic Premature Senescence and Sensitizes Cells to Oxidative Apoptosis. *Cancer Cell* **14,** 458–470 (2008).

125. Onori, P. *et al.* Activation of the IGF1 System Characterizes Cholangiocyte Survival During Progression of Primary Biliary Cirrhosis The Journal of Histochemistry & Cytochemistry. **55,** 327–334 (2007).

126. Seixas, W. *et al.* Mitochondrial Bound Hexokinase Activity as a Preventive. **279,** 39846–39855 (2004).

127. Ward, P. S. & Thompson, C. B. Metabolic reprogramming: a cancer hallmark even warburg did not anticipate. *Cancer Cell* **21,** 297–308 (2012).

128. Kondoh, H., Lleonart, M. E., Bernard, D. & Gil, J. Protection from oxidative stress by enhanced glycolysis; a possible mechanism of cellular immortalization. *Histol. Histopathol.* **22,** 85–90 (2007).

129. Cairns, R. A., Harris, I. S. & Mak, T. W. Regulation of cancer cell metabolism. *Nat. Rev. Cancer* **11,** 85–95 (2011).

130. Wise, D. R. *et al.* Hypoxia promotes isocitrate dehydrogenase-dependent carboxylation of alpha-ketoglutarate to citrate to support cell growth and viability. *Proc. Natl. Acad. Sci. U. S. A.* **108,** 19611–19616 (2011).

131. Vander Heiden, M. G., Cantley, L. C. & Thompson, C. B. Understanding the Warburg effect: the metabolic requirements of cell proliferation. *Science* **324,** 1029–1033 (2009).

132. Lawley, W. *et al.* Rapid lupus autoantigen relocalization and reactive oxygen species accumulation following ultraviolet irradiation of human keratinocytes. *Rheumatology (Oxford).* **39,** 253–261 (2000).

133. Sutendra, G. *et al.* A Nuclear Pyruvate Dehydrogenase Complex Is Important for the Generation of Acetyl-CoA and Histone Acetylation. *Cell* **158,** 84–97 (2014).

134. McLelland, G.-L., Soubannier, V., Chen, C. X., McBride, H. M. & Fon, E. A. Parkin and PINK1 function in a vesicular trafficking pathway regulating mitochondrial quality control. *EMBO J.* **33,** 282–295 (2014).

135. Roberts, R. F. & Fon, E. A. Presenting mitochondrial antigens: PINK1, Parkin and MDVs steal the show. *Cell Res.* **26,** 1180–1181 (2016).

136. Syal, G., Fausther, M. & Dranoff, J. A. Advances in cholangiocyte immunobiology. *Am. J. Physiol. Gastrointest. Liver Physiol.* **303,** G1077–86 (2012).

137. Shimoda, S. *et al.* Biliary epithelial cells and primary biliary cirrhosis: the role of liver-infiltrating mononuclear cells. *Hepatology* **47,** 958–965 (2008).

138. Yasoshima, M. *et al.* Increased expression of interleukin-6 and tumor necrosis factor-alpha in pathologic biliary epithelial cells: in situ and culture study. *Lab. Invest.* **78,** 89–100 (1998).

139. Zhao, J. *et al.* Altered biliary epithelial cell and monocyte responses to lipopolysaccharide as a TLR ligand in patients with primary biliary cirrhosis. *Scand. J. Gastroenterol.* **46,** 485–494 (2011).

140. Mao, T. K. *et al.* Altered monocyte responses to defined TLR ligands in patients with primary biliary cirrhosis. *Hepatology* **42,** 802–808 (2005).

141. Bulua, A. C. *et al.* Mitochondrial reactive oxygen species promote production of proinflammatory cytokines and are elevated in TNFR1-associated periodic syndrome (TRAPS). *J. Exp. Med.* **208,** 519–533 (2011).

Appendix

Group	Patient and Passage Number	Diagnosis	DNA Concentration (ng/ µL)	260/280	260/230
Control	BEC96 P3	Normal Hemangioma	17.34	1.8	12
	BEC101 P3	CRYPTO	71.9	1.8	2.73
	BEC103 P4	ETOH	24.33	1.67	29.46
	BEC122 P4	Budd Chiari Syndrome	14.89	1.98	1.28
	BEC129 P4	ETOH	59.26	1.75	1.97
	BEC155 P3	ETOH	214.55	1.7	1.54
	BEC159 P3	PSC	29.25	1.99	3.86
	BEC163 P2	PSC	25.49	1.76	4.37
	BEC163 P3	PSC	57.43	1.88	2.71
	BEC166 P2	PSC	20.91	1.93	1.45
	BEC178 P2	Sarcoidosis	30.16	2.01	5.85
	BEC223 P2	PSC	19.57	1.74	37.36
	BEC225 P6	HCV/HCC	55.75	1.61	1.1
	BEC226 P4	CRYPTO	39.28	1.84	3.37
	BEC230 P5	CRYPTO	14.69	2.06	1.5
	BEC234 P3	PSC	22.75	1.77	20.56
	BEC237 P2	PSC	34.74	1.75	4.64
	BEC245 P2	PSC	24.01	1.68	2.63
	BEC260 P2	PSC/IBD	83.54	1.95	2.88
	BEC267 P2	PSC	10.26	2.06	1.28
	BEC271 P3	CRYPTO	44.99	1.8	2.49
	BEC301 P5	GSD/Adenoma	27.92	1.66	1.01
	BEC325 P6	PSC	52.12	1.67	1.28
PBC	BEC145 P4	PBC	8.2	2.31	1.65
	BEC183 P1	PBC/AIH	37.13	1.84	6.36
	BEC185 P5	PBC	24.26	1.94	1.69
	BEC201 P5	PBC/ETOH	32.8	1.64	3.01
	BEC229 P2	PBC	25.94	1.73	3.31
	BEC235 P3	PBC	83.29	1.91	2.52
	BEC239 P2	PBC	23.72	1.77	4.54
	BEC243 P2	PBC/ETOH	28.98	1.82	8.4
	BEC258 P2	PBC	64.51	1.84	2.5
	BEC261 P3	PBC	38.18	1.91	2.72
	BEC263 P2	PBC	23.36	1.91	1.94
	BEC288 P4	PBC	35.93	1.8	1.25

Table 5.1. Nanodrop results for BEC DNA samples. PBC=Primary Biliary Cholangitis; ETOH=Alcoholic Liver Disease; PSC=Primary Sclerosing Cholangitis; HCC=Hepatocellular Carcinoma; Crypto=Cryptogenic Cirrhosis; HCV=Hepatitis C-Virus; GSD=Glycogen storage disease; AIH=Autoimmune hepatitis; IBD=Inflammatory bowel disease.

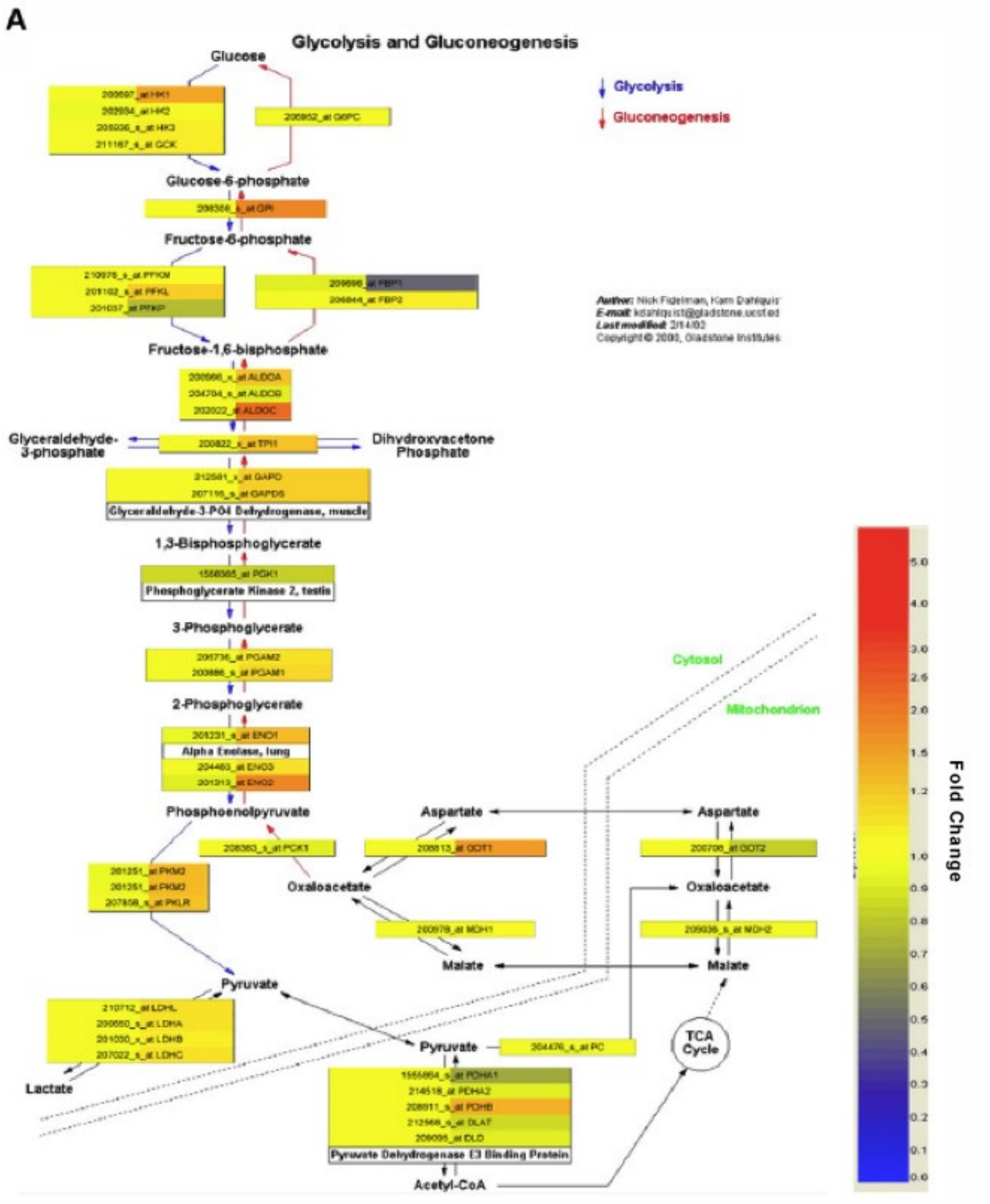
A
Glycolysis and Gluconeogenesis
Glucose
Glycolysis
Gluconeogenesis
Glucose-6-phosphate
Fructose-6-phosphate
Fructose-1,6-bisphosphate
Glyceraldehyde-3-phosphate
Dihydroxyacetone Phosphate
Glyceraldehyde-3-PO4 Dehydrogenase, muscle
1,3-Bisphosphoglycerate
Phosphoglycerate Kinase 2, testis
3-Phosphoglycerate
2-Phosphoglycerate
Alpha Enolase, lung
Phosphoenolpyruvate
Oxaloacetate
Aspartate
Malate
Pyruvate
Lactate
Acetyl-CoA
TCA Cycle
Cytosol
Mitochondrion
Fold Change

Figure 5.1. Cultured biliary epithelial cells (BEC) from patients with Primary Biliary Cholangitis (PBC) display a trend for increased expression of glycolytic enzymes. Using microarray analyses, we observed increased expression of several glycolytic enzymes including glucose-6-phosphate isomerase, aldolase, and enolase up to 1.7-2 fold (in the orange spectrum) in PBC patients' BEC. For these studies, pools of BEC were extracted from livers explanted from 6 patients with PBC, and compared to 4 patients with primary sclerosing cholangitis and 5 other patients with liver failure unrelated to biliary disease. Probes were constructed from total RNA following manufacturer's instructions, hybridized with Affymetrix Plus 2.0 chips and processed for microarray analyses. Data analysis was performed using Affymetrix software (including Microarray Suit 5.0, Micro DB and Data Mining Tool 3.0), and Silicon Genetics' GeneSpring 6.0 program to provide robust and reproducible algorithms for distinguishing biochemical pathways specific to PBC. [Studies performed by Dr. L. Xu: because some of the BEC from both PBC and controls were grown up using different growth media, these data were not included in the thesis defence. However, they provided an impetus for further study of a glycolytic phenotype.]

Up regulated in PBC BEC

Uniprot Accession #	Gene Name	Annotation	p value	change fold
P27144	AK4	Adenylate kinase isoenzyme 4	0.000889088	3.236668802
P09104	ENO2	Gamma-enolase	0.001256577	18.38984117
Q9NRV9	HEBP1	Heme-binding protein 1	0.001288626	3.155741172
Q13162	PRDX4	Peroxiredoxin-4	0.001653788	1.497531368
P42224	STAT1	Signal transducer and activator of transcription 1-alpha/beta	0.001701392	2.231111544
Q9NZN4	EHD2	EH domain-containing protein 2	0.002278944	2.736834106
P17813	ENG	Endoglin	0.002492826	2.666915699
P55084	HADHB	Trifunctional enzyme subunit beta, mitochondrial	0.003584619	2.394966963
O95340	PAPSS2	Bifunctional 3'-phosphoadenosine 5'-phosphosulfate synthase 2	0.004073627	3.679169454
P05121	SEPINE1	Plasminogen activator inhibitor 1	0.004348858	2.151148222
P00338	LDHA	L-lactate dehydrogenase A chain	0.006063924	1.83295741
Q07960	ARHGAP1	Rho GTPase-activating protein 1	0.007321323	2.152010056
Q04446	GBE1	1,4-alpha-glucan-branching enzyme	0.007513368	3.665590485
P53007	SLC25A1	Tricarboxylate transport protein, mitochondrial	0.007705167	2.08629255
P04632	CAPNS1	Calpain small subunit 1	0.008190551	1.652920502
Q14247	CTTN	Src substrate cortactin	0.008649707	3.069622733
P16070	CD44	CD44 antigen	0.00922269	2.060217081
O00429	DNM1L	Dynamin-1-like protein	0.009307978	2.344039677
P07384	CAPN1	Calpain-1 catalytic subunit	0.009385119	2.251802038
Q13404	UBE2V1	Ubiquitin-conjugating enzyme E2 variant 1	0.010685585	3.392363057
Q6NZI2	PTRF	Polymerase I and transcript release factor	0.012184714	2.14660051
P84095	RHOG	Rho-related GTP-binding protein RhoG	0.012626021	2.574483465
P00441	SOD1	Superoxide dismutase [Cu-Zn]	0.013621776	3.159714121
P40261	NNMT	Nicotinamide N-methyltransferase	0.013729096	2.045888698
P11216	PYGB	Glycogen phosphorylase, brain form	0.014216532	3.030130766
Q14315	FLNC	Filamin-C	0.01456578	1.421311646
P30041	PRDX6	Peroxiredoxin-6	0.014717509	1.414114384
Q9H299	SH3BGRL 3	SH3 domain-binding glutamic acid-rich-like protein 3	0.016245709	3.115146416
P28161	GSTM2	Glutathione S-transferase Mu 2	0.01697704	2.116051816
P02751	FN1	Fibronectin	0.01701424	2.666292222
Q9UDY4	DNAJB4	DnaJ homolog subfamily B member 4	0.017420337	2.157807185
Q14112	NID2	Nidogen-2	0.017428403	2.697357172
P07686	HEXB	Beta-hexosaminidase subunit beta	0.017533381	2.150243994
Q16881	TXNRD1	Thioredoxin reductase 1, cytoplasmic	0.017605294	1.401725628
P06733	ENO1	Alpha-enolase	0.019321476	2.076366821
P13674	P4HA1	Prolyl 4-hydroxylase subunit alpha-1	0.019955869	1.598747934
P40939	HADHA	Trifunctional enzyme subunit alpha, mitochondrial	0.020011832	1.647775913

P55290	CDH13	Cadherin-13	0.021209676	2.428639827
P30046	DDT	D-dopachrome decarboxylase	0.022073314	2.533020467
P04406	GAPDH	Glyceraldehyde-3-phosphate dehydrogenase	0.02338631	1.52323395
P49748	ACADVL	Very long-chain specific acyl-CoA dehydrogenase, mitochondrial	0.023832039	2.644764679
P51452	DUSP3	Dual specificity protein phosphatase 3	0.029453101	2.143182875
P17655	CAPN2	Calpain-2 catalytic subunit	0.030724213	1.455330639
P04075	ALDOA	Fructose-bisphosphate aldolase A	0.032903007	1.424736962
O95782	AP2A1	AP-2 complex subunit alpha-1	0.036417983	1.948199398
P36871	PGM1	Phosphoglucomutase-1	0.037040763	2.552721669
P13987	CD59	CD59 glycoprotein	0.038739188	2.501235675
P02786	TFRC	Transferrin receptor protein 1	0.03898607	1.869829907
P41250	GARS	Glycine--tRNA ligase	0.041252415	1.207363992
P35080	PFN2	Profilin-2	0.042940949	2.178002294
Q03135	CAV1	Caveolin-1	0.044668856	1.890078114
P14618	PKM	Pyruvate kinase isozymes M1/M2	0.047504872	1.272316315
P31150	GDI1	Rab GDP dissociation inhibitor alpha	0.047537299	3.446111673

Down regulated in PBC BEC

Uniprot Accession #	Gene Name	Annotation	p value	change fold
Q08211	DHX9	ATP-dependent RNA helicase A	4.56117E-05	0.29619153
Q92945	FUBP2	Far upstream element-binding protein 2	0.000154184	0.314558146
P61978	HNRPK	Heterogeneous nuclear ribonucleoprotein K	0.000241223	0.560291185
P51991	ROA3	Heterogeneous nuclear ribonucleoprotein A3	0.000634279	0.345571626
Q15717	ELAV1	ELAV-like protein 1	0.000670926	0.29728701
Q14103	HNRPD	Heterogeneous nuclear ribonucleoprotein D0	0.000695545	0.548084311
P31943	HNRH1	Heterogeneous nuclear ribonucleoprotein H	0.001208158	0.61341343
Q00839	HNRPU	Heterogeneous nuclear ribonucleoprotein U	0.001599383	0.569006564
P26599	PTBP1	Polypyrimidine tract-binding protein 1	0.001649059	0.645936716
Q9UJZ1	STML2	Stomatin-like protein 2	0.001926019	0.332493021
Q6IBS0	TWF2	Twinfilin-2	0.002527335	0.463297681
P07910	HNRNPC	Heterogeneous nuclear ribonucleoproteins C1/C2	0.003931148	0.526456178
P16403	HIST1H1C	Histone H1.2	0.004401339	0.272070211
Q15233	NONO	Non-POU domain-containing octamer-binding protein	0.004494165	0.290946307
P55769	NHP2L1	NHP2-like protein 1	0.004579946	0.435056579
P35579	MYH9	Myosin-9	0.005375616	0.568165599
Q15366	PCBP2	Poly(rC)-binding protein 2	0.006662018	0.601414977
Q13263	TRIM28	Transcription intermediary factor 1-beta	0.006785131	0.392238774
P31942	HNRNPH3	Heterogeneous nuclear ribonucleoprotein H3	0.007786229	0.456459307
Q12905	ILF2	Interleukin enhancer-binding factor 2	0.009025164	0.493353726
P49915	GMPS	GMP synthase [glutamine-hydrolyzing]	0.012542001	0.474339784

O15372	EIF3H	Eukaryotic translation initiation factor 3 subunit H	0.012724643	0.512893321
Q13185	CBX3	Chromobox protein homolog 3	0.014232522	0.390925508
P20700	LMNB1	Lamin-B1	0.015734735	0.277655395
P43243	MATR3	Matrin-3	0.015973852	0.491302582
P35580	MYH10	Myosin-10	0.017555983	0.196779089
P17174	GOT1	Aspartate aminotransferase, cytoplasmic	0.01789829	0.503509941
P78371	CCT2	T-complex protein 1 subunit beta	0.018000109	0.703456492
Q9UBS4	DNAJB11	DnaJ homolog subfamily B member 11	0.01932754	0.595639632
P68431	HIST1H3A	Histone H3.1	0.024240761	0.454417912
P19338	NCL	Nucleolin	0.024960207	0.750736582
Q09666	AHNAK	Neuroblast differentiation-associated protein AHNAK	0.025421148	0.188498841
P34897	SHMT2	Serine hydroxymethyltransferase, mitochondrial	0.026804333	0.492348817
P14866	HNRNPL	Heterogeneous nuclear ribonucleoprotein L	0.03073878	0.421994266
Q02952	AKAP12	A-kinase anchor protein 12	0.031564712	0.348649665
Q13148	TARDBP	TAR DNA-binding protein 43	0.03356693	0.516426816
Q9H0U4	RAB1B	Ras-related protein Rab-1B	0.033672384	0.298931555
Q02790	FKBP4	Peptidyl-prolyl cis-trans isomerase FKBP4	0.03475669	0.537657194
Q14195	DPYSL3	Dihydropyrimidinase-related protein 3	0.034859714	0.368726957
P22626	HNRNPA2 B1	Heterogeneous nuclear ribonucleoproteins A2/B1	0.039414266	0.590948654
Q86V81	ALYREF	THO complex subunit 4	0.043974952	0.756078848
Q15819	UBE2V2	Ubiquitin-conjugating enzyme E2 variant 2	0.045208839	0.422417924
P11177	PDHB	Pyruvate dehydrogenase E1 component subunit beta, mitochondrial	0.046860079	0.564265215
P62979	RPS27A	Ubiquitin-40S ribosomal protein S27a	0.046880897	0.203530124
P12268	IMPDH2	Inosine-5'-monophosphate dehydrogenase 2	0.047250715	0.533682014
Q16822	PCK2	Phosphoenolpyruvate carboxykinase [GTP], mitochondrial	0.048069909	0.501852045

Table 5.2. **Table of protein candidates shown by shotgun-proteomics to be differentially regulated in cultured Primary Biliary Cholangitis (PBC) patients' biliary epithelial cells compared to liver disease control BEC.** DanteR software was used for normalization and statistical analysis, determining the p-values and fold changes shown here.

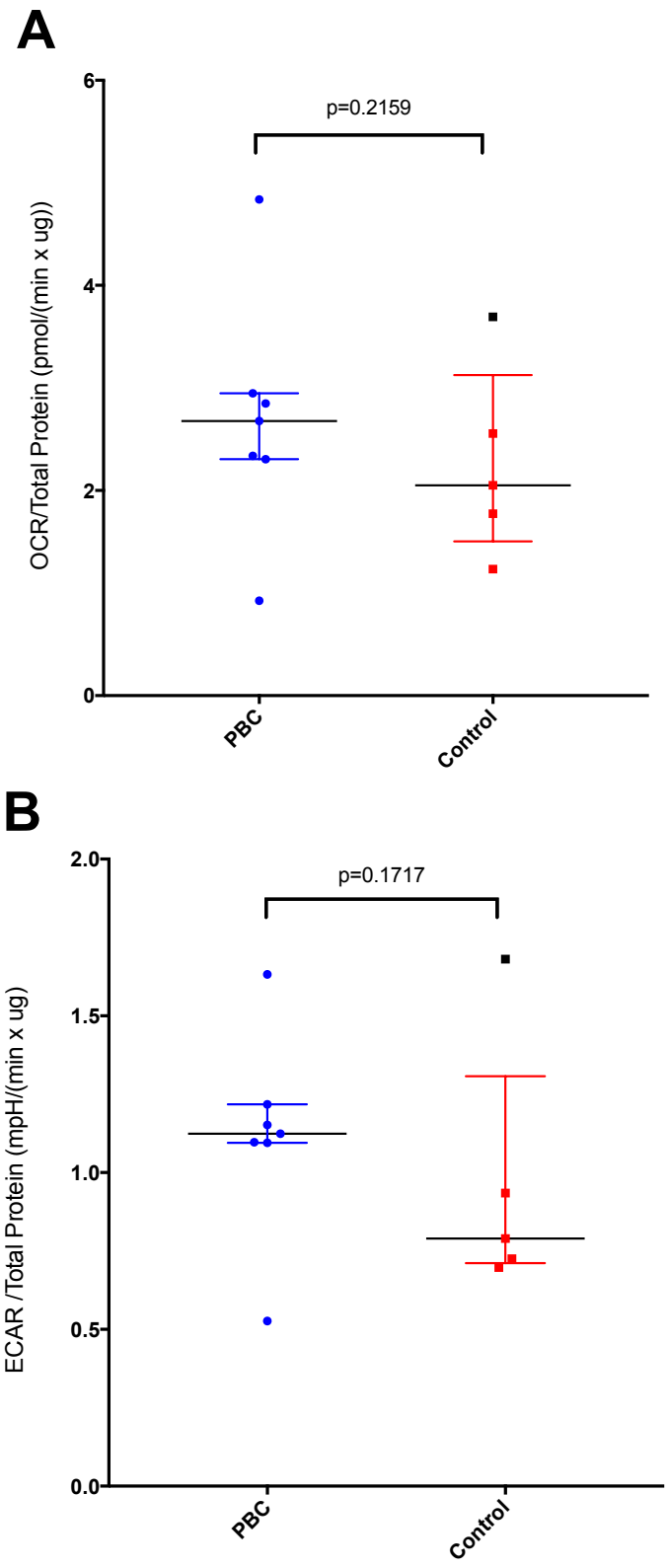
A
p=0.2159
OCR/Total Protein (pmol/(min x ug))
6
4
2
0
PBC
Control
B
p=0.1717
ECAR /Total Protein (mpH/(min x ug)
2.0
1.5
1.0
0.5
0.0
PBC
Control

Figure 5.2. Seahorse XF24 assay results prior to outlier removal. Oxygen consumption rate (OCR, A) and extracellular acidification rate (ECAR, B) before outlier was removed. The outlier sample (BEC334 p3) is highlighted in black. The outlier (BEC334 p3) was 112% higher than the ECAR median and 1.74 standard deviations above the ECAR mean. The outlier was 80% higher than the OCR median and 1.53 standard deviations above the OCR mean. Groups were compared using a 1-tailed Mann Whitney test with Prism 7 software. Shown are medians +/- IQR.

A

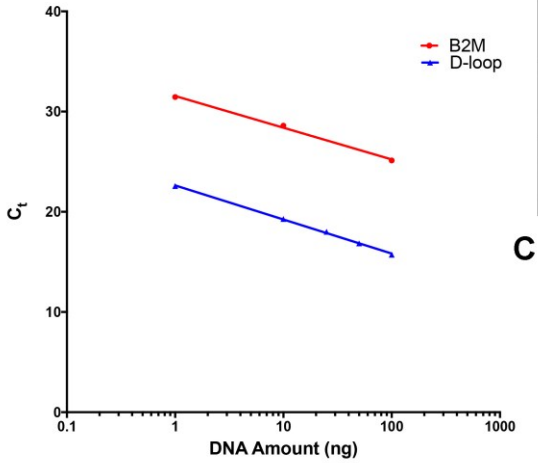

B

		Mean	Standard Error	95% CI (Lower Bound)	95% CI (Upper Bound)
B2M	Slope	-3.165	0.127	-3.518	-2.812
	E_x (%)	106.99			
	Y-Int	31.55	0.164	31.1	32.01
	R^2	0.9936			
D-Loop	Slope	-3.4	0.06759	-3.511	-3.288
	E_x (%)	96.84			
	Y-Int	22.63	0.04818	22.47	22.79
	R^2	0.9984			

C

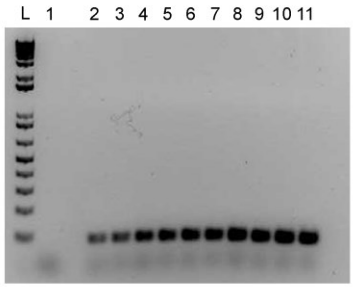

Figure 5.3. Quality control (QC) for mitochondrial DNA (mtDNA) quantitative PCR (qPCR) studies. QC of both the D-loop and Beta-2-Microglobulin (B2M) qPCR assays shows that they perform at acceptable levels. A. Standard curves for the SybrGreen B2M assay (red) and the TaqMan D-loop (blue) qPCR assays show strong correlations with similar slopes. One BEC DNA sample was serially diluted and assessed in duplicate for each assay. Error bars were too small to visualize and were left out of the plot. B. Descriptive statistics for slope, amplification efficiency (E_x), Y-intercept (Y-int.) and correlation coefficient (R^2) for each standard curve. Both targets are optimized, with high R^2 values (≥0.99) and high amplification efficiency (≥95%). C. 2% Agarose gel of B2M PCR products from the standard curve shows only one amplified product. 25ng of DNA was used for the TaqMan D-loop assay and 10ng of DNA was used for the B2M SybrGreen assay. Fluorescence spectra were monitored by the ABI7300 Real-Time PCR system. Standard curve and line of best fit were produced using PRISM 7 software. L=1kb DNA ladder, 1=0ng 2-3=0.01 ng, 4-5=0.1ng, 6-7=1 ng, 8-9=10 ng, 10-11=100ng. CI=confidence interval, ng=nanogram, B2M=beta-2-microglobulin

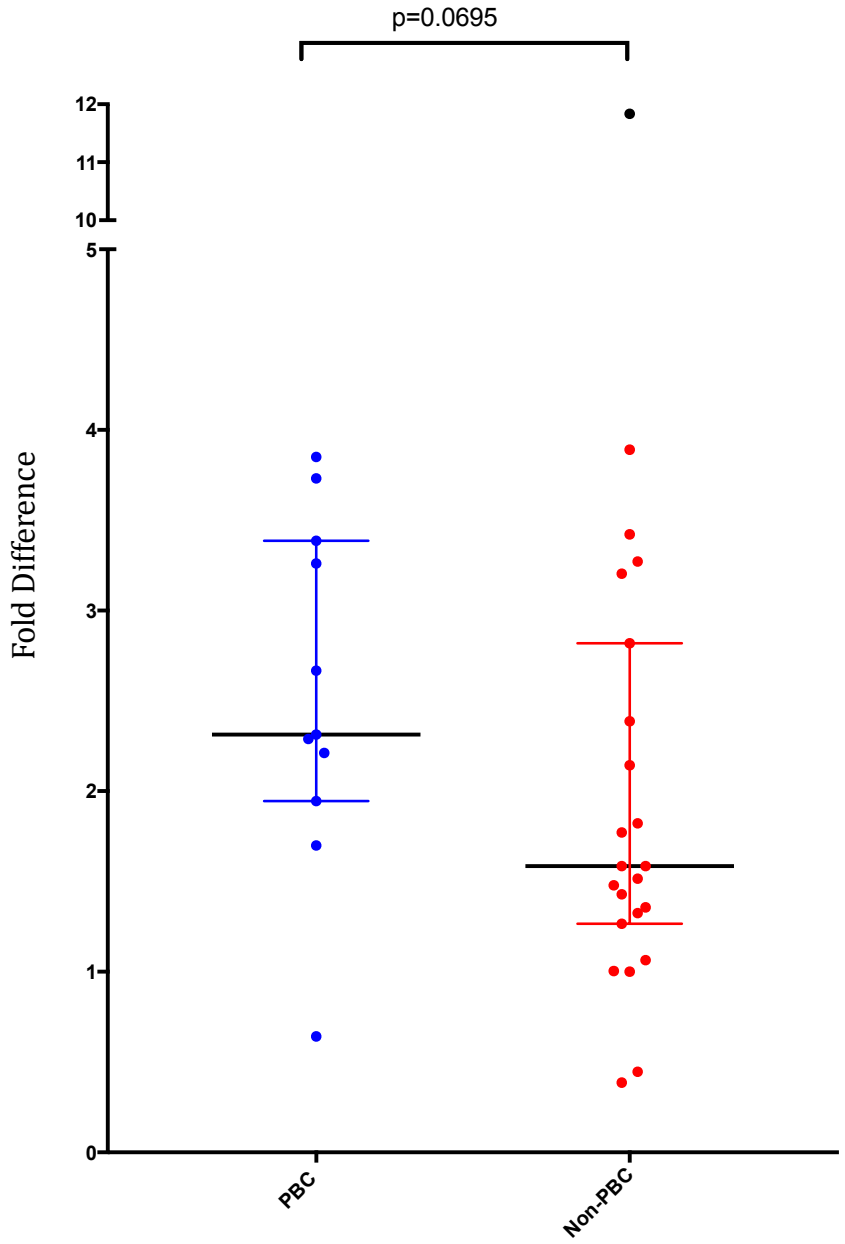

Figure 5.4. Mitochondrial DNA quantitative PCR results before the outlier was removed. The outlier sample (BEC245 p2) is highlighted in black. The outlier (BEC245 p2) was 650% higher than the Non-PBC median and greater than 4 standard deviations away from the mean. Groups were compared using a 2-tailed Mann Whitney Test with Prism 7 software. Shown are medians +/- IQR.